Role of Polyprotic Acids as Inhibitors of Calcium Oxalate Crystallization

A Dissertation

Presented to

the Faculty of the Department of Chemical and Biomolecular Engineering

University of Houston

In Partial Fulfillment

of the Requirements for the Degree

Doctor of Philosophy

in Chemical and Biomolecular Engineering

by

Jihae Chung

May 2017

Role of Polyprotic Acids as Inhibitors of Calcium Oxalate Crystallization

Jihae Chung

Approved:

Chair of the Committee
Dr. Jeffrey D. Rimer, Associate Professor,
Chemical and Biomolecular Engineering

Committee Members:

Dr. Peter G. Vekilov, Professor,
Chemical and Biomolecular Engineering

Dr. Megan L. Robertson, Assistant Professor,
Chemical and Biomolecular Engineering

Dr. Ognjen S. Miljanic, Associate Professor,
Chemistry

Dr. Michael A. Reynolds,
Staff Production Engineer
Shell Exploration and Production Company

Dr. Suresh K. Khator, Associate Dean
Cullen College of Engineering

Dr. Michael P. Harold, Chair,
Chemical and Biomolecular Engineering

Acknowledgments

First, I would like to thank my PhD advisor, Dr. Jeffrey D. Rimer, for giving me the opportunity to conduct research in his group. His relentless pursuit of scientific facts inspired all his students to do the same. I will forever be grateful for all the lesson, guidance, and support he has given me over the past six years.

I would also like to thank all my committee members, Dr. Peter G. Vekilov, Dr. Megan L. Robertson, Dr. Ognjen S. Miljanic, and Dr. Michael A. Reynolds, for their insightful and valuable discussion. It was an honor presenting my work to them.

I thank all my collaborators, Dr. John R. Asplin and his colleague, Ignacio Granja, and Dr. Giannis Mpourmpakis and his student, Michael G. Taylor, without whom my this thesis would have been incomplete.

I thank each and every Rimer group members, both former and current, for the supportive environment and also for making this journey more enjoyable.

I thank all my friends, Matt Oleksiak, and my cats, Manny and Patty, for my sanity. I give special thanks to Matt for being by my side and to my cats for giving me such affection and emotional comfort.

I dedicate my work to my family who has motivated me from the start. I thank you for your unconditional love and support throughout my existence. I could not have done this without you.

Role of Polyprotic Acids as Inhibitors of Calcium Oxalate Crystallization

An Abstract

of a

Dissertation

Presented to

the Faculty of the Department of Chemical and Biomolecular Engineering

University of Houston

In Partial Fulfillment

of the Requirements for the Degree

Doctor of Philosophy

in Chemical and Biomolecular Engineering

by

Jihae Chung

May 2017

Abstract

Crystallization is a ubiquitous phenomenon in many synthetic, natural, and biological systems that is often mediated by the action of foreign molecules (or modifiers) to tune the physicochemical properties of crystalline materials. Pathological biomineralization is an example of an undesirable crystallization process where modifiers act as inhibitors to reduce the rate of crystal growth. Here, we focus on the effects of modifiers and parametric studies of the growth medium on the crystallization of calcium oxalate monohydrate (COM), which is the most prevalent constituent of human kidney stones. We performed a systematic study to observe the specificity and efficacy of polyprotic organic acids, including the current drug citrate and its structural analogues, on COM crystallization. Interestingly, we identified modifiers that exhibit different modes of inhibitory action. A notable example is that of hydroxycitrate, which induces dissolution of the crystal surface in highly supersaturated growth solutions. Combined results from in situ atomic force microscopy studies and density functional theory calculations support our hypothesis that modifier-crystal interactions induce localized strain on the crystal lattice, which, in turn, leads to surface dissolution. We also studied the effects of solute and modifier speciation on COM crystallization under varying solution alkalinity that encompasses physiological conditions. We observe a pronounced disparity in the efficacy of modifiers with solution alkalinity owing to changes in local supersaturation near the crystal surface. Collectively, the improved fundamental understanding of modifier-crystal interactions coupled with high-resolution characterization techniques serve as a platform

to developing new therapeutics for kidney stone disease as well as elucidating the role of natural biomolecules in the pathological biomineralization of calcium oxalate stones.

Table of Contents

List of Figures

List of Tables

Chapter 1

Crystallization of Calcium Oxalate

1.1 Background on Kidney Stone Disease

Biomineralization is a ubiquitous process in many living organisms that has several functions, such as formation of bone in human body (Dunlop and Fratzl 2010), shells of molluscs (Falini, Albeck et al., 1996; Meldrum 2003; Evans 2008), and exoskeleton of coccoliths (Young, Didymus et al., 1992) which are essential to the mentioned organism. However, there are also undesirable biomineralization processes such as pathological crystallization which leads to various types of ailments in humans. These include (but are not limited to) cataract (i.e., protein crystallization in lens) (Pande, Pande et al., 2001), atherosclerosis (i.e., formation of solid composite of cholesterol with calcium orthophosphates in blood vessel) (Dorozhkin 2007), gallstones (cholesterol crystallization in gallbladder) (Holan, Holzbach et al., 1979), and kidney stones. The latter is the main area of interest in this thesis.

Kidney stone disease or nephrolithiasis is a common renal pathological disorder that influences about 10% of the population in the United States in which men are reported to have higher propensity to be afflicted than women (i.e., 12% men and 7% women) (Pearle, Calhoun et al., 2005). Unfortunately, even though researchers predict the number of inflicted people to rise due to increasing sedentary life style, choice of food consumption, and even global warming (i.e., expansion of ‘kidney stone belt’) (Brikowski, Lotan et al., 2008), the medicinal field have not witnessed significant development in treatments for the past three decades (Coe and Asplin 2010).

Kidney stones are classified as different types depending on the major constituent of the stones and most stones collected from patients are in the form of mixture of stones. About 10% of stones contain uric acid while ca. 5% exist in pure uric acid form and ca. 10 - 20% contains struvite (magnesium ammonium phosphate). About 75% of all nephrolithiasis cases involve calcium oxalate as its major component, in which most contain small amounts of hydroxyapatite. Calcium oxalate crystals may exist in three hydrate forms: calcium oxalate monohydrate or whewellite (COM), dihydrate or weddellite (COD) and trihydate (COT) (Millan 2001). COM is the most thermodynamically stable hydrate and the most common component in kidney stones. COD is less thermodynamically stable and is proposed to be a benign crystalline form of calcium oxalate due to the fact that it is often observed in urine in single crystal form (Dyer and Nordin 1967; Elliot and Rabinowitz 1980). COT is the least thermodynamically stable and less physiologically relevant (Sheng, Jung et al., 2005).

Formation of renal stones is a complex process with multiple steps and involves various components that form a matrix of stones. There are four processes associated with the formation of COM stones: nuclei formation in supersaturated solution, growth of crystals, aggregation of single crystals (or clusters thereof) into polycrystalline aggregates, and attachment (i.e., retention) of crystals and/or aggregates to epithelial cells (Sheng, Jung et al., 2005).

External factors may also affect stone formation. For instance, Brikowski et al., stated that there is a northward expansion of the distribution of population or ‘kidney stone belt’ which showed strong correlation with the rise in geographical temperature and the number of reported case for stone formers. This may affect the hydration level of

human body and concentration of electrolyte which directly influences the urinary environment where the stone formation transpires (Brikowski, Lotan et al., 2008). Dehydration also affects stone formation in a similar manner, in which the supersaturation with respect to the solute in urine increases providing a greater driving force for crystallization (Pak, Sakhaee et al., 1980; Borghi, Meschi et al., 1996).

Current therapies for COM kidney stones include dietary adjustment, which depends on the cause of stone formation, such as avoiding high oxalate-containing food or reducing consumption of high protein and increasing fluid intake, and taking supplements such as potassium citrate. Traditionally, lithotripsy procedure are performed in which stones are removed by breaking them into smaller fragments for them to readily pass through the urethra; however, it was reported that it may inflict side effects such as damaged tissues (Evan, Willis et al., 1998) to the cells. As mentioned above, there has not been a substantial advancement in kidney stone treatment therapeutics (Chen, Xie et al., 2007; Coe and Asplin 2010) which is in dire need for improvement.

This thesis will present research efforts aimed at inhibiting the formation of COM stones, focusing on arresting crystal growth via various classes of foreign additives or crystal growth modifiers (i.e., inhibitors) which may serve as model compounds for preventative drug molecules for renal stone disease. Before delving into my own research, this chapter will provide background information required to understand the project. First and foremost, the theory behind crystallization will be discussed. Second, the material of interest, calcium oxalate monohydrate will be presented. Third, the theory and mechanisms governing crystal growth inhibition via modifiers will be discussed.

Finally, previous research on the role of various classes of growth modifiers on COM crystallization will be presented.

1.2 Crystal Growth

Crystallization is a ubiquitous separation process that occurs in nature and also synthetically. Many industries including pharmaceutical companies utilize the knowledge of crystallization to manufacture, purify, and/or recover solid products with high purity. Crystallization from solution can be considered a two-step process. The first step is the birth of a new phase by nucleation in which the nuclei form from a supersaturated solution. This process may occur homogeneously (although this is rare) or heterogeneously wherein the energy barrier for nucleation is reduced by solute adsorption to solid substrates. The second step is crystal growth leading to bulk crystals with various sizes and habit.

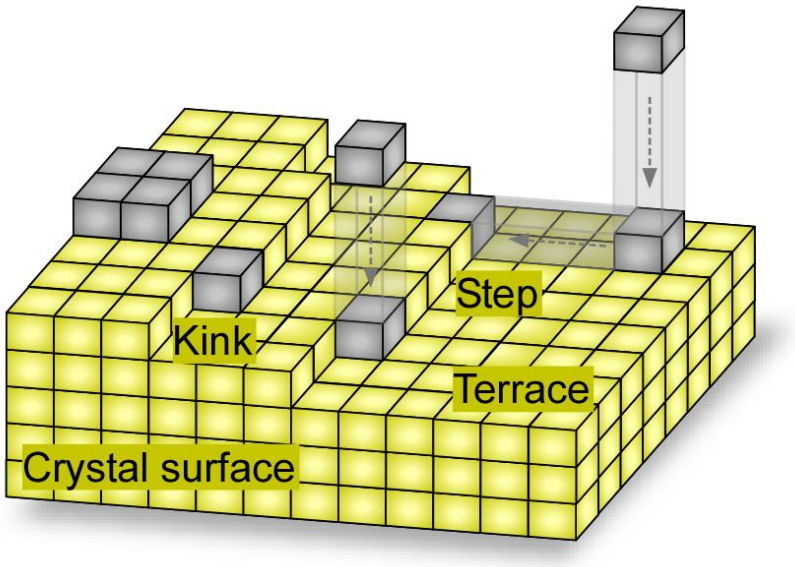

Figure 1.1 A schematic of a crystal surface depicting three possible sites for solute molecule attachment: terraces, steps, and kinks. Bulk and surface diffusion are also shown.

One important aspect of crystal growth is determining the rate of crystal growth. There may be numerous ways to obtain a linear growth rate: one example is to observe the change in certain dimension of the crystal over time and another example is to measure the change in mass of crystal over time. In the former case, the choice dimension may differ depending on the shape of the crystal i.e., radius for spherical crystals and the second longest dimension for nonspherical morphology. When measuring the linear growth velocity which is the growth rate normal to surface, it is essential to focus on the particular face of interest especially in the case of anisotropic crystals. The simplest classical example for crystal growth is the growth of (001) face on a cubic crystal i.e., Kossel crystal, in which an incomplete lattice layer on (001) face is terminated by a step and an incomplete row of molecules along either [100] or [001] directions forms a kink site. As shown in Figure 1.1, crystal growth via solute attachment on a crystal surface is possible at three sites: terraces with one nearest neighbor or bond, steps with two bonds, and kink sites with three nearest neighbors. The latter are the most energetically favorable sites for solute addition due to their low free energy of binding. Moreover, solute attachment/detachment on kink sites brings no change in the surface energy of crystal (Markov 2003).

There are several theories and mechanisms to describe crystal growth. One theory describes the birth of a step as ‘birth and spread model’, which is derived from the same logic that explains the two dimensional nucleation theory in which the Gibbs free energy favors the formation of nuclei when it has reached critical size, otherwise it will dissolve. Using the same logic, when the cluster of molecules reaches a critical size, it will grow on a flat surface. Once a surface nucleus is formed, it will either spread across the surface

(i.e., mononuclear model) or enough two dimensional nuclei will be generated on the surface to cover the entire layer (i.e., polynuclear model). The combination of these two extreme cases is the 'birth and spread model' that states the nuclei can spread at a finite constant rate, can form at any location of the surface, and there is no intergrowth between nuclei (Moe, Pearle et al., 2011). There are some limitations associated with this model. The mononuclear model predicts a proportional relationship between the crystal growth fate of a face and the area of the face, which contradicts the observation that the slowest growing face is the most dominantly expressed face and vice versa. The polynuclear model predicts a linear relationship between growth rate and the rate of nucleation and critical nuclei size; however, the size of nuclei will decrease with increasing supersaturation which leads to a more complex growth rate model with respect to supersaturation.

Burton-Cabrera-Frank (BCF) model was first based on Frank's idea of self-perpetuating steps via screw dislocations in the crystals which serve as the source of new steps that continues to grow suggesting that surface nucleation is unnecessary and that surface growth may occur at low supersaturation. This model was further developed by Burton et al., in which the diffusion of solute was assumed to be the determining step in the growth rate model (Burton, Cabrera et al., 1951; Frank 1952). The BCF model explains that the crystal growth rate varies from a parabolic dependence on supersaturation at low supersaturation to a linear dependence at high supersaturation.

The diffusion layer model correlates the boundary layer thickness and the growth rate for crystal growth from a supersaturated solution. The concentration of solute will be depleted at the crystal-solution interface as the solute molecules are incorporated into the

crystal lattice, which leads to continuous diffusion of solute from bulk to crystal interface. This region where the constant change in concentration occurs due to diffusion is called the ‘concentration boundary layer’ and the distance between the crystal surface and the region where the concentration is the same as bulk is called the ‘boundary layer thickness’. This model is based on the logic that solute diffuses through the boundary layer and incorporates into crystal lattice and the rate law provides information whether the diffusion or incorporation is the rate limiting step.

One important aspect of observing crystal growth is assessing the kinetics of crystal growth. As shown in Figure 1.1 and mentioned previously, kink sites are the most energetically favorable for solute incorporation due to the strong bonds available to be formed as well as the least number of bonds to break during solute detachment. Kink density, which determines the rate of crystal growth, is determined by the strength of bonds and the anisotropy in bonding, i.e., high kink density will be possible if a crystal has weak bonds parallel to step edges and strong bonds normal to step edges since the energy penalty for creating kink site will be small.

1.3 Calcium Oxalate Monohydrate (COM) Crystals

Calcium oxalate monohydrate is the most thermodynamically stable hydrate of calcium oxalate (Tomazic and Nancollas 1979) and it is also the most relevant form in kidney stone disease. There are two different monoclinic space groups assigned to COM crystals in other publications. One is $P2_1/n$ space group reported by Deganello and Piro with unit cell dimension of a = 9.978 Å, b = 14.5884 Å, c = 6.2913 Å, and β= 107.05˚. (Deganello and Piro 1981). The second is a $P2_1/c$ space group with unit cell dimension of

a = 6.290 Å, b = 14.5803 Å, c = 10.116 Å, and β = 109.46˚ (Tazzoli and Domeneghetti 1980). As shown in Figure 1.2A and B, COM crystals exhibit a hexagonal platelet morphology that is bounded by four crystallographically relevant surfaces: {100}, {010}, {12-1}, and {021}. Researcher have used in situ atomic force microscopy to observe the growth of (100) and (010) faces, which follow a layer-by-layer growth model with step propagating from screw dislocation sources (Gvozdev, Petrova et al., 2004). On the (100) face, the growth hillock is triangular with {12-1} steps that propagate in c-direction. On the (010) face, the growth hillock is bounded by {12-1} and {021} steps. Figure 1.2C shows that each plane on COM crystal has different density and spatial orientation of calcium and oxalate ions. We color coded the calcium ions (green) to emphasize their spatial arrangement on each plane while oxalate molecules are shown in gray and water molecules are omitted for clarity and easy visualization.

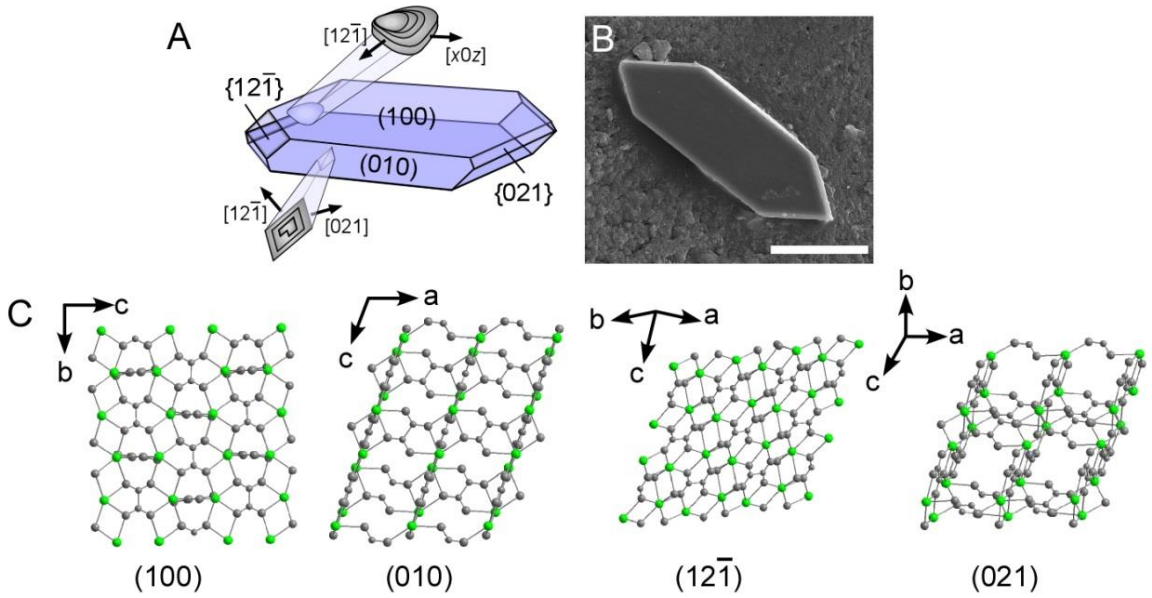

Figure 1.2 Schematic of calcium oxalate monohydrate crystal (A) and scanning electron micrograph of COM crystal (B) is shown. Cross-sectional images of each crystallographically significant plane are shown (C). Scale bar equals 20 μm.

Millan reported a thorough analysis of the equilibrium structure and morphology of whewellite and the ionic interaction between calcium and oxalate within the structure (Millan 2001). Calcium ions interact with oxalate in two different positions as shown in Figure 1.3. Calcium ion may be in close distance between two oxygen atoms in oxalate and form a chelato bond with oxalate (I in Figure 1.3). It can also form a single bond with oxygen atom (II in Figure 1.3). The interaction between calcium and oxalate or Ca – O interaction is a purely ionic interaction according to the interatomic distances, as measured by ultraviolet and infrared absorption spectroscopy (Krishnamurty and Harris 1961; Millan 2001). However, calculations of quantum potentials around oxalate performed by the author showed that calcium ions near oxalate ions are located where oxalate potential is minimum and there is electron density accumulation in the sp^2 hybridation of oxygen in oxalate in the direction of the O – Ca bonds. Collectively, the author concluded that calcium – oxalate interactions are ionic in character, but the bonds resemble covalent bonds due to the directionality. One more notable point is that COM (100) surfaces consist of alternating layers of oxalate,$_2$ ions and calcium – oxalate,$_1$ pair which leads to double charge layer under ion-rich aqueous environment (Figure 1.3). This would cause growth inhibition in the [100] direction due to restricted diffusion of ions from bulk to surface resulting in thinner crystal than the equilibrium morphology. It was suggested that the growth modifiers introduced to inhibit the growth should be chosen to target surfaces exhibiting the fastest rates of growth. This will be discussed in further detail in later section of this chapter.

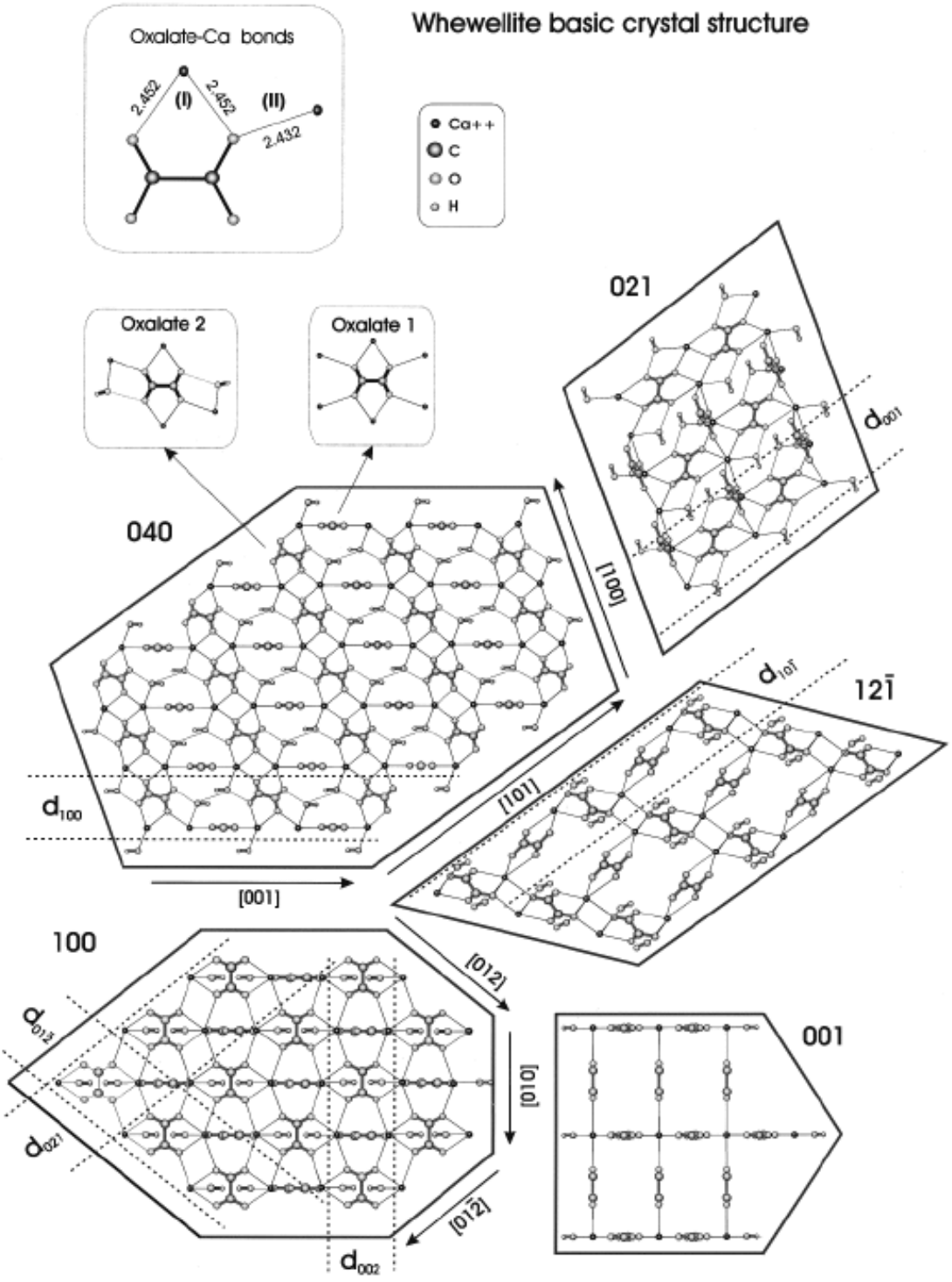

Figure 1.3 COM crystal structure on each face and two kinds of calcium-oxalate bonds and coordination of each oxalate ion are shown. Molecular graphs are slices with d_{hkl} thickness cut along crystal edges.

1.4 Modification of Crystallization

There are numerous factors to consider when designing any crystallization processes in solution that includes (but are not limited to) solute concentration, temperature, additives and the choice of solvent, which collectively alters the crystalline products. These may in fact improve the quality of crystalline products. For instance, solubility of active pharmaceutical ingredient can be improved by forming a co-crystal with an additive (Chung and Kim 2011) or inhibit the crystallization. Either way, the impact of these factors is paramount. Herein, we focus on the effect of additive and solvent on the crystal habit and the rate of crystallization.

The crystal habit is determined by the growth rate of individual faces of a crystal which may be affected by foreign molecules or the solvent. As shown in Figure 1.4 (Weissbuch, Addadi et al., 1991), faces with slow normal growth will be more dominantly expressed than the fast growing faces; however, when an additive interacts specifically with the fast growing direction, such as the B direction in Figure 1.4, growth in the B direction will be stunted resulting in larger B surfaces and affecting the final crystal habit.

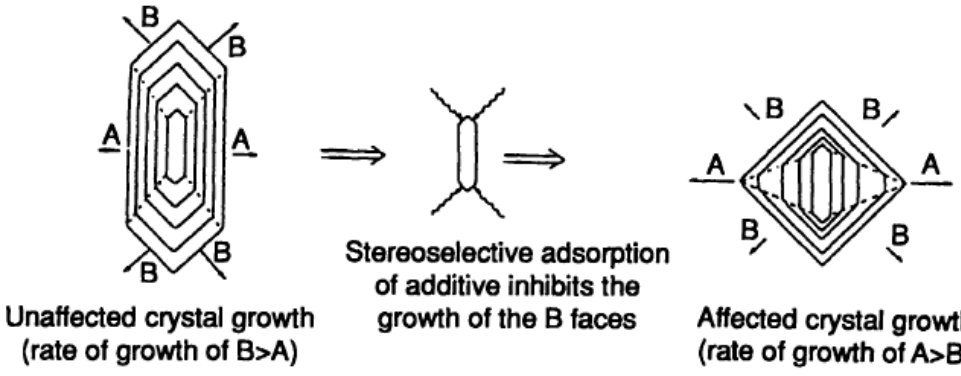

Figure 1.4 A schematic of an anisotropic crystal growth and the effect of a site-specific additive interacting with the crystal.

Thermodynamics dictates the final crystal habit in the case of very slow growth, which results in faces with the minimum surface free energy being expressed. Crystals in an equilibrium state follow the following Gibbs condition in which the sum of surface free energy times the corresponding surface area is minimum. However, under most conditions, crystal habit is dictated by kinetics, which can be affected by numerous external factors such as supersaturation, temperature, and agitation.

In the case of crystal growth in solution, the rate limiting step of crystal growth is the mass transport at the interface of crystal where the transport in restricted to the solute molecules diffusing through the diffusion boundary layer (Rosenberger 1986). This volume diffusion can be influenced by the diffusivity of the solute molecule, the solvent viscosity, and hydrodynamics at the interface. Once the solute diffused through the boundary layer near the interface, it will absorb on the crystal surface and diffuse in a two dimensional manner until it finds a site to be incorporated. Desolvation is a process in which a solute-solvent bond breaks in order for the solute-crystal bond to be formed. This may be a rate limiting step (Chernov 1989) for certain crystal systems such as potassium hydrogen phosphate (Hottenhuis and Lucasius 1989). However, with the advance of theoretical calculations and simulations, it has been reported that the lifetime of hydrogen bonding in structured water molecules on the surface of a protein molecule is many orders of magnitude shorter than the formation of bond of protein molecules to the surface (Makarov, Andrews et al., 2000). Thus, the solvation/desolvation effect is dependent on the system and the solution properties (e.g., pH and ionic strength).

In some processes, additives or impurities are considered undesirable; however, the impact of additives on modifying the crystallization process may be beneficial and

highly effective. If we consider crystallization in terms of the 'energy landscape', we can describe the process as a phase transition from a matter in a solvated state with high free energy into a crystalline state with low free energy. This energy landscape can explain much about the crystallization of the matter of interest, such as the crystal habit and the rate of crystallization, which can be dramatically altered by the use of additives. Additives are referred to by many different names, such as impurities, inhibitors, auxiliaries, and modifiers (Weissbuch, Lahav et al., 2003), as well as imposters (Sizemore and Doherty 2009). Herein, growth *modifier* will be used as the representative term (or alternative *inhibitor* or *promotor* of crystallization).

Modifiers operate by three possible modes of action to inhibit crystallization: step pinning, kink blocking, and incorporation as shown in Figure 1.5 (Dove and De Yoreo 2004). The step pinning mode of action occurs when modifiers adsorb on terraces and impede the advancement of layers (Cabrera and Vermileya 1958). Steps with pinned sites can still advance forward, albeit with reduced rate of advancement due to decrease in the driving force for growth (Lovette, Browning et al., 2008), if the distance between the pinned sites by adsorbed growth modifiers is much greater than the critical radius of the step curvature. However, when the distance between adsorbed modifiers is less than the critical curvature of the step, arrest of step movement occurs. According to Gibbs-Thompson equation, supersaturation is a function of curvature so if the curvature becomes less than its critical value the solution at the interface in fact becomes undersaturated and steps retreat to bring the curvature above the critical value. The so-called *dead* zone is a range of concentration marked by critical supersaturation in which no growth occurs. As shown in Figure 1.5A, the dead zone expands as the concentration

of impurity increases (i.e., the critical supersaturation is proportional to the square root of impurity concentration) but the rate of step advancement can be restored upon being exposed to a pure solution. This mode of action has been reported for COM crystals in the presence of citrate and osteopontin (Qiu, Wierzbicki et al., 2004; Qiu, Wierzbicki et al., 2005), in which citrate only pins the step on {100} face and osteopontin merely affects {010} surfaces. This implies that step pinning inhibition mode is dependent on a specific modifier-step interaction.

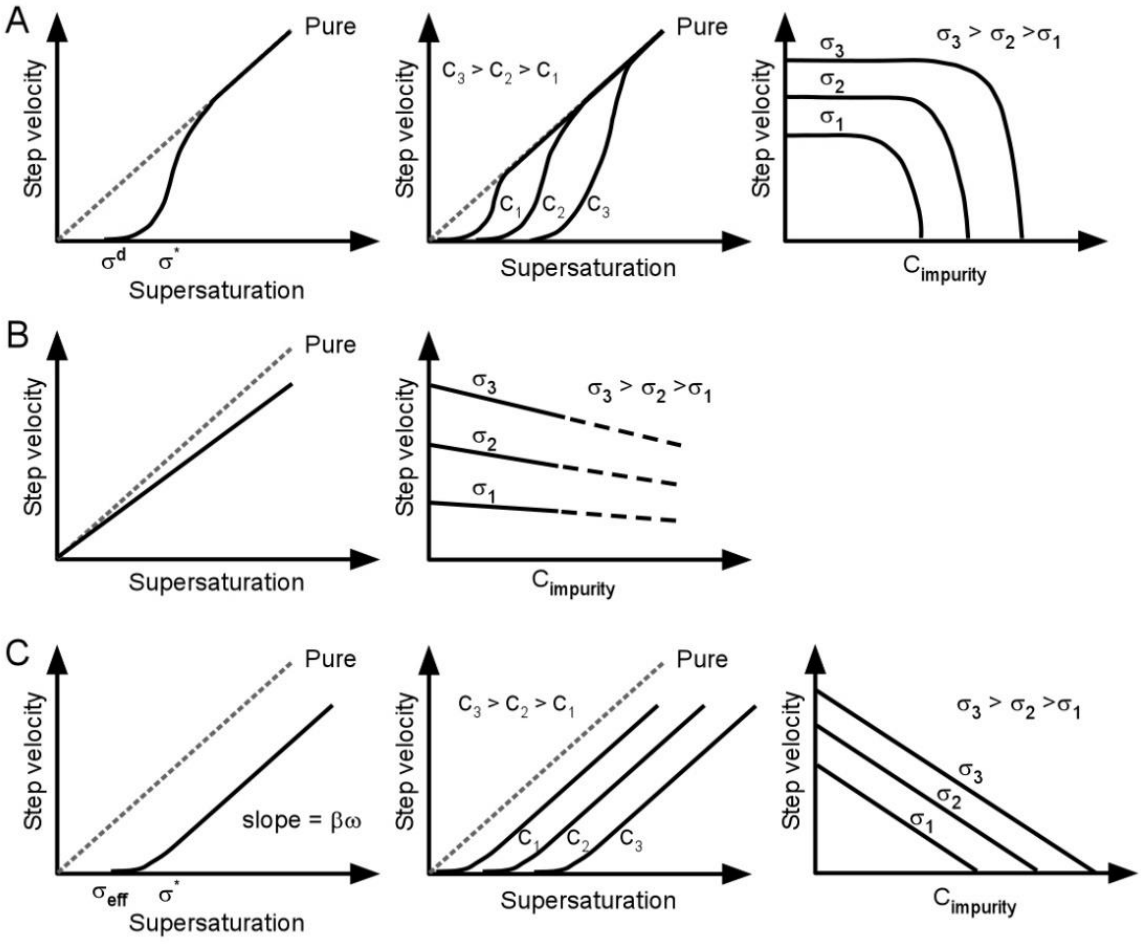

Figure 1.5 A representative step velocity versus supersaturation and impurity concentration plot in the presence of modifier with step pinning (A), kink blocking (B), and incorporation (C) mode of action.

Kink blocking is when the modifier blocks the kink site and reduces the effective kink density for solute to attach leading to halt of kink propagation. Similar to growth, kink sites are also the most energetically favorable sites for growth modifiers to attach (De Yoreo and Vekilov 2003). If an inhibitor occupies a crystal vacancy at kink sites, the inhibitor blocks further attachment of solute molecules; and since the total number of kink sites is relatively few, only a few inhibitor molecules are required to block growth. Unlike step pinning, this is not a thermodynamic effect and the solubility is unaffected but the kinetic coefficient is affected (See Figure 1.5B) Similar to step pinning, kink blocking is also dependent on the specific modifier-site interaction and can possibly lead to changes in the final morphology of crystals.

The incorporation mode of action is when a modifier becomes trapped by the advancing step or at kink sites and becomes incorporated into the crystal which leads to a distortion in the crystal lattice. This can either result in an increase or decrease in free energy and solubility, thereby affecting the effective supersaturation. As shown in Figure 1.5C, the kinetic coefficient (i.e., slope of velocity vs. concentration plot) remains unchanged, meaning that modifier incorporation does not impact the kinetics of solute attachment. For example, the effect of strontium ions and magnesium ions on calcium carbonate crystallization involves modifier incorporation (Nielsen, De Yoreo et al., 2013). The presence of strontium on calcite crystal surfaces results in the promotion of step velocity at low modifier concentration and switches to the inhibition of step velocity at high modifier concentration. This is due to strontium ion incorporation, which contributes to the overall precipitation rate of solute by enhancing solute attachment to

the crystal surface by modifying the structure of kink sites (Nielsen, De Yoreo et al., 2013).

1.5 Inhibition of COM Crystallization

As mentioned in the previous section, site specific interactions between modifiers and crystal surfaces are crucial in inhibiting crystallization. COM is a non-Kossel crystal with many types of kink sites, thus offering many diverse binding sites for modifiers. As shown in Figure 1.6, calcium ions on COM crystal surface dissociate into diffuse double layer, which leaves the COM crystal surface negatively-charged in aqueous media.

A study by Shirane et al., suggested that the calcium ions are the binding sites on COM crystals which can readily interact with negatively-charged moieties on modifiers (Shirane, Kurokawa et al., 1999). There have been numerous reports identifying effective modifiers of COM growth as molecules or macromolecules rich in negatively-charged groups, such as carboxylate and phosphate groups (Friddle, Weaver et al., 2010). There moieties are believed to mimic the vacancy of oxalate groups. To this end, anionic moieties bind to COM interfaces via calcium bridges: $_{(COM)}COO^{-}\ldots Ca^{2+}\ldots {}^{-}OOC_{(modifier)}$, as illustrated in Figure 1.6; and since the spatial arrangement of calcium and oxalate on each COM surface is different, the alignment of oxalate molecules or modifiers with negatively-charged moieties (Figure 1.7) may exhibit a preferential binding when adsorbing on COM crystal faces.

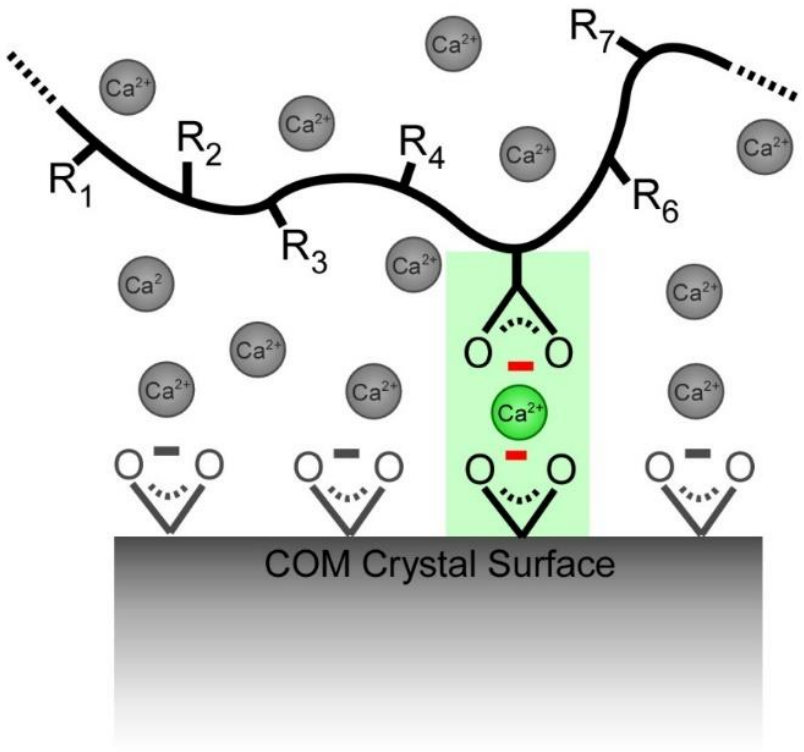

Figure 1.6 A schematic of an interaction between a growth modifier with negatively-charged groups i.e., carboxylate, and negatively-charged COM crystal surface via calcium-bridge is illustrated.

Aside from their physicochemical properties, modifiers can be classified into different types depending on the nature of modifier-crystal interaction. Tailor-made modifiers are structural analogues of the solute molecule that mimic the binding mode of the solute, but contain different functional groups (e.g., modified functional moieties) that perturb further building of solute molecules. The specific binding affinity of tailor-made modifiers can alter the anisotropic growth rate(s), which can lead to dramatic changes in the final morphology of crystals (Weissbuch, Addadi et al., 1991; van Enckevort and Los 2008). Citrate is an example of a molecular tailor-made modifier for COM crystallization, as it exhibits similar molecular structure as that of oxalate (Qiu, Wierzbicki et al., 2005; Chung, Granja et al., 2016). Indeed, citrate exhibits preferential binding to COM (100)

faces and impedes growth in the *c* direction, leading to blunted (and thinner) hexagonal platelets.

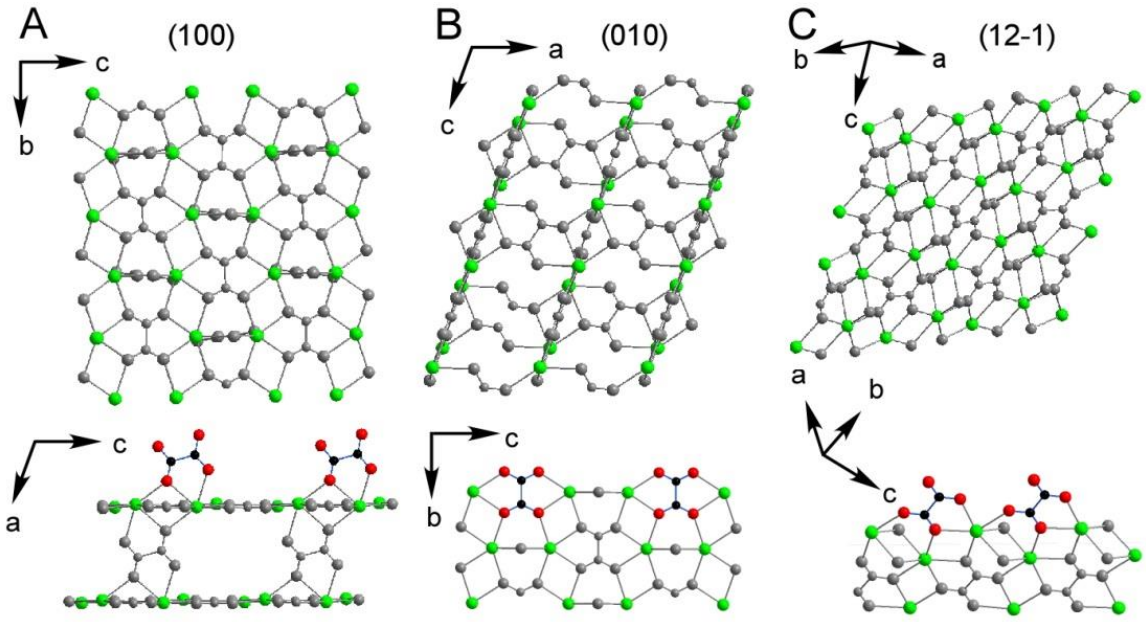

Figure 1.7 Cross-sectional images of (100) (A), (010) (B), and (12-1) (C) planes are shown (top) as well as the orientations of oxalate interacting with each surface are shown along the planes (bottom).

Not all modifiers are structural analogues of the solute molecule, but rather can exhibit epitaxial matching with the crystal surface. A popular example is antifreeze proteins present in cold weather species (e.g., fish, insects, plants, etc.), which suppress ice formation (Graether, Kuiper et al., 2000; Huang, Ehre et al., 2012). It has been shown that antifreeze proteins contain binding moieties, such as threonine groups (Graether, Kuiper et al., 2000) that form an array with geometric feasibility to interact with ice crystals via lattice matching, which leads to suppression of ice crystal growth as well as freezing point depression.

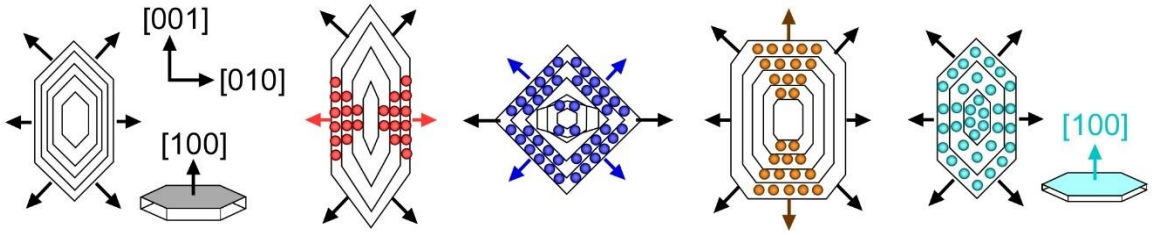

Figure 1.8 A schematic of specific binding of modifiers (represent as colored circles) on hexagonal COM crystal surfaces, which results in suppression of growth normal to that direction and change in final morphology.

Crystals prepared in the presence of growth modifiers may exhibit altered morphology owing to the specific binding of modifiers to crystal surfaces wherein the adsorbed modifier inhibits further attachment of solute to sites and reduces the growth rate normal to the affected surface (Weissbuch, Addadi et al., 1991). As shown for COM crystals in Figure 1.8, modifiers that preferentially bind to the (010) face increase the [001] length of hexagonal platelets which elongates the resulting COM crystals. Modifiers with specific binding to {12-1} and {021} faces lead to the formation of diamond-shaped crystals. Modifiers with specificity for (100) faces would lead to thinner COM crystals (i.e., reduced [001] dimensions relative to that of the control).

1.5.1 Past Studies on COM Growth Inhibitors

Past studies have identified modifiers of COM crystallization spanning from natural modifiers such as urinary constituents (Asplin, Deganello et al., 1991; Millan, Sohnel et al., 1997)), amino acids (Fleming, van Bronswijk et al., 2001; Sayan, Sargut et al., 2009) as well as synthetic modifiers such as peptides (Wang, Qiu et al., 2006; Weaver, Qiu et al., 2009) and peptoids (Chen, Qi et al., 2011; Huang, Ehre et al., 2012) which are poly-N-substituted glycine (i.e., the side chains are attached to the nitrogen

atom of peptide backbone rather than to the α carbons). Additional examples include small organics, such as citrate (Qiu, Wierzbicki et al., 2004; Qiu, Wierzbicki et al., 2005; Sheng, Jung et al., 2005; De Yoreo, Qiu et al., 2006; Wang, De Yoreo et al., 2006; Weaver, Qiu et al., 2006; Weaver, Qiu et al., 2007), and alkali metals (Farmanesh, Alamani et al., 2015).

One of the most extensively studied urinary constituent with respect to its effect on COM crystallization is osteopontin (OPN). It is a ubiquitous protein in physiological processes (e.g., bone formation) and is a potent inhibitor of COM crystallization capable of inhibiting all four critical steps of COM kidney stone formation: nucleation, growth, aggregation, and retention (Wesson, Johnson et al., 2003; An, Lee et al., 2010). Due to the high population of aspartic acid-rich domains e.g., amino acid 70 to 105 is comprised of 19 aspartic acids (53%) (Hoyer, Asplin et al., 2001) in its primary sequence, OPN exhibits a similar mode of interaction with COM crystal as that of polyaspartic acid. This led to many studies elucidating the effect of spatial positioning of aspartic acid and glutamic acid arrangements in the primary amino acid sequence of OPN (Wang, Qiu et al., 2006; Taller, Grohe et al., 2007; Farmanesh, Chung et al., 2013). It was also reported that acidic amino acids are not the only factor affecting OPN-COM crystals interactions. Notably, the presence of phosphate groups in OPN is also an important factor. Phosphate groups help promote specific protein-crystal interactions (Hoyer, Asplin et al., 2001; Wesson, Johnson et al., 2003; Grohe, O'Young et al., 2007; Wang, Guan et al., 2008; Langdon, Wignall et al., 2009; Grohe, Chan et al., 2011; Chan, Vincent et al., 2012; Hug, Grohe et al., 2012) and may alter the preferential binding affinity to COM crystals, which may be explained via the surface free energy of the sites (Taller, Grohe et al., 2007) and

nonspecific electrostatic interactions between calcium ions of the crystal and the phosphate groups of the protein (Langdon, Wignall et al., 2009). Although phosphorylation enhances the inhibition of COM crystal growth, there is no detectable change in secondary structure of OPN (which is mainly β-sheet conformation) in the presence and absence of phosphate groups so the effectiveness might be attributed to the local patterns of charge density (Hoyer, Asplin et al., 2001; Wang, Guan et al., 2008).

The influence of protein modification has also been noted for Tamm-Horsfall protein (THP), the most abundant protein in urine and a major component of the stone matrix. The reported effects of THP on COM crystallization and aggregation are widely varying in their claims of THP acting as a stone inhibitor (Scurr and Robertson 1986; Ronco, Brunisholz et al., 1987; Hess, Nakagawa et al., 1991; Mo, Liaw et al., 2007) and promoter (Boyce and King 1963; Hallson and Rose 1979), due in part to the large variation in sialic acid content (i.e., the functional groups present in glycosyl side groups of THP) (Viswanathan, Rimer et al., 2011). Several clinical studies have shown that when comparing THP extracted from stones of former stone-forming patients and a control group, the level of sialic acid in THP was reduced for stone-forming patients (Knorle, Schnierle et al., 1994; Pragasam, Kalaiselvi et al., 2005). Viswanathan et al., investigated the relative effects of THP and desialylated THP on crystal aggregation and reported that the latter promoted COM aggregation (Viswanathan, Rimer et al., 2011). They hypothesized that sialic acid (consisting of one carboxyl group) contributed to the overall negative charge of THP, and that by eliminating these residues from the protein, the modified protein may function as a promoter of COM aggregation.

Ryall and coworkers investigated the adsorption affinity of amino acids on calcium oxalate crystals (Fleming, van Bronswijk et al., 2001). They prepared a saturated aqueous solution of calcium oxalate and placed COM crystals and single amino acid in the solution. After the crystals were in contact with amino acids for 15 hours, the supernatant solutions were filtrated and the remaining concentration of amino acid was monitored using HPLC. From these studies it was shown that the most effective amino acids were aspartic acid, glutamic acid, and γ-carboxyglutamic acid (i.e., these amino acids most strongly adsorbed to COM crystal surfaces). Based on the strong adsorption affinity of dicarboxylic acids and tricarboxylic acids, it was proposed that proteins rich in such amino acids would have higher impact on crystals compared to those with fewer negatively-charged groups (Fleming, van Bronswijk et al., 2001).

Citrate is a small organic acid with three carboxylic acids that is a common urinary constituent and is also an over-the-counter supplement commonly administered to stone patients as a potassium salt (Ettinger, Pak et al., 1997). Citrate has been extensively studied due to its moderate inhibitory effect on COM crystallization, as reported in both clinical and *in vitro* studies. It was found that citrate was capable of forming a complex with calcium and can inhibit the nucleation, growth, and aggregation of COM crystals (Pak 1994). Moreover, citrate reportedly enhances the inhibitory effect of THP (Hess, Zipperle et al., 1993). Bulk crystallization studies of COM crystals in the presence of citrate reveal that the morphology of resulting crystals become disc-shaped hillock geometry on the (100) face (Qiu, Wierzbicki et al., 2004; Wang, Zhang et al., 2006; Grohe, O'Young et al., 2011). The aspect ratio of COM crystals as well as the thickness decreases with increasing concentration of citrate present (note aspect ratio is defined as

the ratio of [001] to [010]). It is intuitive that the surface area of the (010) faces would also decrease as the rate of growth in the [010] direction becomes more dominant (Qiu, Wierzbicki et al., 2005). In a non-clinical setting, the effect of citrate on the COM growth kinetics was observed by *in situ* atomic force microscopy. Qiu et al., reported that citrate preferentially affects the growth hillock on COM (100) surfaces via a step pinning mode of action wherein the authors observed characteristic jagged steps in the presence of the modifier (Qiu, Wierzbicki et al., 2004; Qiu, Wierzbicki et al., 2005; Weaver, Qiu et al., 2006). Molecular modeling reveals that the specific binding affinity can be explained through the maximum bonding energy exerted on step sites due to the orientation of calcium and oxalate ions (Qiu, Wierzbicki et al., 2004). Also, the effect of citrate is low on COM (010) surface due to the electrostatic repulsion between oxalate on the surface and carboxylate groups in citrate molecule (Qiu, Wierzbicki et al., 2005; Cho, Salter et al., 2013).

Trace elements are also detected in urine (Elliot and Eusebio 1967; Hofbauer, Steffan et al., 1991; Pearle, Calhoun et al., 2005) and in the calcium oxalate monohydrate (COM) stone matrix (Levinson, Nosal et al., 1978; Wandt and Pougnet 1986; Wandt and Underhill 1988; Hofbauer, Steffan et al., 1991; Abboud 2008). These species are reported to interact with COM crystal surfaces and affect crystallization (Munoz and Valiente 2005). For instance, Fe^{3+}, Al^{3+}, and Cr^{3+} were reported to inhibit the growth of COM crystals by interacting with oxalate ions on crystal surfaces (Meyer and Thomas 1982; Pearle, Calhoun et al., 2005)). Trace metals such as Mg^{2+} (Elliot and Eusebio 1967; Streit, Tran-Ho et al., 1998) and K^{+} (Yachantha, Hossain et al., 2009) were reported to inhibit COM crystallization by increasing the solubility.

1.5.2 Previous Studies on COM Growth Inhibitors

Our group has been actively investigating growth modifiers of COM crystallization including macromolecules such as protein and polysaccharide, synthetic peptide, and alkali metal ions and systematically studied their effect on the bulk crystallization to elucidate the modifier-crystal interaction, quantified their efficacy in terms of inhibiting crystallization by measuring kinetics of crystallization in the presence of modifiers, and delve into the modifier-crystal interaction at a near molecular lever by observing the growth and inhibition phenomena in real time using in situ atomic force microscopy. Lastly, we combined our experimental finding with colloidal theory to explain the phenomena. This section will provide a short summary of our previous findings.

1.5.2.1 High-Throughput Platform for Design and Screening of Peptides

This study was performed in collaboration with the Karande group at Rensselaer Polytechnic Institute and was published in the Journal of Crystal Growth (Farmanesh, Chung et al., 2013).

Peptides are an attractive template for designing tailored growth modifiers due to its amenable synthesis which enables size, sequence, secondary structure, and stereochemical modularity control by substituting different residues. This also makes it easier to design its physicochemical properties such as solubility and bioavailability. Rimer, Karande, and coworkers systematically observed the effectiveness of 18-mer peptide with varying sequences on COM crystallization where we studied their preferential binding on COM crystal as well as their efficacy on the kinetics of COM crystallization. Design of peptides was inspired by the proteins that tune

biomineralization process of calcium-based minerals, which tend to be rich in aspartic acid and glutamic acid with different periodicity i.e., singlet, doublet, triplet of acids with a non-binding amino acid. Peptide sequences selected for this study represented a combination of randomly selected alanine (A, spacer) and aspartic acid (D, binder) sequences with the motif of singlet, doublet, and triplet (Table 1.1). Note that alanine was chosen as a spacer because of its small side group (methyl group) which would minimize any steric hindrance and may promote peptide-COM interaction through entropic effect and release unfavorable hydration layer on COM surface.

Table 1.1 List of peptides used in this study.

	1	2	3	4	5	6	7	8	9	10	11	12	13	14	15	16	17	18
D1	**D**	**D**	**D**	A	A	A	A	A	**D**	**D**	**D**	A	A	A	A	A	**D**	**D**
D2	A	A	**D**	A	A	A	A	A	**D**	**D**	A	A	A	A	**D**	A	A	A
D3	A	**D**	A	A	A	**D**	A	A	**D**	A	A	**D**	**D**	A	A	**D**	A	A
D4	A	**D**	A	A	**D**	A	A	**D**	A	A	**D**	A	A	**D**	A	A	**D**	A
D5	A	**D**	A	A	**D**	**D**	A	A	**D**	A	A	**D**	**D**	A	A	A	A	A
D6	A	**D**	A	A	A	**D**	**D**	**D**	A	A	A	**D**	A	A	A	**D**	**D**	**D**
D7	A	**D**	A	A	A	**D**	**D**	A	A	A	A	A	A	A	A	**D**	A	A
D8	A	**D**	A	A	A	**D**	**D**	A	A	A	**D**	A	A	A	A	**D**	A	A
D9	A	**D**	A	A	A	**D**	**D**	A	A	A	**D**	A	A	A	**D**	**D**	A	A
D10	A	**D**	A	A	**D**	A	A	A	**D**	A	A	**D**	**D**	A	A	**D**	A	A
D11	A	**D**	A	A	**D**	**D**	A	A	A	A	A	A	**D**	A	A	**D**	A	A
D12	A	**D**	**D**	A	A	**D**	A	A	**D**	A	A	**D**	**D**	A	A	**D**	**D**	A
D13	A	**D**	A	**D**	A	**D**	A	**D**	A	**D**	A	**D**	A	**D**	A	**D**	A	**D**

The most notable outcome of this study was the design of a high-through put system for screening the efficacy of peptides on inhibiting COM crystallization. Calcium

ion selective electrode (ISE) was used to track the temporal depletion of free calcium ion concentrations during COM crystallization in the absence and in the presence of each peptides. The efficacy of each peptide in inhibiting COM crystallization was determined by comparing the COM growth rate in the presence of peptide to that of absence. Performing an extensive study of an 18-mer peptide with all natural amino acids is virtually impossible and even an exhaustive study of 18-mer peptides with just alanine and aspartic acid would result in a library of 10^5 different combination of peptides. Our approach of using the motif from a known potent inhibitor provided a good starting point for a systematic study. Another important finding is that this study systematically demonstrated the significance of subtle changes in peptide sequence. One example is the comparison between the efficacies and sequences of peptide D8 and D9 where the two peptides share the same sequence with D9 possessing one additional aspartic acid on the 15^{th} position making a doublet. This subtle change in structure improved the peptide's efficacy to ca. 40% as shown in Figure 1.9.

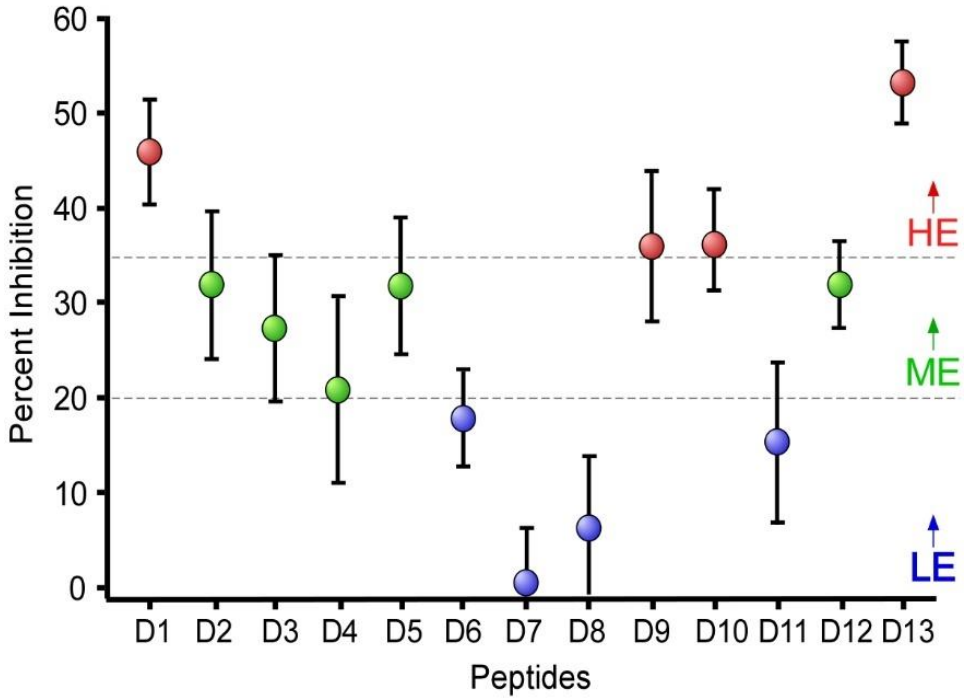

Figure 1.9 Percent inhibition of COM crystallization in the presence of $C_{peptide}$ = 20 μg/mL was categorized as high (HE), medium (ME), and low (LE) efficacy.

Peptides are an attractive construct for engineering chemical and structural motifs of growth modifiers that provide effective crystal growth control. This work demonstrated the efficacy of short peptide sequences (18 amino acids in length) as effective growth modifier of COM crystallization and also shows that simple design rules based on mimicking observations in the natural world can lead to the rational design of crystal growth modifiers. While there have been many reports on the growth modifiers of COM crystallization in which subtle differences in the sequence of macromolecules resulted in profound improvement/change in their inhibitory potential, this work shows for the first time a systematic demonstration of the role of sequence in custom-designed peptides. The most salient feature of this work is the use of ISE-based high-throughput screening and identification of potent peptides, and their validation as effective inhibitors

in bulk crystallization studies. This work may be used as a basis for more systematic analysis of peptide structure, including varying amino acid motifs and sequences, which will undoubtedly lead to the discovery of inhibitors with increased efficacy. Indeed, it is reasonable to expect that the application of our design algorithm using biomimetic peptide sequences derived from targeted segments of known calcium-binding proteins has the potential to further improve peptide performance as potent growth modifiers of COM crystallization. Furthermore, molecular-level studies that address fundamental aspects of peptide–crystal interactions will establish an improved understanding of structure–function properties as input into the design algorithm for further refinement and testing. Collectively, the versatile approach utilized in this work has broader applicability for a variety of inorganic and organic materials.

1.5.2.2 Specificity of Growth Modifiers and Their Cooperative Effects

This study was performed in collaboration with the Karande group at Rensselaer Polytechnic Institute and Dr. Asplin at Litholink Corporation and was published in the Journal of the American Chemical Society (Farmanesh, Ramamoorthy et al., 2014).

The interactions between ions or molecules with crystalline interfaces play an integral role in fine tuning the design of materials. These modifiers interact with crystal surfaces via a range of intermolecular forces, such as van der Waals, hydrogen bonds, ionic bonds, or in rare cases covalent bonds. The ability to characterize these modifier-crystal interactions can provide a deep understanding of the phenomena influencing crystal growth inhibition and can be utilized to rationally design materials. Modifiers may be used individually and in cooperation with multiple modifiers to alter crystallization. This study entailed the examination of chondroitin sulfate, serum albumin, and transferrin

all of which are known putative modifiers of COM crystallization. Systematic study of each modifiers as well as binary combinations thereof was carried out to investigate their specificity and efficacy on COM crystallization.

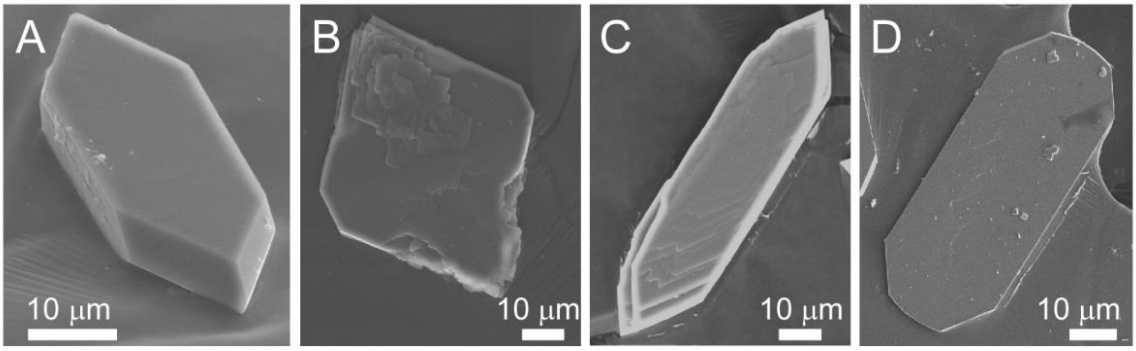

Figure 1.10 Scanning electron micrographs of COM crystals in the absence (A) and in the presence of serum albumin (B, BSA), chondroitin sulfate (C, C4S), and citrate (D).

Bulk crystallization assays revealed discrepancies with previous findings from literature regarding modifier specificity. Cook et al., reported that serum albumin preferentially interacts with the COM (010) surface by using fluorescent-labeled proteins (Cook, Grover et al., 2009) whereas a study by Sheng et al., suggested that serum albumin should bind to all COM surfaces nonspecifically. The latter study also proposed that chondroitin interacts with the (010) and {12-1} surfaces, and that transferrin binds to the (100) and {12-1} faces (Sheng, Jung et al., 2005). Our findings, however, showed the following: (1) serum albumin preferentially binds to {12-1} and {021} surfaces, which correspond to the apical tips of COM crystals; (2) chondroitin specifically binds to the (010) surface, leading to an elongated COM crystal morphology; and (3) transferrin binds to the apical tips of COM crystals, but not as effectively as serum albumin (Figure 1.10).

Modifier specificity was confirmed using a combination of atomic force microscopy (AFM) and fluorescent-labelling.

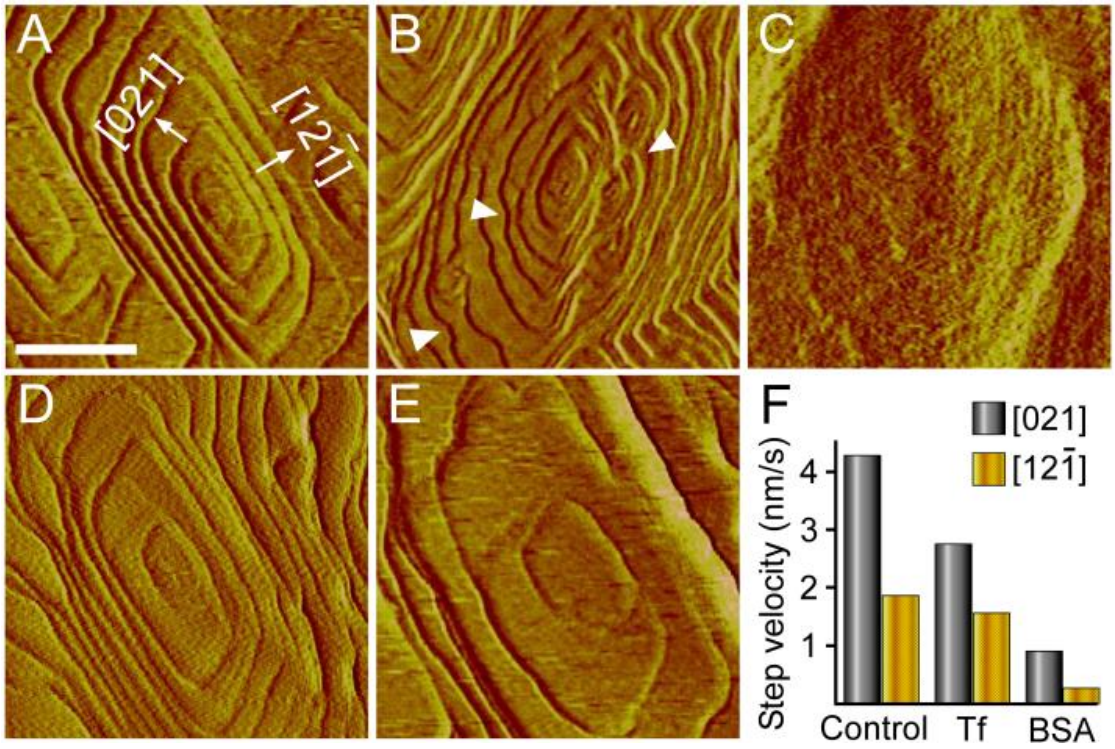

Figure 1.11 Snapshots from *in situ* AFM studies on COM (010) surface in the absence (A) and presence of C_{C4S} = 0.5 μg/mL (B), C_{C4S} = 2.5 μg/mL (C), C_{Tf} = 2.5 μg/mL (D), and C_{BSA} = 0.25 μg/mL are shown (E). Step velocities are compared (F). Scale bar equals 1 μm.

In situ AFM was used to observe the effect of chondroitin sulfate, serum albumin, and transferrin on the rate of step growth on COM (010) surfaces, which contain hillocks bounded by {12-1} and {021} steps as shown in Figure 1.11A. The findings from this study were consistent with that of bulk assay (i.e., chondroitin sulfate preferentially binds to the (010) surface). At lower concentration (Figure 1.11B), chondroitin is shown to adsorb on the terraces and impede step advancement. At higher concentration (Figure 1.11C), there is a significant inhibition in step growth rendering the steps

indistinguishable. Layer advancement in the presence of transferrin resulted in increased interstep distance in [021] directions while reducing step velocity in the same direction, whereas step propagation in the [12-1] direction was unimpeded. Serum albumin had significant impact on both directions i.e., increasing interstep distance as well as reducing step velocity, as shown in Figure 1.11F.

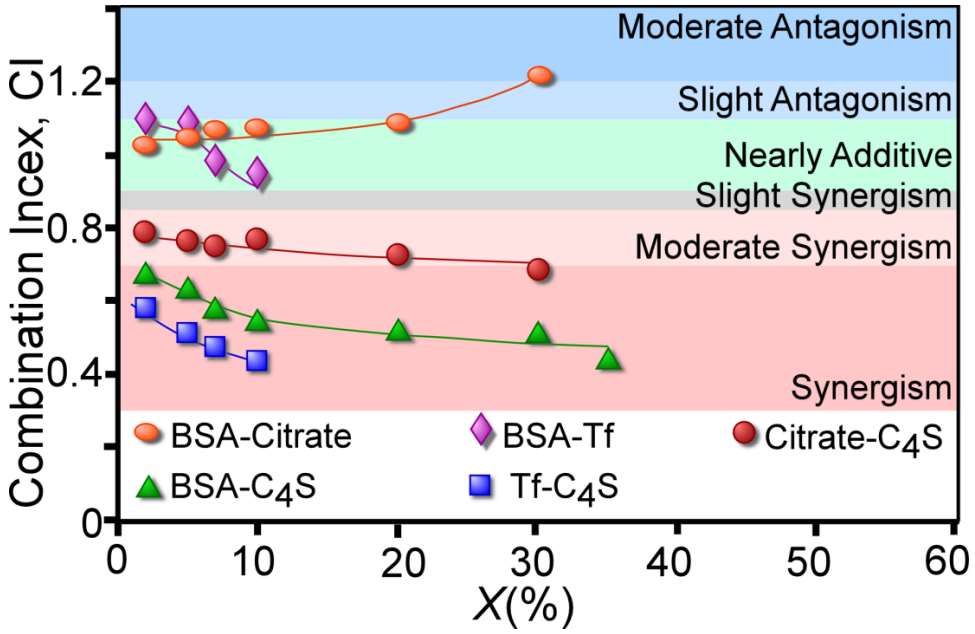

Figure 1.12 Combination index for growth modifiers used in this study is shown. This is a common method in combination drug therapy to observe whether the pair will have synergistic, antagonistic or additive effect.

The combination index (CI) was calculated by comparing the efficacy of modifiers individually and as a pair based on how much total modifier concentration was needed to reach the same efficacy as individual and binary combination,

$$CI = \frac{(D)_1}{(D_x)_1} + \frac{(D)_2}{(D_x)_2}, \tag{1.1}$$

where $(D)_i$ is the does (i.e., concentration) of species *i* in the binary mixture with percent inhibition of *x*, and $(D_x)_i$ is the concentration of species *i* used as an individual modifier to

achieve the same percent inhibition as the binary mixture. This mathematical expression facilitates the comparison of modifier combinations that exhibits synergism (CI < 1), additivity (CI = 1), or antagonism (CI > 1). Figure 1.12 shows where the pair exhibited synergism, antagonism or merely act as additives which is a method proposed by Chou to determine the effectiveness of combination drug therapy (Chou 2006). Combinations of serum albumin-chondroitin sulfate and transferrin-chondroitin sulfate showed synergistic effects, which may be attributed to their different binding affinity to COM crystals that allows each modifier to target the surface without competition. In contrast, combinations of serum albumin-citrate and serum albumin-transferrin exhibited antagonistic effects because these modifiers have the same specificity to COM crystal surface that created competition among modifiers.

The most interesting aspect of this study was the use of combination of techniques to determine the specificity of modifiers on the crystalline surface and draw kinetic data which improved our understanding of modifier-crystal interaction and the mechanism by which the modifiers inhibit crystal growth. Also, the combination study demonstrated the importance of designing site-specific modifiers and judiciously selecting modifiers as putative drugs for COM stone disease. To do so, a fundamental understanding of the interfacial phenomena is required which may be achieved by combination of techniques such as AFM and molecular modelling.

1.5.2.3 Growth Promoters of Calcium Oxalate Crystals

This study was performed in collaboration with the Karande group at Rensselaer Polytechnic Institute and was published in the Journal of the American Chemical Society (Farmanesh, Chung et al., 2014).

As mentioned in the previous sections, putative inhibitors of COM crystallization are abundant in negatively-charged moieties that enable interactions with COM crystal surfaces via calcium bridging. However, proteomic studies of organic constituents within the COM stone matrix also show the presence of positively-charged moieties in addition to negatively-charged molecules (Canales, Anderson et al., 2008). In our previous study, we selected lysozyme and lactoferrin as proteins identifies in proteomic studies that are both rich in positively-charged groups, such as lysine and arginine, and constructed a series of experiments to determine their potential impact on COM crystallization.

Kinetic studies in the presence of lysozyme and lactoferrin revealed that these proteins promote COM crystallization, as shown in Figure 1.13, whereby the relative growth rate is greater than unity. There have been several mechanisms for crystal growth promotion that postulates the following: (1) local supersaturation at the crystal interface may be increased due to attraction of solute molecules to the crystal surface via solute-promoter interaction (Fu, Qiu et al., 2005); (2) promoter-crystal interaction may perturb the hydration layer at the crystal interface and reduce the energy barrier for solute attachment (Elhadj, De Yoreo et al., 2006); and (3) the adsorbed promoter may decrease the edge energy for steps to advance (Madsen 2008).

Bulk crystallization assays reveal that lysozyme and lactoferrin increase COM crystal dimensions in *c* and *a* directions, resulting in elongated crystals as well as thicker

crystals. *In situ* atomic force microscopy studies also reveal that the advancement of steps on COM (010) surfaces is enhanced in the presence of lysozyme (Figure 1.14), which is in agreement with kinetic studies shown in Figure 1.13 as well as bulk assays where elongated crystal morphology was observed.

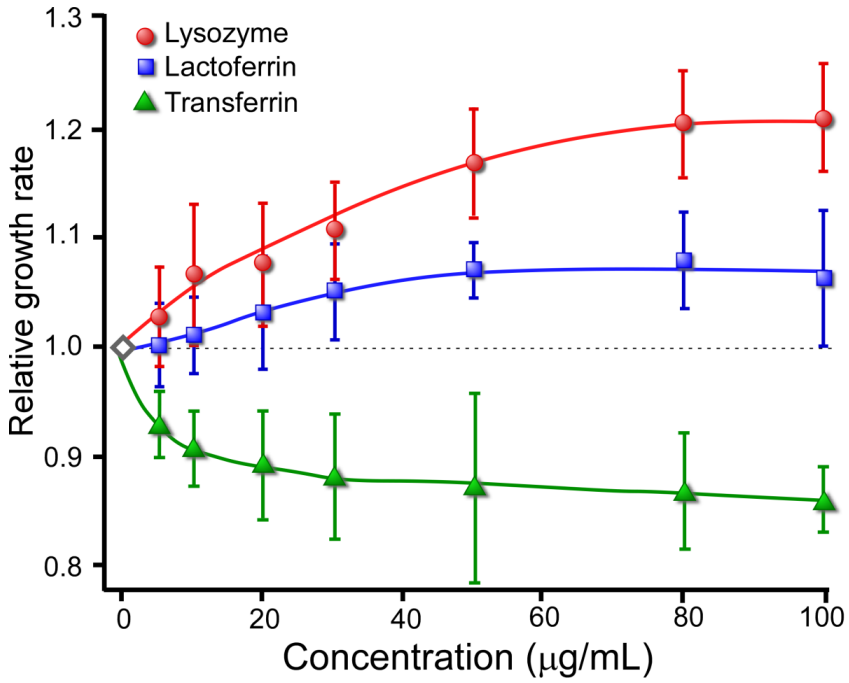

Figure 1.13 Relative growth rate ($r_{modifier}/r_{control}$) of COM crystallization in the presence of lysozyme, lactoferrin, and transferrin are shown at varying concentrations. Solid lines are extrapolated and error bars equal two standard deviations.

Lysozyme is consisted of both acidic and basic regions in its sequence and according to the proteomic studies as well as molecular modelling study, both negatively-charged and positively-charged moieties are capable of interacting with COM crystal surface. This led to exploring the role of each segment in lysozyme and determining whether the segments serve as inhibitor or promoter and correlate the result to its charge. The general trend was that the segments with many positively-charged groups and with isoelectric points greater than 7 primarily showed promotion, whereas the segments with

more negatively-charged moieties and with lower isoelectric points inhibited COM crystallization. However, the efficacy of certain segments revealed that the net charge is not the only factor governing the peptide's role. It is crucial to consider the amino acids in the sequence as well as the spatial pattern of amino acids in the sequence.

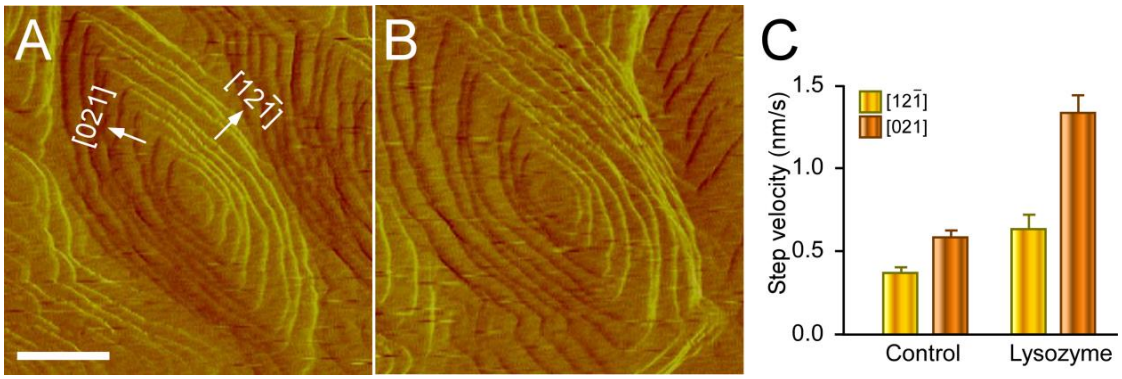

Figure 1.14 Snap shots from in situ AFM studies of COM (010) surface growth in the absence (A) and presence of $C_{lysozyme}$ = 2.5 μg/mL (B). Step velocities are compared (C). Scale bar equals 0.5 μm and error bars equal one standard deviation.

In summary, we identified two proteins that promote COM growth by accelerating the rate of layer advancement on crystal surfaces. A systematic analysis of lysozyme was performed where its entire amino acid sequence was subdivided into contiguous peptides (10−20 amino acids in length). This study revealed that the sequences responsible for growth promotion are rich in basic side chains. We observed that lysozyme is composed of subdomains that function as either promoters or inhibitors of COM growth. Peptides identified as inhibitors are located in the middle of the primary amino acid sequence, which suggests that steric restrictions may limit their interaction with COM surfaces. Conversely, it is reasonable to expect that peptide promoters (located on either terminus) exhibit fewer steric restrictions.

There are few examples of crystal growth promoters. Among those identified in the literature, a common phenomenon is that the promotion effect of the modifier is concentration dependent (i.e., modifiers promote crystallization only at low concentrations and inhibit crystallization at high concentrations). Our findings seem to suggest that lysozyme and lactoferrin operate by a different mechanism. Indeed, the characteristic ISE profile of crystal growth promoters closely resembles the Langmuir-like behavior of COM growth inhibitors. What is currently lacking from this analysis is a molecular-level description of modifier−crystal interactions that identifies the exact mechanism of COM growth promotion. Defining an inclusive set of heuristic guidelines capable of predicting the role of growth modifiers is challenging, yet general trends have been proposed to estimate modifier efficacy on the basis of its physicochemical properties.

The observation that lysozyme and lactoferrin promote COM crystallization may reflect a more universal role of these proteins in biomineralization. Results of this study are qualitatively consistent with observations that cationic proteins are observed in three types of pathological stones (kidney, pancreas, and prostate). Although it is not feasible to draw definitive conclusions of *in vivo* processes from *in vitro* assays, it can be suggested that lysozyme and lactoferrin may play an active role in stone pathogenesis. In a broader context, the pathway of crystal growth promotion may allude to a more widespread mechanism of biogenic mineral formation (e.g., bone or exoskeletal structures). From a practical standpoint, the design of growth promoters offers a potential route to reduce the time of commercial crystallization, and, in certain applications, growth promoters may prove to be useful for tailoring crystal size and/or habit. The fact

that such effects can be achieved with small peptides (i.e., constitutive segments of larger proteins) is advantageous for the design of biomimetic modifiers for applications that span pharmaceuticals to materials synthesis.

1.6 Thesis Outline

The primary objective of this thesis is to examine methods of inhibiting calcium oxalate monohydrate crystallization via the use of growth modifiers, and to determine the corresponding mechanism by which these modifiers alter the rate of crystallization. Previously, our group focused on the use of natural macromolecules, such as proteins, that function as growth modifiers; however, my thesis focuses on the use of small organic growth modifiers (OGMs) such as citrate, a known inhibitor of COM crystallization that is used as a therapeutic for calcium oxalate kidney stone disease. In order to better understand modifier-crystal interactions, we employ a combination of characterization techniques that include bulk crystallization assays, kinetics studies, and observation of surface phenomena experimentally and with theoretical calculation.

In Chapter 2, we present the experimental methods, analytical techniques, and conditions employed in studies of COM crystallization. In Chapter 3, we discuss the impact of citrate and its structural analogue, hydroxycitrate on COM crystallization and propose a new mechanism of crystal growth inhibition. We present a combination of experimental data, theoretical calculations as well as preliminary human urine studies. In Chapter 4, we explore the effects of a range of structural analogues of citrate. We report the importance of the subtle differences in the molecular structure of modifiers that influence modifier-crystal interactions. In Chapter 5, we focus on the effect of growth

solution alkalinity and speciation of polyprotic solute and growth modifiers on COM crystallization. We use a combination of experimental data and colloidal theory to refute prior findings that the pH of the growth medium does not govern COM crystallization. Lastly, in Chapter 6, we present a summary of results from this thesis and an outline for future studies which may serve as a unique platform for tailoring any crystallization process of interest as well as heuristic guidelines for modifying other crystalline materials. The literature references in this thesis are listed in alphabetical order (by first author) at the end Chapter 6. Also, supplementary information for each chapter is presented as Appendices.

Chapter 2

Experimental and Computational Methods

2.1 Calcium Oxalate Monohydrate Bulk Crystallization

Batch crystallization was carried out in a 20 mL glass vial by dissolving NaCl in deionized (DI) water, then adding 0.7 mL of 10 mM $CaCl_2$ stock solution. A clean glass slide (ca. 1.3 x 1.3 cm^2) was placed at the bottom of the vial for ease of collection of the crystals for microscopy. The sample vial was then placed in an oven set to 60°C for ca. one hour to ensure the solution reached the set point temperature for crystallization. Subsequently, 0.7 mL of 10 mL $Na_2C_2O_4$ stock solution was added to the vial dropwise while continuously stirring at a rate of ca. 400 rpm using magnetic stir bars. To investigate the effect of growth modifiers on COM crystallization, a desired quantity of the modifier was added to the growth solution prior to $Na_2C_2O_4$ addition. The amount of added water was adjusted to ensure that the final growth solution had a composition of 0.7 mM $CaCl_2$: 0.7 mM $Na_2C_2O_4$: 150 mM NaCl: x μg/mL modifier (where x = 0 – 100) and a total volume of ca. 10 mL. Similar protocol was used to study the effect of pH on COM crystallization, in which an appropriate amount of either HCl or NaOH was added to adjust the pH of the CaOx growth solution. Crystallization was performed at 60°C for 3 days at static conditions (i.e., without stirring or agitation). The glass slide (substrate) was removed from the solution, gently washed with DI water, and dried at room temperature prior to morphological analysis.

2.2 Characterization of COM Crystallization

2.2.1 Morphology Observation

The size and morphology of COM crystals prepared in the absence and presence of inhibitors was assessed by optical microscopy using a Leica DM2500-M instrument. Brightfield micrographs were obtained in reflectance mode to quantify the crystal dimensions, which we report as length *L* in the [001] direction, width *W* in the [010] direction, and the length-to-width (L/W) aspect ratio, or *AR* (Figure 2.1). A minimum of 150 crystals from three separate batches were measured to obtain an average *AR* for any study. COM crystal number density, ρ_{COM}, was measured as the number of crystals formed per area of glass slide. Number density data was obtained with an average of at least ten areas on glass slides from three separate batches (each micrograph area is 647 x 484 μm^2 for the x100 magnification setting used throughout the study) for any study.

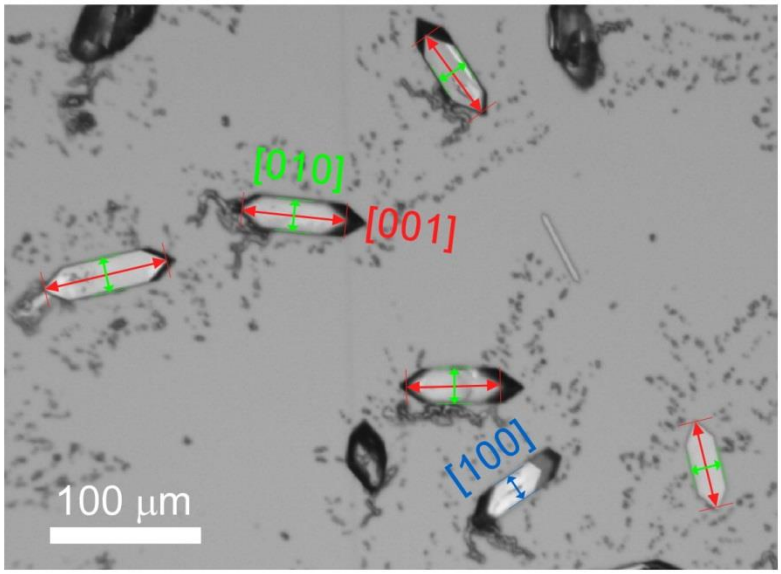

Figure 2.1 An optical micrograph of COM crystals and measurements of crystal dimensions such as aspect ratio i.e., [001]/[010] and thickness i.e., length in [100].

The COM [100] thickness was measured from a combination of optical and electron micrographs. Scanning electron microscopy (SEM) was performed using a FEI 235 Dual-Beam Focused Ion-beam instrument equipped with a SEM sample extraction probe. SEM samples were prepared by gently pressing COM crystals on the glass slide to carbon tape in order to transfer crystals to the sample disk. Each sample was coated with a layer of carbon (ca. 20 nm) to reduce the effects of electron beam charging.

2.2.2 Bulk Kinetics of COM Crystallization

The rate of COM crystallization was measured using a calcium ion selective electrode (ISE) from ThermoScientific equipped with an Orion 9720BNWP ionplus® electrode. ISE measurements track the temporal reduction in free calcium ion concentration in the growth solution during crystallization (including the effects of both nucleation and crystal growth) (Farmanesh, Chung et al., 2013). Growth solutions were prepared similar to COM bulk crystallization, but at room temperature using a solution with a composition of 0.5 mM $CaCl_2$: 0.5 mM $Na_2C_2O_4$: 150 mM NaCl: x μg/mL modifier (where x = 0 – 100) and supersaturation ratio S = 3.8. Supersaturation ratio is defined as the ratio of bulk concentration to solubility concentration ($S = \frac{C}{C_s}$) or the equilibrium concentration of solute,

$$C_s = \sqrt{K_{sp}\gamma_{Ca}^{-1}\gamma_{Ox}^{-1}}, \tag{2.1}$$

where K_{sp} is the solubility product (1.66 x 10^{-9} mol^2/L^2 at 25˚C)(Tomazic and Nancollas 1979) and γ_i is the activity coefficient where that of calcium and oxalate were calculated respectively using the Debye-Hűckel equation

$$\log \gamma = \left(\frac{-0.51\, z^2\sqrt{\mu}}{1+(\alpha\sqrt{\mu}/305)}\right), \tag{2.2}$$

where z is ion valence, μ is ionic strength ($\mu = \frac{1}{2}\sum_i c_i z_i^2$), and α is hydrated radius of ions ($\alpha_{Ca^{2+}} = 600\, pm,\ \alpha_{Ox^{2-}} = 450\, pm$).

For ISE studies, we used the calcium oxalate (CaOx) solubility product reported by Tomazic et al., (Tomazic and Nancollas 1979) in order to calculate the CaOx supersaturation. ISE measurements were performed at room temperature under constant stirring (ca. 1200 rpm) to minimize the induction time (Farmanesh, Chung et al., 2013; Farmanesh, Ramamoorthy et al., 2014). Plots of consumed calcium ion concentration as a function of time were generated for each study. A minimum of eight measurements were performed for each data point for all studies conducted. The data were normalized by subtracting the concentration of the initial time point (Figure 2.2). The approximate linear slope of these curves during the first 40 minutes of crystallization corresponds to the rate of Ca^{2+} depletion. The efficacy of growth modifiers was determined by either the percent inhibition,

$$\frac{(\frac{dC}{dt})_{control} - (\frac{dC}{dt})_{modifier}}{(\frac{dC}{dt})_{control}}\ x\ 100 = \frac{r_{control} - r_{modifier}}{r_{control}}\ x\ 100 \tag{2.3}$$

or relative growth rate (RGR)

$$\frac{r_{modifier}}{r_{control}}, \tag{2.4}$$

which was calculated by comparing the change in slope of the growth curve in the presence of modifier relative to that in the absence of modifier (i.e., the control). Prior to ISE measurements, the electrode was calibrated using a standard calcium solution (0.1 M, Orion Ion Plus), which was diluted with DI water to three concentrations: 0.1, 1.0, and

10.0 mM. The ionic strength of each solution was adjusted using a standard solution (ISA, Thermo Scientific), which was added in a 1:50 volume ratio of ISA-to-standard.

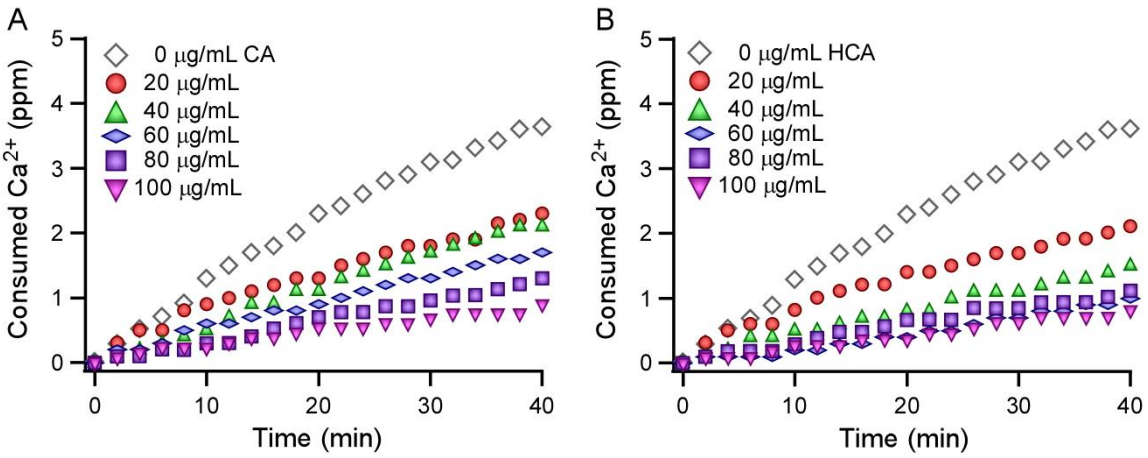

Figure 2.2 An example of in situ ISE measurements in the absence and in the presence of citrate (A) and hydroxycitrate (B) at varying concentrations. Slope of each curve represents crystal growth rate.

2.2.3 Surface Growth

In situ atomic force microscopy (AFM) was performed using a Digital Instruments Multimode III and IV (Santa Barbara, CA) to examine topographical images of COM crystals and capture the dynamics of surface growth in real time. COM crystals prepared following the method in section 2.1 (ca. 50 μm in length) were mounted on an AFM specimen disk (Ted Pella) covered with a thin layer of thermally curable epoxy (MasterBond EP21AOLV), in accordance with previously reported protocols (Farmanesh, Chung et al., 2014; Farmanesh, Ramamoorthy et al., 2014; Lupulescu and Rimer 2014). The epoxy was partially cured in an oven for ca. 20 minutes at 60°C. COM crystals on glass slides from bulk crystallization assays (in the absence of modifier) were immobilized on the partially-cured epoxy by gently pressing the glass slide to transfer crystals with either their (100) or (010) faces oriented normal to the specimen surface.

The sample was then placed in an oven at 60°C for an additional 3 hours to completely cure the epoxy. All AFM measurements were performed using silicon nitride probes with gold reflex coating and a spring constant of 0.15 N/m (Olympus, TR800PSA). *In situ* experiments were performed to monitor surface growth in supersaturated CaOx solution.

We measured the velocity of step advancement and changes in hillock morphology on COM (010) and (100) surfaces in the absence or presence of modifiers. We have adopted a method reported by Gvozdev et al., in order to quantify the step velocity from *in situ* AFM studies (Gvozdev, Petrova et al., 2004). As shown in Figure 2.3, there are two main methods to measure the step velocity. First method involves disabling the slow axis scan (i.e., y-direction) during *in situ* AFM studies, which allows a single line scan to capture the dynamic changes of steps. When slow axis scan is disabled, the image is rendered a plot of time versus the line scan. An arbitrary reference line can be drawn (Figure 2.3A) and the distances between the reference line and each step on the growth hillock can be measured at different time points.

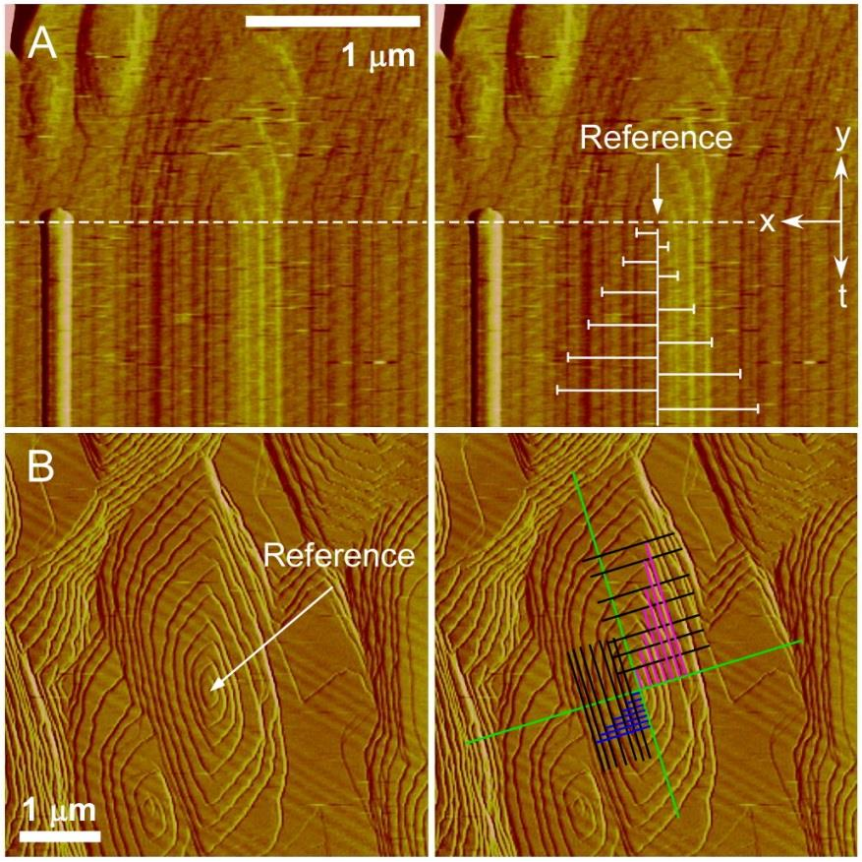

Figure 2.3 Two methods to calculate step velocity from in situ AFM studies are shown. Velocities obtained from both disabling the slow scan axis (A) and using consecutive images (B) were in good agreement.

Second method employed was a more traditional 2D imaging in contact mode to capture the growth of steps on the COM surfaces. The step velocity was obtained by measuring the distance between each step within the hillock and a preset reference line as shown in Figure 2.3B (i.e., some defect or surface feature that is consistent throughout the duration of AFM imaging). Since the AFM probe is rastered up and down the scanning area images selected for analysis should be scanned in the same direction (i.e., scanning upward or scanning downward) to avoid any distortions due to the scan direction. Velocities obtained using either method was in good agreement with one another and we opted to use the second method for all step velocity analysis. An average

of at least 5 measurements of different steps is reported. For *in situ* AFM measurements, a growth solution with supersaturation ratio S = 4.1 was prepared similar to the solution used for ISE measurements, but with a composition of 0.18 mM $CaCl_2$: 0.18 mM $Na_2C_2O_4$: x μg/mL modifier. The modifier concentration used in AFM measurements is lower than that employed in bulk crystallization (Farmanesh, Chung et al., 2014; Farmanesh, Ramamoorthy et al., 2014) owing to fewer crystals (i.e., smaller COM surface area) on the AFM specimen disk. The AFM instrument was equipped with a fluid cell (model MTFML) containing two ports for inlet and outlet flow to maintain constant supersaturation during continuous imaging. A silicon O-ring was used to ensure no liquid leakage would occur while solutions were being continuously replenished. The growth solution was delivered to the liquid cell using a dual syringe pump (CHEMYX, Fusion 200) with an in-line mixing configuration (Jung, Sheng et al., 2004) to combine $CaCl_2$ and $Na_2C_2O_4$ solutions with a combined flow rate of 0.2 mL/min.

Other research groups who also studied COM growth using *in situ* AFM, including DeYoreo, Ward and Rashkovich, have employed different flow rates according to their purpose of work. For instance, DeYoreo's group used 2 mL/min to ensure that growth was limited by surface kinetics and not by diffusion. They noted that at a given supersaturation, the rate of step advancement did not change when the flow rate was further increased (Gilmer, Ghez et al., 1971; Stephenson, Hunter et al., 2011), Ward and coworkers did not use in line flow, but replenished solutions at 5 minute intervals to maintain a relatively constant supersaturation (Guo, Ward et al., 2002). Rashkovich's group used a constant flow rate of 0.3 – 0.5 mL/min since they reported that the rate of

crystal growth and dissolution were independent of solution flow rate in this range (Gvozdev, Petrova et al., 2004; Petrova, Gvozdev et al., 2004).

The flow rate used in this study was 0.2 mL/min, which is an order of magnitude smaller than that used by DeYoreo and similar to the value used by Rashkovich. This rate was selected at a maximum value that also minimized the effects of fluid flow on the cantilever imaging of COM crystal surfaces. It is possible that due to the lower flow rate, the rate of COM crystal growth observed in this study was influenced by mass transfer limitations; however, higher flow rates sacrificed the resolution of *in situ* images.

Modifiers were introduced into the $Na_2C_2O_4$ solution at the appropriate concentration (taking into account the effect of dilution at the in-line flow connection). Continuous imaging was performed in contact mode with a scan rate of 7.0 – 9.2 Hz at 256 lines/scan.

2.2.4 Zeta Potential Measurement

Zeta potential (ζ) of COM crystals were measured using Zetasizer Nanoseries (Malvern Instruments) at room temperature. Samples were prepared by adding ca. 1 μg seed COM crystals to 10 mL of a 0.15 mM saturated calcium oxalate solution. Measurements were performed in the absence and presence of 50 μg/mL growth modifiers at pH 4 to 8 (pH 9 and 10 were not measured due to electrode stability issue in the cell). Prior to measurement, sample solutions were stirred for approximately 1 hour to allow sufficient time for modifier to interact with COM crystal surfaces. Universal 'dip' cell kit (ZEN 1002, Malvern Instruments) was submerged into 1 mL volume of each

sample solution to measure the electrophoretic mobility of COM crystals which was calculated using Smoluchowski equation.

2.3 Density Functional Theory (DFT) Calculation

This section of the work was done by our collaborator, Dr. Giannis Mpourmpakis and his student Michael G. Taylor, at the University of Pittsburgh.

Molecular orbital DFT calculations were performed using the Turbomole/6.6 program package (Ahlrichs, Bar et al., 1989). We used the BP86 functional (Perdew 1986; Becke 1988) and accounted for dispersion energy corrections through the D3 method (Grimme, Antony et al., 2010) appropriate for capturing hydrogen bonds originating by the presence of HCA and CA modifiers. The BP86 method has been shown to successfully capture the aggregation behavior of metal-cation complexed organic acids (Mpourmpakis, Caratzoulas et al., 2010). The resolution of identity (RI) (Feyereisen, Fitzgerald et al., 1993) approximation along with multipole accelerated resolution of indices (MARI-J) (Weigend and Haser 1997) were used to accelerate the calculations. We used the def2-SV(P) basis set (Weigend, Haser et al., 1998) and accounted for solvent effects through the COSMO continuum solvation model (solvent = water, ε = 78.46) (Klamt and Schuurmann 1993). The COM nanoparticle with a (100) surface termination consisted of 168 atoms ($Ca_{24}C_{48}O_{96}$), whereas the one with a (021) termination consisted of 133 atoms ($Ca_{19}C_{38}O_{76}$). The (100) and (021) surfaces were kept frozen and the modifiers were allowed to fully relax in our calculations. We also performed calculations where the surface of COM was allowed to relax and the overall adsorption trends remained the same. The isomer of HCA in *garcinia cambogia* was

taken into account, consistent with the natural extract used in human trials (Boll, Sorensen et al., 1969). The binding energy (BE) of modifiers and oxalate to crystal surfaces is defined as:

$$BE = E_{modifier+COM} - E_{modifier} - E_{COM}, \quad (2.5)$$

where E_x represents the total electronic energy of species *x*. For calculations of the "modifier+COM" species, the deprotonated forms of the acids were placed on the COM surfaces and their hydrogens (from the deprotonation) were placed at a position far away from the interaction center and anti-diametric on the COM nanoparticle to bring the system to a neutral charge state and avoid calculations under high charge states (i.e., charge counterbalance). The energy of the modifier in the gas phase, labelled as $E_{modifier}$, corresponds to molecules in their protonated (neutral) state. Analogous to the previous expression, the BE of the complexes used in determining the affinity of HCA, CA, and OX for Ca^{2+} is defined as

$$BE(complex) = E_{complex} + n\frac{d}{2}E_{H_2} - n\frac{d}{2}E_{Ca} - nE_{modifier}, \quad (2.6)$$

where *n* represents the number of organic molecules in the complex, *d* is the deprotonation state of the modifier (*i.e.*, d = 1 corresponds to single, d = 2 to double, and d = 3 to triple deprotonated states, equivalently), and E_x represents the electronic energy of species *x*. The modifier is in the protonated form in the gas phase and we use H_2 as a reference state for the hydrogen of the acids. Approximately four different initial conformations were taken into consideration for each modifier-surface and complexation calculation wherein we report the lowest energy conformations. Our obtained minima from the optimization calculations were further validated by the absence of any

imaginary frequencies on the complexes and on the modifiers interacting with COM crystal surfaces.

In order to quantify crystal lattice strain, we employ a geometric comparison between the frozen and relaxed structures of COM surfaces in the presence and absence of adsorbates (growth modifiers). We developed a distance metric to quantify the displacement of relaxed atoms (relative to their frozen state) on COM crystal surfaces by taking the average absolute value of the (x,y,z) coordinate displacements. The average displacement δ is represented as:

$$\delta = \frac{\sum_{i=1}^{n} \sqrt[2]{\left(x_{i,frozen} - x_{i,relaxed}\right)^2 + \left(y_{i,frozen} - y_{i,relaxed}\right)^2 + \left(z_{i,frozen} - z_{i,relaxed}\right)^2}}{N_{atoms}}, \qquad (2.7)$$

where N_{atoms} represents the number of atoms that are relaxed on the surface of the COM crystallographic plane.

2.4 Human Urine Studies

This section of the work was done by our collaborator, Dr. John R. Asplin and his colleague Ignacio Granja at Litholink, a LabCorp Company.

2.4.1 *In Vitro* Assays of COM Crystallization in Human Urine

The upper limit of metastability was measured using a modified version of the method described by Asplin et al., (Asplin, Parks et al., 1999). Urine aliquots were obtained over a 24-h urine collection period from eight patients with kidney stones. All urine samples were brought to a pH of 5.7 by the addition of potassium hydroxide or HCl as needed. Each urine sample was studied with no additive or with either CA or HCA added to increase their concentration by 2 mM. For each sample, 200 μl of urine was added to 12 wells of a 96-well microliter plate. Solutions of increasing concentration of

OX were pipetted into the urine aliquots in the wells. The plate was placed on a shaker for 3 h at 37°C and then the turbidity of solutions in each well were measured at 620 nm wavelength using a VMax kinetic ELISA microplate reader (Molecular Devices, Sunnyvale, CA). The well at which turbidity increased determined the point of crystallization and the OX concentration at this point is the amount of OX in the urine measured at baseline plus the amount of OX added to the urine in the well showing increased turbidity. The results are presented as the calcium oxalate concentration product (used as a surrogate of supersaturation) at the point of crystallization (see Chapter 3). In addition to their crystal inhibition activity, both CA and HCA complex calcium in solution, lowering the concentration of ionized calcium. Both mechanisms should contribute to changes in the upper limit of metastability relative to the control, indicative of an inhibition of nucleation. Each urine sample was run in duplicate and the results were averaged. Statistical comparison was performed using the non-parametric Wilcoxon test.

2.4.2 Human Trials of HCA Bioavailability

There were no prior reports of measurements of HCA in human urine in people not consuming HCA supplement. We tested the hypothesis that HCA is not a normal constituent of human urine by measuring the concentration of HCA in random urine samples from five healthy subjects (protocol number 1061857 Western Institutional Review Board).

The hypothesis of the human trial study was that HCA, when orally administered, will be excreted in urine. To test this hypothesis, we assessed urinary excretion to

confirm the bioavailability of HCA through oral administration. The protocol was approved by the University of Houston Internal Review Board (case 15176-01). Recruitment was limited to subjects between 21 and 65 years of age. Pregnant women and subjects with known severe chronic kidney disease (stage 4 or 5) were excluded. All samples were collected and analyzed with informed consent.

The supplement used in the human trial was Super CitriMax Clinical Strength Garcinia Cambogia Extract. The active ingredient, HCA, is an inhibitor of ATP citrate lyase and is presumed to reduce lipogenesis as its mechanism of action for inducing weight loss (van Loon, Van Rooijen et al., 2000). Each serving (2 capsules) contained 1.5 g garcinia cambogia extract with 900 mg active ingredient. The subjects were asked to take garcinia cambogia extract for three days at the dose recommended by the manufacturer (that is, two capsules three times a day). On the third day of garcinia cambogia treatment, the subjects collected urine for 24 h. The urine was collected unrefrigerated using an antimicrobial preservative.

HCA concentration was measured by ion chromatography using an ICS-2000 system (Dionex Corp., Sunnyvale, CA) with AS11 guard and analytic columns, potassium hydroxide eluent, and a conductivity detection system. Because isocitrate co-elutes with HCA on this system, urine samples were pre-treated with isocitrate dehydrogenase to remove isocitrate interference. Hydroxycitric acid calcium salt, (−)-(P), purchased from ChromaDex Inc. (Irvine, CA) was used as a standard.

Chapter 3

Molecular Modifiers Reveal a Strain Induced Dissolution Mechanism

The material discussed in this chapter has been published. The format of figures and tables has been modified for dissertation consistency.

Crystalline materials are crucial to the function of living organisms, in the shells of molluscs (Falini, Albeck et al., 1996; Meldrum 2003; Evans 2008), the matrix of bone (Dunlop and Fratzl 2010), the teeth of sea urchins (Killian, Metzler et al., 2009), and the exoskeletons of coccoliths (Young, Didymus et al., 1992). However, undesirable crystallization processes, such as pathological biomineralization, can be associated with human diseases (Weissbuch and Leiserowitz 2008; Rimer, An et al., 2010; Olafson, Ketchum et al., 2015). The crystal growth of biogenic, natural and synthetic materials may be regulated by the action of modifiers, which range from small ions and molecules (Davis, Dove et al., 2000; Orme, Noy et al., 2001) to large macromolecules (Graether, Kuiper et al., 2000). Modifiers adsorb on crystal surfaces and impede the addition of solute, thereby reducing the rate of growth (Weissbuch, Addadi et al., 1991; Sizemore and Doherty 2009). Complex modifier–crystal interactions in biomineralization are often not well elucidated (Dey, de With et al., 2010). Here we show that two molecular modifiers of calcium oxalate monohydrate crystallization—citrate and hydroxycitrate—exhibit a mechanism that differs from classical theory in that modifiers adsorption on crystal surfaces induces dissolution of the crystal at specific conditions rather than a reduced rate of crystal growth. This phenomenon occurs even in supersaturated solutions where modifier concentration is three orders of magnitude less than that of the solute. The results of bulk crystallization, *in situ* atomic force microscopy, and density functional

theory studies are qualitatively consistent with a hypothesis that modifier–crystal interactions impart localized strain to the crystal lattice and that oxalate and calcium ions are released into solution to alleviate this strain. Calcium oxalate monohydrate is the principal component of human kidney stones (Nancollas and Gardner 1974; Coe, Parks et al., 1992; Wesson and Ward 2007) and citrate is an often-used therapy (Phillips, Hanchanale et al., 2015) but hydroxycitrate is not. For hydroxycitrate to function as a kidney stone treatment, it must be excreted in urine. We report that hydroxycitrate ingested by non-stone-forming humans at an often-recommended dose leads to substantial urinary excretion. *In vitro* assays using human urine reveal that the molecular modifier hydroxycitrate is also as effective in inhibiting the nucleation of calcium oxalate monohydrate nucleation as citrate. Our findings support further exploration of the clinical potential of hydroxycitrate as an alternative treatment to citrate for kidney stones.

3.1 Effect of Citrate and Hydroxycitrate on COM Crystallization

Here, we examine COM crystallization in the presence of two modifiers with nearly identical structure: CA and HCA. These two molecules are tricarboxylic acids and their structures differ only by a single alcohol group, yet this subtle difference markedly alters their specificity for binding to COM crystal surfaces as discussed in the previous chapter. Figure 3.1 shows the scanning electron microscopy (SEM) images of COM crystals in the absence and in the presence of CA and HCA, respectively, and the schematic of modifier-crystal interaction is illustrated in the bottom of Figure 3.1, in which the modifiers are represented as colored circles. In the absence of modifiers, COM crystals exhibit well-defined hexagonal platelet morphology (Figure 3.1A). It is evident

that CA alters growth in the *c* direction and blunts the apical tip of COM crystals (Figure 3.1B), which is consistent with results from prior atomic force microscopy measurements where the authors showed rounding of growth hillocks on (100) surface (Qiu, Wierzbicki et al., 2004). Conversely, HCA preferentially binds to the apical tips (i.e., the {12-1} and {021} surfaces) of COM crystals and generates diamond-shaped crystals (Figure 3.1C).

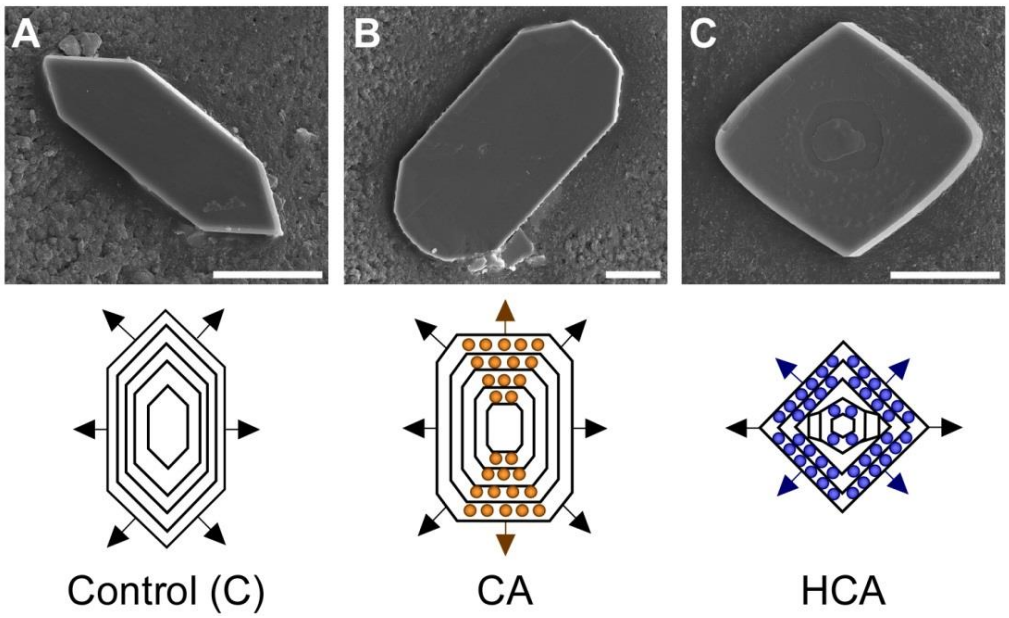

Figure 3.1 Scanning electron micrographs of COM crystals prepared in the absence (A) and in the presence of C_{CA} = 20 μg/mL (B) and C_{HCA} = 20 μg/mL (C). Schematic of modifier interaction with COM surface is shown in the bottom. Scale bar equals 20 μm.

We also report a quantitative analysis of modifier-crystal interactions by measuring the dimensional ratio of [001] to [010] (or *c/b* aspect ratio) of the resulting COM crystals as well as the thickness of the crystals i.e., [100] dimension. Figure 3.2A shows the reduction in the *c/b* aspect ratio of COM crystals with increasing modifier concentration. Figure 3.2B represents the reduction in [100] dimension of COM crystals in the presence of CA and HCA; however, interestingly both modifiers show similar

effectiveness in interacting with (100) surface in bulk crystallization. Kinetic studies using an ion selective electrode (ISE) to track the temporal depletion of free Ca^{2+} ions (Farmanesh, Ramamoorthy et al., 2014) in supersaturated calcium oxalate solution indicate that HCA is a more potent growth modifier (Figure B4.1). It should be mentioned that the third dissociation constant of CA (pKa = 6.4) is close to the nominal pH of COM growth solution in this study (pH 6.2), thus indicating a distribution of CA species with either -3 or -2 charge (Figure B4.2a). To ensure that we are comparing the effects of fully dissociated HCA and CA, we performed ISE measurements of COM growth at pH 8.0 (Figure B4.2b), well above the pKa of CA, and found that HCA is the more effective modifier, irrespective of solution alkalinity.

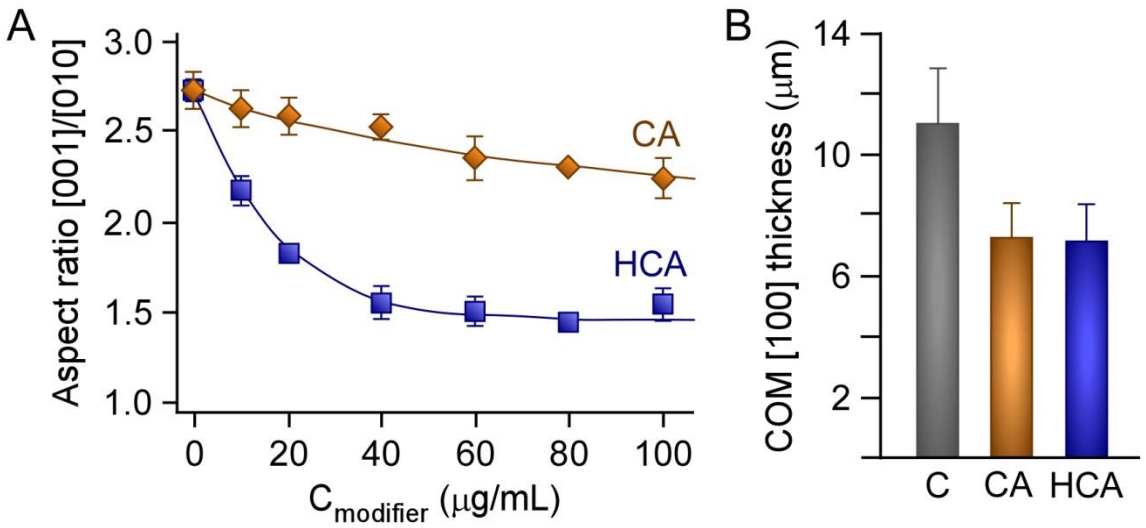

Figure 3.2 Scanning electron micrographs of COM crystals prepared in the absence (A) and in the presence of C_{CA} = 20 μg/mL (B) and C_{HCA} = 20 μg/mL (C). Schematic of modifier interaction with COM surface is shown in the bottom. Scale bar equals 20 μm.

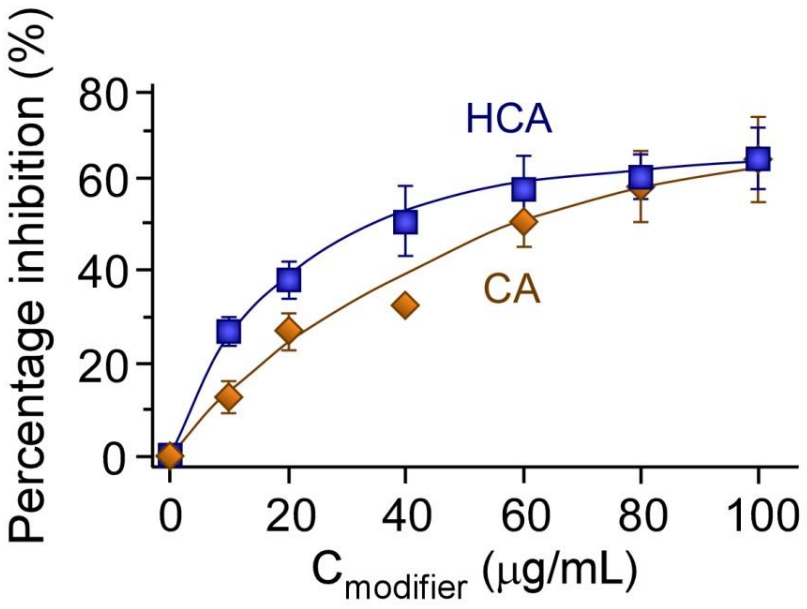

Figure 3.3 Percentage inhibition of COM crystallization in the presence of CA and HCA is shown as increasing concentration of modifiers, respectively.

Figure 3.3 shows the percentage inhibition of COM crystallization in the presence of CA and HCA as a function of increasing modifier concentration. At concentration lower than 60 μg/mL, HCA has a greater efficacy in inhibiting COM crystallization compared to CA; however, at higher concentration, i.e., $C_{modifier}$ > 60 μg/mL, both CA and HCA lead to a maximum 60% inhibition of COM crystallization. This net effect reflects the reduction in crystal growth rate as well as the potential inhibition of COM nucleation due to the nature of ISE measurement which merely detects the concentration of free calcium ion in the solution. To assess the latter, we measure the number of crystals collected on substrates per unit area, or the crystal number density ρ_{COM}. As shown in Figure 3.4, HCA and CA both inhibit COM nucleation, resulting in 62 ± 15% and 39 ± 17% reductions in ρ_{COM}, respectively.

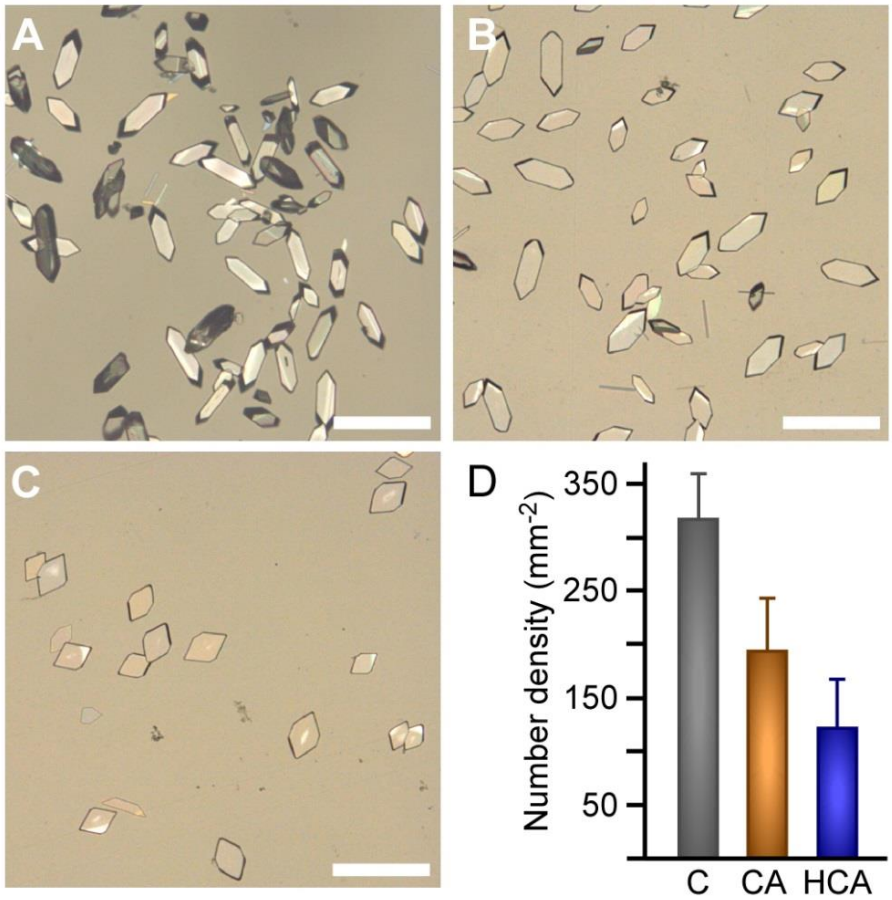

Figure 3.4 Optical micrographs of COM crystals prepared in the absence (A) and in the presence of C_{CA} = 20 μg/mL (B) and C_{HCA} = 20 μg/mL. Number density is decreased in the presence modifiers (D). Scale bars equal 100 μm.

3.2 Interesting Surface Growth Observed with Citrate and Hydroxycitrate

Modifier interactions with hillocks presented on the surfaces of COM crystals reduce the rate of step advancement. *In situ* atomic force microscopy (AFM) measurements confirm CA exhibits specificity for steps on the basal (100) surface of COM crystals that advance in the *c* direction. Time-resolved images also show that CA concentration > 1 μg/mL reduces interstep distance, decreases step velocity, and generates protrusions on steps (Figure 3.5A). Continuous imaging of COM (100) hillocks reveal that 1 μg/mL HCA reduces interstep distances near the origin of screw dislocations

(arrow in Figure 3.5B) and slows the rate of step advancement. *In situ* AFM measurements of the COM (010) surface indicate that HCA inhibits the growth of hillocks bounded by {12-1} and {021} steps leading to the disappearance of distinct step edges within minutes of introducing the modifier (Figure 3.5C). Prior *in situ* AFM studies of COM have been reported wherein macromolecular modifiers, such as proteins (Qiu, Wierzbicki et al., 2004; Wang and Nancollas 2008) and glycosaminoglycans (Farmanesh, Ramamoorthy et al., 2014), have similar effects on surface growth.

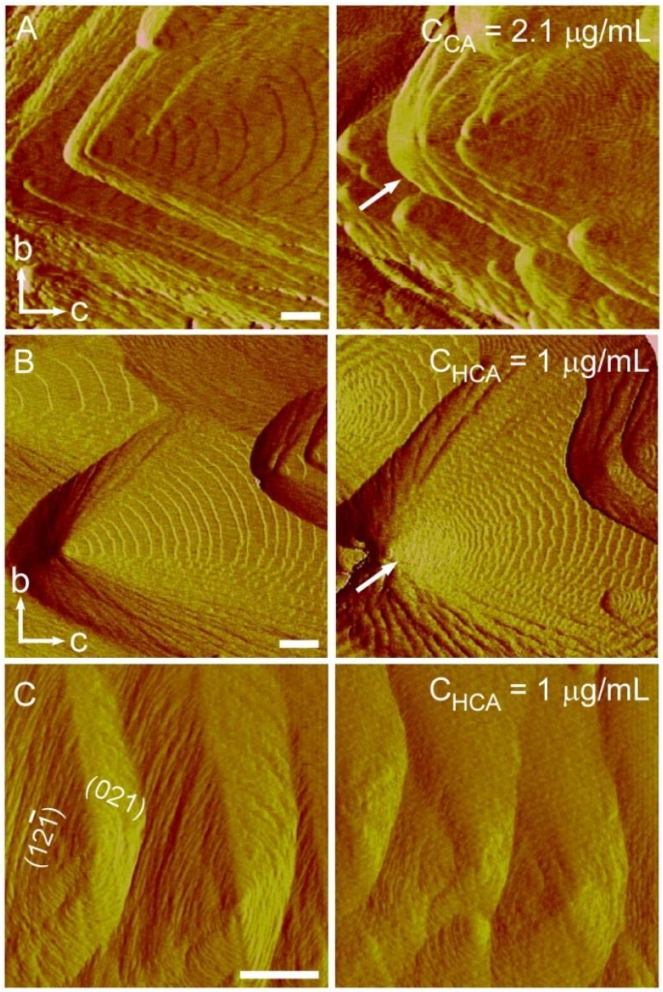

Figure 3.5 Snapshots from *in situ* AFM studies are shown for COM (100) surface in the presence of CA (A) and HCA (B) and (010) surface in the presence of HCA (C). Scale bars equal 1 μm.

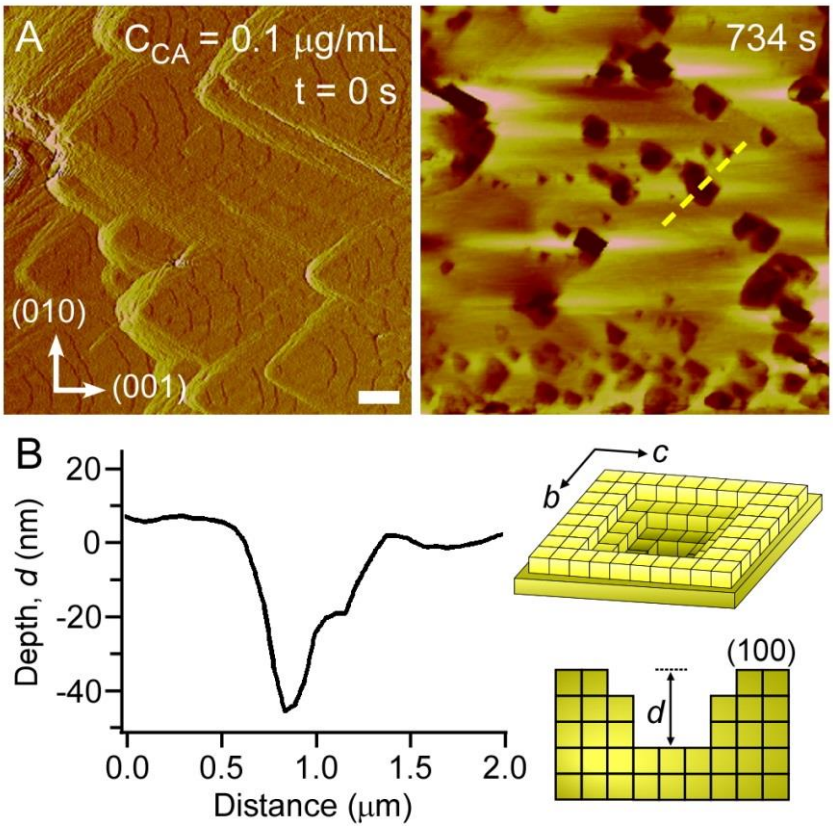

Figure 3.6 Snapshots from *in situ* AFM studies are shown for COM (100) surface in the presence of C_{CA} = 0.1 μg/mL (A, right) and depth profile of the etch pit corresponding to the yellow dashed line of the right image in A (B). Scale bar equals 1 μm.

When evaluating the lower limits of CA and HCA efficacy by AFM, a unique mode of action compared to conventional mechanisms (Chernov 1989; Weissbuch, Addadi et al., 1991; De Yoreo and Vekilov 2003) of crystal growth inhibition was noted at modifier concentrations < 0.25 μg/mL. Time-resolved images of COM (100) growth in the presence of CA reveal the appearance of etch pits (Figure 3.6A) that evolve in depth *d* with continuous imaging (Figure 3.6B). A similar phenomenon was observed on COM (100) surface in the presence of HCA. Periodic snapshots from *in situ* AFM study presented in Figure 3.7 show a hillock on the (100) surface that is initially growing in the

absence of modifier at supersaturation ratio S = 4.1, and is then subjected to the same growth solution containing HCA with a molar ratio Ca^{2+}/HCA ≈ 10^3. Etch pits immediately form once HCA is introduced into the AFM liquid cell. The etch pits appear to originate at step edges and evolve in both depth and width with imaging time (Figure B4.3). To our knowledge, this is the first observation of crystal dissolution in a highly supersaturated growth environment. This effect cannot be attributed to modifier complexation with free Ca^{2+} ions in solution, which would require comparable concentrations of modifier and solute to reduce calcium concentration below the solubility of COM crystals. Here the modifier concentration is nearly three orders of magnitude less than that of calcium, suggesting the effect is related to specific modifier-crystal interactions.

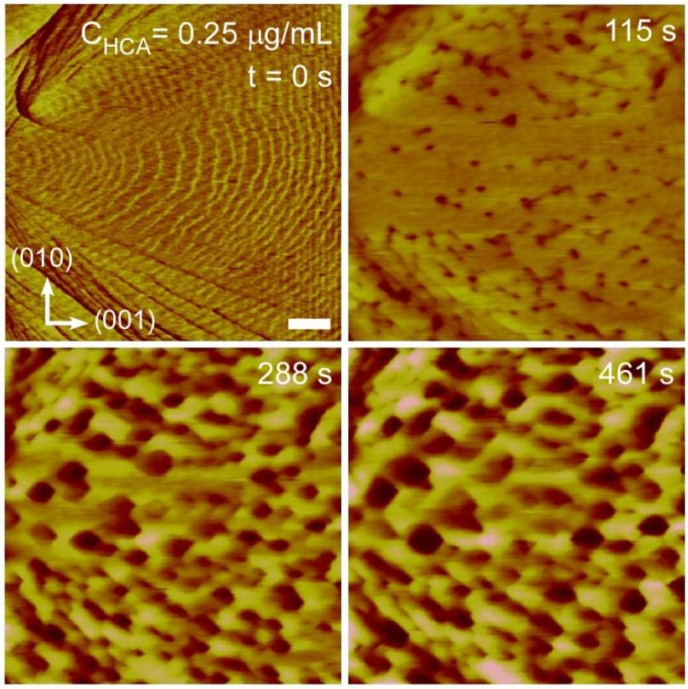

Figure 3.7 A series of snapshots from *in situ* AFM studies are shown for COM (100) surface in the presence of C_{HCA} = 0.25 μg/mL at t = 0 – 461 s. Scale bar equals 1 μm.

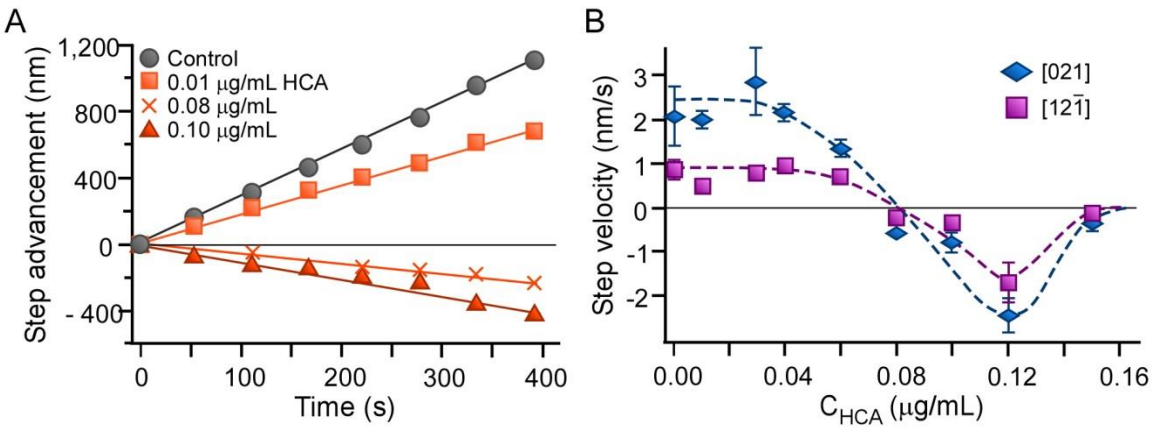

Figure 3.8 Step advancement in [12-1] direction was monitored over time at varying C_{HCA} (A) and linear regression of each curve in A was used to obtain step velocity of both [021] and [12-1] directions at varying C_{HCA} (B).

Time-resolved *in situ* AFM images of COM (010) surface growth indicate that dissolution occurs within a narrow range of HCA concentration, C_{HCA}. As shown in Figure 3.8, modifier-crystal interactions reduce step velocity in the [12-1] and [021] directions at $C_{HCA} < 0.08$ μg/mL. The velocity monotonically decreases with increasing C_{HCA} (Figure 3.8A and B) in a manner that suggests HCA preferentially binds to step sites on the COM (010) surface. Figure 3.7B shows that within the range $0.08 \leq C_{HCA} \leq 0.15$ μg/mL, step velocities become negative and layers uniformly dissolve. At $C_{HCA} > 0.15$ μg/mL we begin to observe the disappearance of distinct steps, as indicated in Figure 3.5C. Snapshots from *in situ* AFM study of COM (010) surface in the presence of $C_{HCA} = 0.10$ μg/mL show the explicit effect of HCA on [12-1] and [021] step advancement (Figure 3.8). Immediately upon introducing a supersaturated solution (S = 4.1) with $C_{HCA} = 0.10$ μg/mL into the AFM liquid cell, steps recede towards the center of the hillock and etch pits (arrows in Figure 3.9A) appear on terraces at later imaging time.

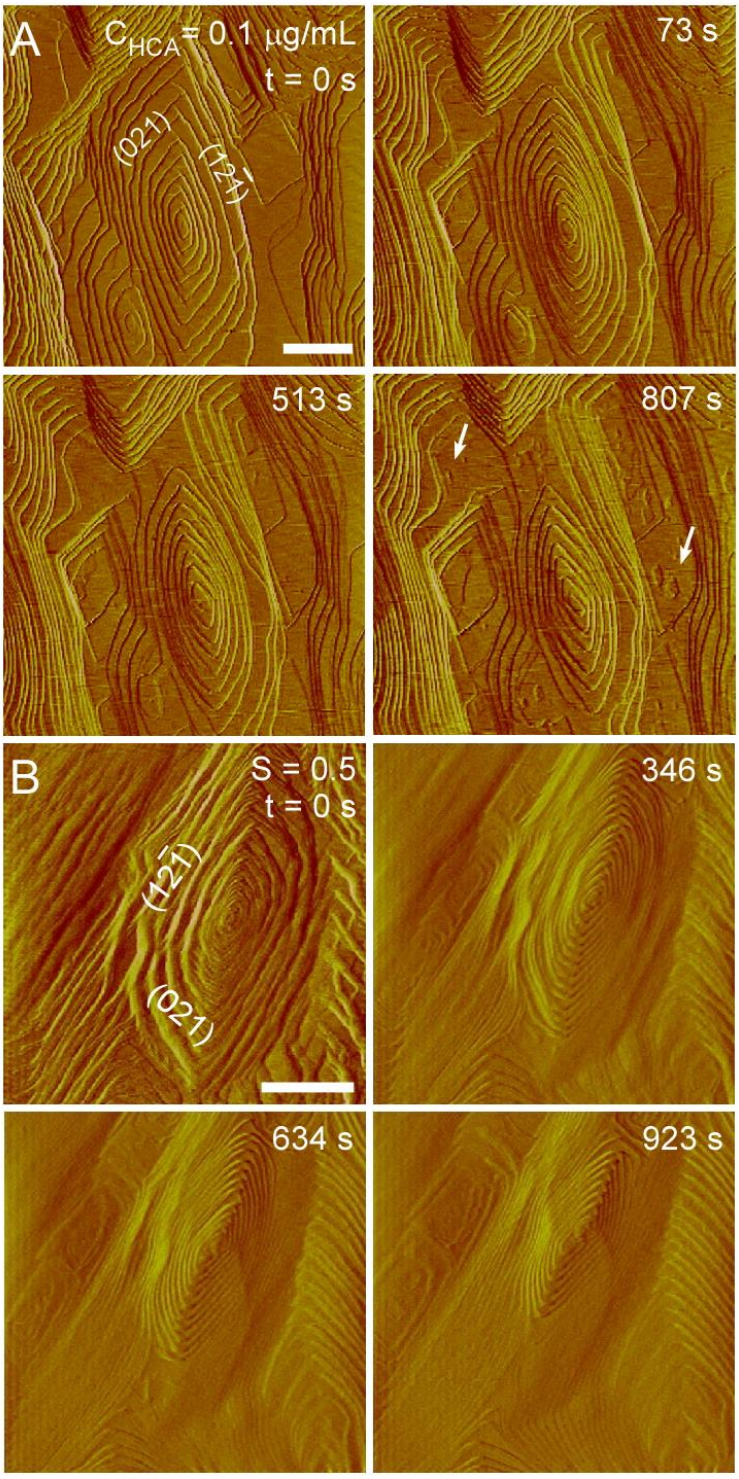

Figure 3.9 A series of snapshots from *in situ* AFM studies are shown for COM (010) surface in the presence of C_{HCA} = 0.1 μg/mL at t = 0 – 807 s (A) and in the absence of modifiers at S = 0.5 (B). Scale bar equals 1 μm.

As a means of comparison, we also assess COM (010) surface dissolution in an undersaturated solution (S = 0.5) without any modifier. Time-elapsed images in Figure 3.9B reveal negative step velocity and layers uniformly receding in a manner that is almost identical to the effect of HCA in supersaturated solution.

3.3 Proposed Mechanism: Strain-Induced Dissolution

Few studies in literature postulate that modifiers are capable of inducing crystal dissolution in supersaturated solution. Lutsko et al., (Lutsko, Gonzalez-Segredo et al., 2014) simulated the effect of occluded impurities in crystals (illustrated in Figure 3.10A) and showed that negative step velocity can be achieved when the impurity is sufficiently large and reaches a high surface coverage (i.e., small separation distances Δx between occluded impurity molecules). An alternative hypothesis for localized (or *virtual*) dissolution along step edges (Sizemore and Doherty 2009) describes the effect of imposters on spiral growth originating from screw dislocations. This mode of action leads to a reduced rate of spiral growth (illustrated in Figure 3.10B). The reduced velocity of steps on COM (010) surfaces at low modifier concentration is qualitatively consistent with this theoretical mechanism; however, the trend deviates from preexisting models at higher modifier concentration. For COM growth inhibition at this condition, we propose a new mechanism to describe the effect of CA and HCA based on changes in surface energy γ when the modifier adsorbs on COM crystal steps (Figure 3.10C) or terraces. For cases when modifier-crystal interactions are more energetically favorable than solute-crystal interactions, the adsorbed modifier imparts an interfacial strain on the crystal lattice.

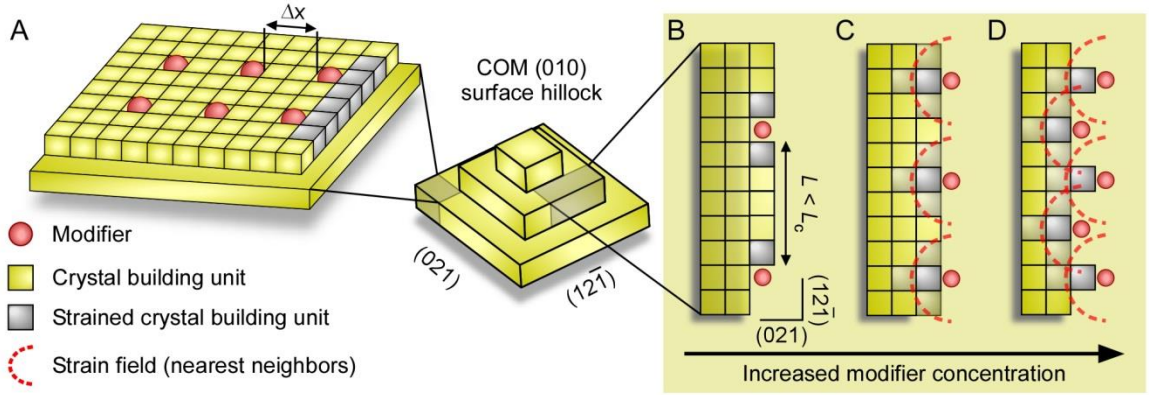

Figure 3.10 Schematic of strain imposed by modifiers incorporated within an advancing, unfinished layer as a result of step pinning (A). Step growth inhibition by kink blocking at low inhibitor concentration (B). Mechanism of strain-induced surface dissolution at moderate (C) and high (D) inhibitor concentration, respectively.

Strain fields are illustrated in Figure 3.10C and D with an arbitrary radius of curvature that includes nearest neighbor interactions between carboxylic acids of the modifier and the carboxylic acid of surface oxalates formed via a calcium bridge, $_{(modifier)}COO^{-}\ldots Ca^{2+}\ldots {}^{-}OOC_{(oxalate,\ COM)}$. We postulate that steps dissolve and release oxalate and calcium ions into solution to alleviate this strain, thus generating fresh crystal interfaces for additional modifier-crystal interactions to perpetuate dissolution, causing steps to recede toward the center of the hillock (i.e., negative step velocity). At higher modifier concentration, increased coverage of modifier on COM crystal surfaces places the adsorbed molecules in closer vicinity to each other on nearby step sites. This seemingly slows the release of solute from crystal surfaces due to mass transport limitations, or steric hindrance, wherein modifier diffusion on and/or desorption from the COM surface is rate limiting. The competing effects of modifier adsorption/desorption and solute attachment/dissolution produce corrugated steps (illustrated in Figure 3.10D),

which is consistent with AFM topographical images of COM (010) surfaces at high HCA concentration (see Figure 3.5C).

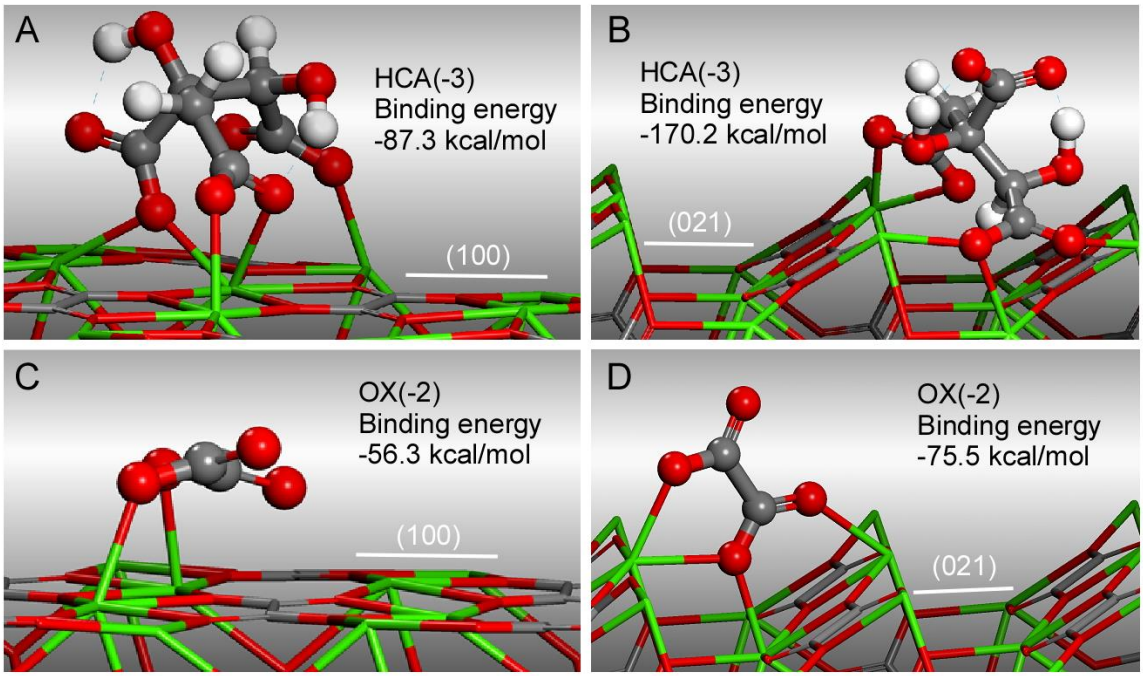

Figure 3.11 Binding energies of fully dissociated HCA on (100) surface (A) and on (021) surface (B) are shown as well as binding energies of fully dissociated oxalate on (100) surface (C) and (021) surface (D).

We used density functional theory (DFT) calculations to rationalize the observed experimental trends and shed light into the action of modifiers on COM crystal growth. The calculated HCA binding strength on COM (100) and (021) surfaces (Figure 3.11A and B) relative to that of an oxalate (OX) molecule (Figure 3.11C and D) indicates that HCA-crystal interactions are more energetically favorable. The net difference between HCA and OX binding to the COM (100) surface is –31.0 kcal/mol (BE_{HCA} = –87.3 and BE_{OX} = –56.3 kcal/mol), and the corresponding difference on the (021) surface is –94.7 kcal/mol (BE_{HCA} = –170.2 and BE_{OX} = –75.5 kcal/mol). The binding preference of HCA for the (021) surface is qualitatively consistent with experimental findings that HCA

exhibits a specificity for the apical tips of COM crystals, thus explaining its ability to reduce [021] step velocity.

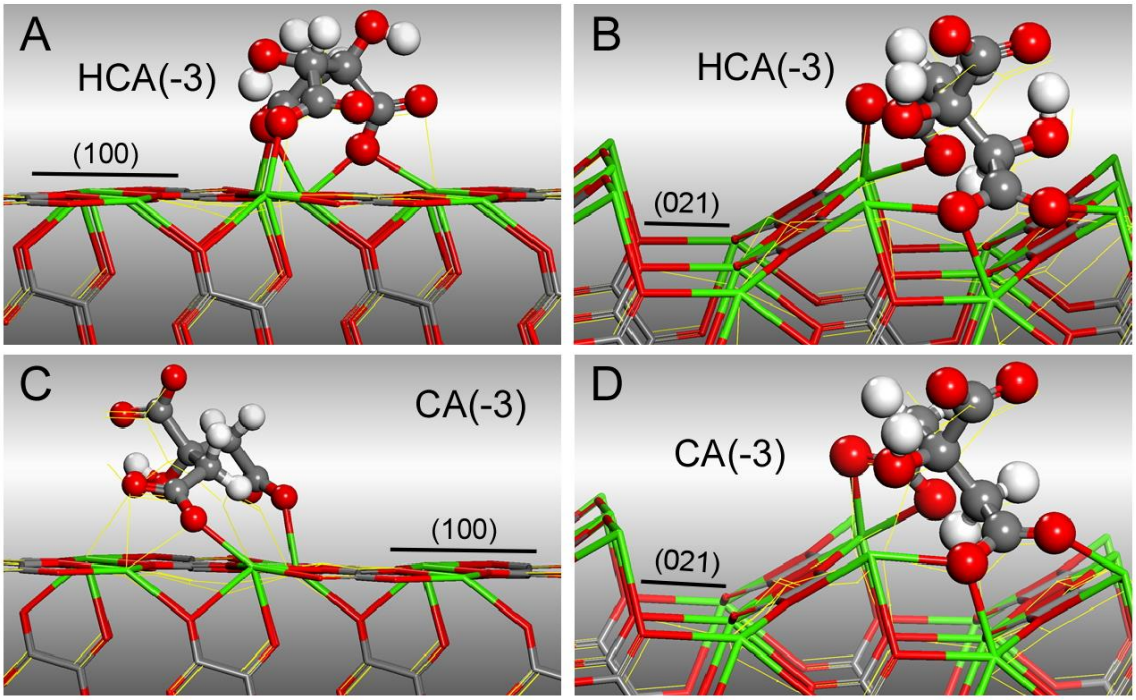

Figure 3.12 Comparison of the interaction between fully dissociated HCA and CA on frozen (colored balls and sticks) and partially relaxed (yellow sticks) COM (100) and (021) surfaces are shown.

On this basis, we expect that HCA adsorption induces higher strain on the (021) face than the (100) face. Superimposed structures of HCA and CA interacting with unrelaxed (coloured balls and sticks) and partially relaxed (yellow sticks) surfaces of COM crystals are shown as side-view snapshots depicting HCA interaction with (100) and (021) surfaces and CA interaction with (100) and (021) surfaces (Figure 3.12). Atoms are coloured as hydrogen (white), carbon (gray), oxygen (red) and calcium (green). We indeed observe that the (100) surface is practically unaffected by the presence of HCA, whereas the (021) surface shows dislocations due to strain induced by

the high binding affinity of the inhibitor. This finding is consistent with the proposed mechanism of crystal dissolution in Figure 3.10B – D where modifier-induced strain alters surface free energy γ of crystal faces in a thermodynamically unfavorable manner. The total energy of the (100) face changes by +18.8 kcal/mol owing to HCA adsorption compared to the +28.1 kcal/mol energy change of the (021) face (Note that positive signs are endothermic and energy values correspond to the difference between single point energy calculations of the COM surface with inhibitors removed). The corresponding values for the total energy change of the (100) and (021) faces from the presence of the CA are +14.2 kcal/mol and +25.7 kcal/mol, respectively.

Table 3.1 Quantification of lattice strain in the presence of CA and HCA.

	Average displacement on COM (100), δ (values in Å)	Average displacement on COM (021), δ (values in Å)
Pristine	0.17	0.38
CA (-3)	0.25	0.55
HCA (-3)	0.25	0.71

To quantify the strain of HCA and CA binding to COM surfaces, we calculated the average displacement δ of atoms in the crystal lattice (Table 3.1). Our calculations reveal that modifier adsorption on the (100) face has a marginal impact on δ; however, HCA binding to the (021) face leads to higher strain (δ = 0.71 Å) compared to CA (δ = 0.55 Å), consistent with HCA's specificity for inhibiting [021] growth. These findings seemingly agree with general observations reported by Wojciechowski and coworkers (Ristic, Sherwood et al., 1988), who showed that strain induced in ductile crystals subjected to constant tensile stress exhibit reduced rates of growth.

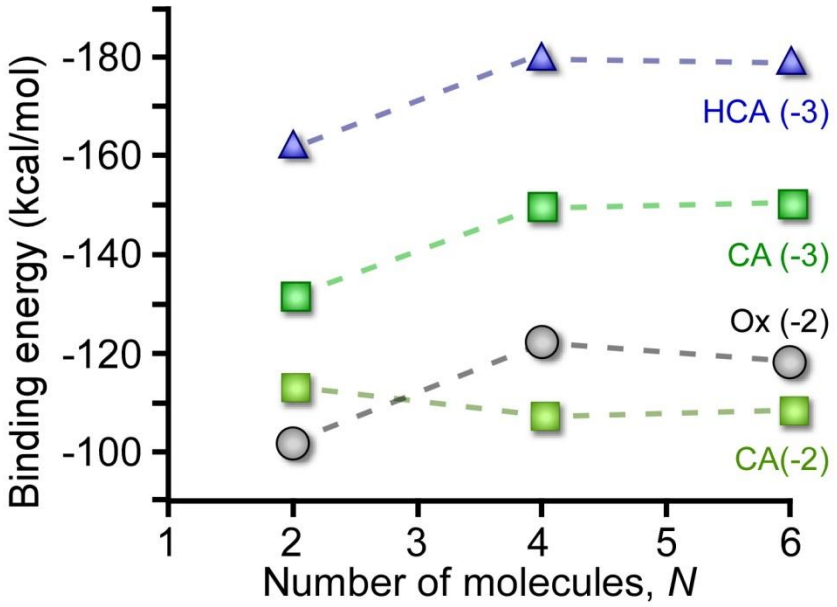

Figure 3.13 DFT-calculated binding energies for the complexation of partially dissociated CA and fully dissociated HCA, CA, and OX molecules with calcium ions are shown.

Beyond COM surface interactions, we analyzed the coordination of organic anions with Ca^{2+} ions in simulations where the number of molecules increases. Comparison of HCA, CA, and OX complexation with Ca^{2+} ions (Figure 3.12) reveals a binding energy (BE) of -174, -144, and -114 kcal/mol, respectively. The corresponding number of Ca^{2+} ions complexed per organic anion is 1.5, 1.5, and 1.0. These calculations indicate that HCA and CA display a higher affinity for Ca^{2+} ion complexation relative to OX. HCA–Ca^{2+} binding is the most energetically favorable, which is attributed to increased hydrogen bonding in the complexes, due to the presence of an additional hydroxyl group on HCA compared to CA, in conjunction with an observed molecular flexibility of HCA to fold around and protect Ca^{2+} ions (Figure 3.13B). Based on these findings, we propose that a modifier must satisfy the criterion $BE_{modifier\text{-}crystal} >> BE_{solute\text{-}}$

$_{crystal}$ (or alternatively $BE_{modifier\text{-}calcium}$ >> $BE_{solute\text{-}calcium}$) in order to induce crystal dissolution.

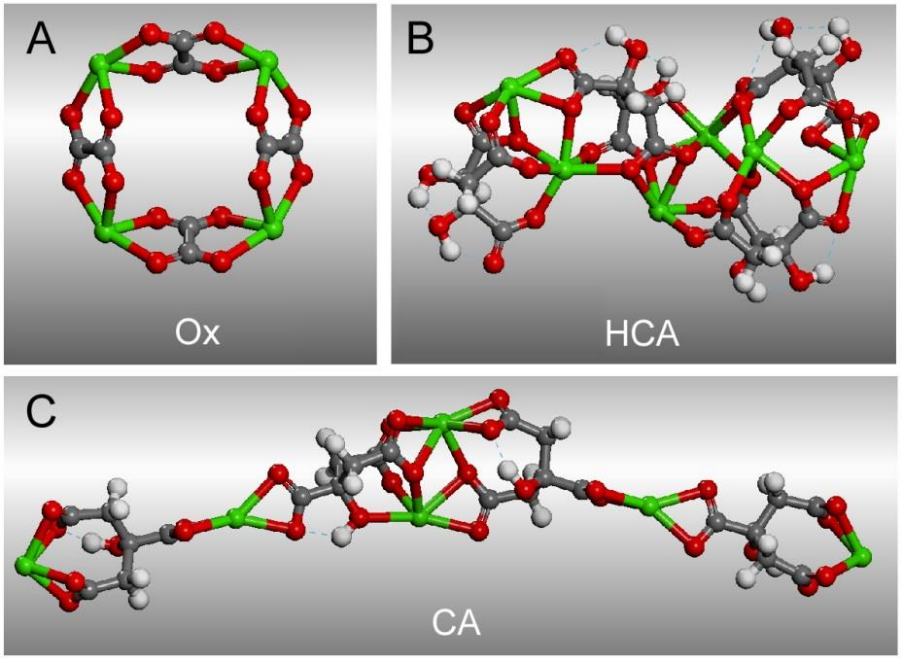

Figure 3.14 Structures of organic anion and calcium ion complexes (shown for N = 4).

3.4 *In Vitro* Assays and Urinary Excretion of Hydroxycitrate

The relevance of COM in pathological crystallization motivated a detailed study of HCA as a potential replacement for potassium citrate (KCA), a supplement that is commonly prescribed to patients with calcium oxalate kidney stone disease. CA is a normal component of human urine, and is thought to prevent kidney stone formation by complexing Ca^{2+} ions and by acting as a modifier of COM crystal growth. Treatment with alkali (most commonly citrate salts) further increases urine CA levels and has been shown to reduce calcium stones formation; however, as many as 16% of patients in treatment trials have discontinued the medication due to side effects (Ettinger, Pak et al., 1997). Moreover, the past 30 years has witnessed no significant advancement in stone

therapy, despite evidence that stone incidence rate is on the rise (Scales, Smith et al., 2012). Here, our findings suggest that HCA has the potential to be an alternative to KCA. To test the effect of modifiers on COM crystallization in a physiologically-relevant environment, we performed an *in vitro* assay (Asplin, Parks et al., 1999) to assess the effect of HCA and CA on the upper limit of metastability (ULM) in urine samples from eight patients with kidney stone disease. This standard assay is used to assess the minimum concentration of oxalate required to induce COM nucleation in the presence of modifiers. Both HCA and CA increased the ULM (Figure 3.14) compared to the untreated urine control ($p < 0.02$ for both modifiers), thus confirming their comparable inhibitory effect on crystal nucleation in the urine milieu.

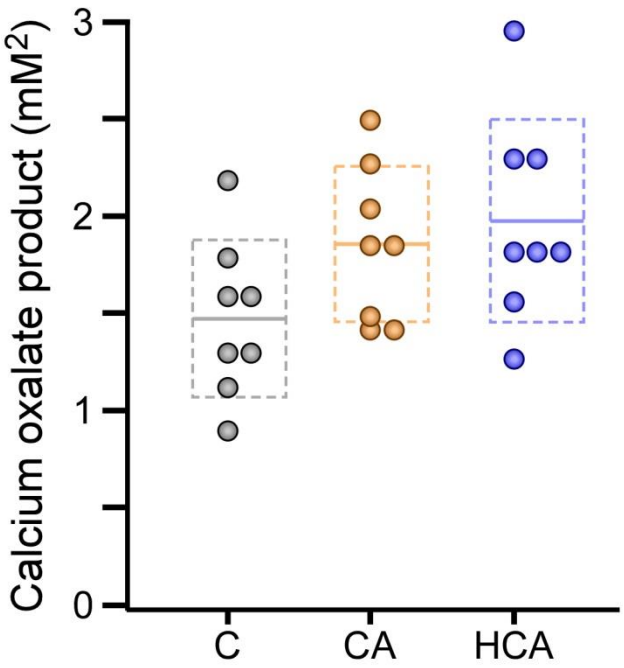

Figure 3.15 The upper limit of metastability in human urine expressed as the calcium oxalate concentration product in the presence of $C_{CA} = C_{HCA} = 2$ mM exceeds that of control (n = 8 subjects). Solid lines are average and dashed boxes extend one standard deviation above and below the average.

Moreover, we purchased clinical-grade *garcinia cambogia* extract for human trials to evaluate HCA bioavailability. In order for HCA to function as a stone treatment, it needs to be excreted in urine. HCA is not a normal component of urine, which we confirmed by measuring HCA concentration in random urine samples in five healthy subjects (three men and two women, mean age 33.4 years) not taking HCA supplement. The result of this control revealed that HCA was below the level of detection (< 0.05 mM) in all five subjects. Prior studies have documented detectable blood levels of HCA after ingestion, though only a fraction of ingested drug is absorbed (van Loon, Van Rooijen et al., 2000; Loe, Bergeron et al., 2001). The drug does not appear to be metabolized by humans, but urine excretion rates of HCA have not been reported previously.

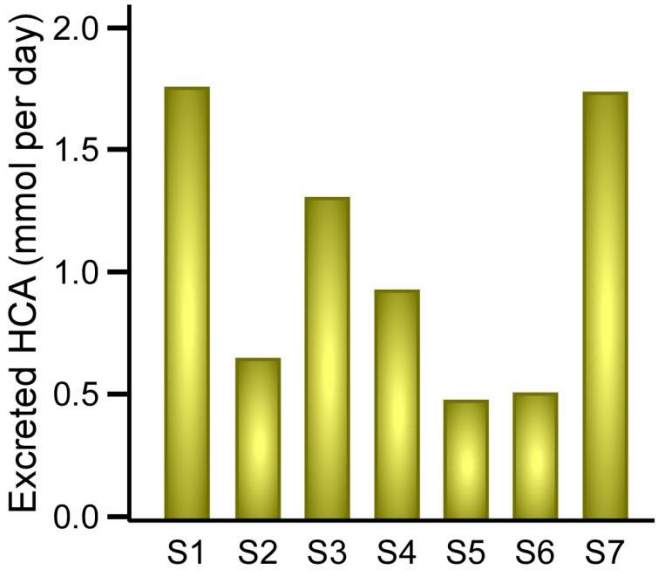

Figure 3.16 Urinary excretion of HCA from oral administration of clinical-grade garcinia cambogia extract in seven human subjects is shown. Each sample was run in duplicate (data are the averages with coefficients of variation $c_v < 1.5\%$).

To this end, we measured urinary excretion of orally ingested HCA in seven non-stone forming subjects (five men and two women with mean age 44.6 years old). The subjects took the recommended dose of the supplement, and on the third day of ingestion urine was collected for 24 hours. All subjects tolerated the short-term dosing protocol with no reported side effects. Excreted HCA was measured by ion chromatography (See Appendix C). As shown in Figure 3.15, the average HCA excretion is 1.1 ± 0.6 mmol/day (with a mean concentration of 0.7 ± 0.6 mM HCA).

3.5 Summary

To summarize, AFM measurements and DFT calculations reveal a new thermodynamic mechanism of crystal growth inhibition that deviates from classical kinetic models of modifier-crystal interactions. We show that two organic anions with high affinity for binding to COM surfaces induce localized strain on the crystal lattice. When adsorbed at moderate coverage, these modifiers cause COM crystal surfaces to dissolve in supersaturated solution. Our proposed criterion based on the relative binding energies of modifier and solute with crystal surfaces may prove to be relevant for predicting dissolution of other crystalline materials. The comparison of HCA and CA in this study also highlights the subtle nuances of rational design wherein a small difference in molecular structure (e.g., insertion of one alcohol group) can substantially alter modifier specificity and efficacy. Moreover, we report that HCA shows promise as a potential therapy to prevent kidney stones. HCA may be preferred as a therapy over KCA, such as in patients with alkaline urine where a further increase in urine pH could cause calcium phosphate stones (Parks, Worcester et al., 2004); however, better

understanding of HCA metabolism in humans, optimal dosing regimens, and long term safety and tolerability are needed before HCA could be studied in a prospective clinical trial of kidney stone prevention.

Chapter 4

Homologous Acids as Inhibitors of Calcium Oxalate Crystallization

Crystallization is a ubiquitous phenomenon with its relevance spanning from nature to industry. Understanding the fundamentals of crystallization process has been a fascinating issue for researchers for many decades. It is a vital knowledge to comprehend in order to manipulate the crystallization process and the property of crystals obtained such as size, shape, and polymorph. Likewise, in-depth researches have been performed to frustrate the crystallization process for undesirable products, most notably for pathological crystallization such as formation of kidney stones.

Various methods for modifying the crystallization have been proven effective including the use of growth modifiers also known as inhibitors, additives, and imposter, which may be utilized in various types of crystalline materials ranging from metals, organic and inorganic crystals. And depending on the material of interest, the growth modifiers used may range from proteins, peptides, and small organics to ions. These growth modifiers often exhibit specific binding affinity to crystal surfaces thereby frustrating the growth of crystals normal to the modifier-interacted plane. They may be structural analogues/derivatives of the solute molecule. One notable example of the effect of imposters was reported by Rimer et al., in which L-cystine dimethylester (L-CDME) and L-cystine methylester (L-CME) was chosen to inhibit the growth of L-cystine crystal growth. These two imposters share the same overall structure with L-cystine with only difference being the end functionality, which enables the imposters to bind to specific step sites of L-cystine crystals (i.e., L-CDME binds to (010) step and L-CME binds to

(001) terrace as well as (010) step) and block further attachment of solute and frustrating the growth. Also, growth modifiers may display stereochemical matching with crystals. Orme et al., observed the effect of D-aspartic acid (D-Asp) and L-aspartic acid (L-Asp) on (104) surface of calcite crystal growth in which the effect of D-Asp and L-Asp on acute steps of resulted in mirrored images of one another due to different binding affinity on acute steps, i.e., D-Asp showed stronger binding energy to (01-4) riser on (104) surface whereas L-Asp showed greater binding to (1-1-4) riser on (104) surface.

In the previous chapter, we discussed the effect of citric acid and hydroxycitric acid on COM crystallization in which the latter with additional hydroxyl group exhibited different interaction with COM crystal surface compared to citric acid. In this study, we performed a more systematic study to understand the effect of subtle structural differences in organic growth modifiers (OGMs) on COM crystallization.

4.1 Homologous Series of COM Growth Modifiers

The organic growth modifiers (OGMs) listed in Figure 4.1 are polyprotic acids with subtle differences in size and functional moieties. Beginning with oxalate (Ox), a principal component of COM crystals, we examined dicarboxylic acids (molecules **1 – 4**) with varying carbon chain length: malonic acid (MA), succinic acid (SA), glutaric acid (GA), and adipic acid (AA). Two OGMs (molecules **8** and **13**) were selected with additional carboxylic groups: tricarballylic acid (TCA) and butanetetracarboxylic acid (BTCA). The systematic addition of alcohols to the aforementioned OGMs increased the pool of candidates to molecules **6**, **7**, and **9 – 12** as a means of examining the impact of alcohol number and spatial positioning along the carbon backbone. Moreover, we

examined the substitution of a carboxylic acid with a methyl ester (molecule **5**), akin to previous studies of L-cystine kidney stones where chemically-modified solute molecules proved to be highly effective growth inhibitors (Rimer, An et al., 2010). Collectively, the molecules in Figure 4.1 are a homologous series of putative modifiers that allow for the most systematic assessment of relationships between the physicochemical properties of OGMs and their relative effect (i.e., efficacy and specificity) on COM crystal growth inhibition.

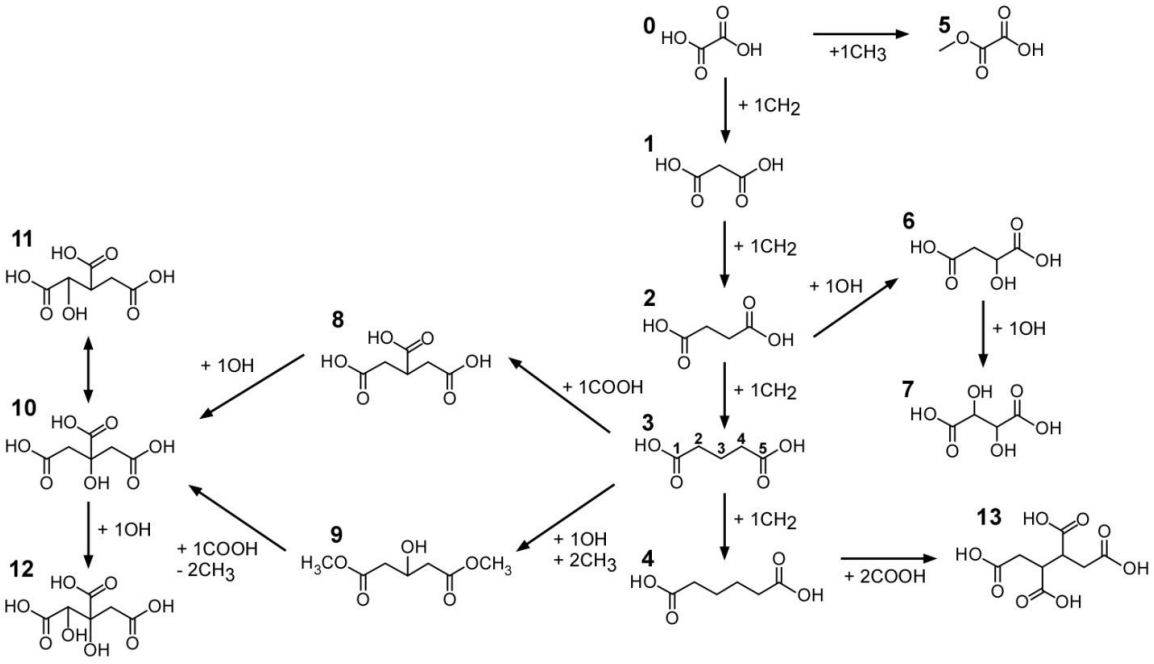

Figure 4.1 (0) oxalic acid, OA; (1) malonic acid, MA; (2) succinic acid, SA; (3) glutaric acid, GA; (4) adipic acid, AA; (5) methyl oxalic acid, MOA; (6) malic acid, MCA; (7) tartaric acid, TTA; (8) tricarballylic acid, TCA; (9) dimethyl hydroxyglutaric acid, DHGA; (10) citric acid, CA; (11) isocitric acid, ICA; (12) hydroxycitric acid, HCA; (13) butanetetracarboxylic acid, BTCA.

A metric for assessing the specificity of OGMs for binding to different COM crystal surfaces is the change in length-to-width aspect ratio of COM crystals, which is measured along crystallographic [001] and [010] directions, respectively. Using optical

microscopy, we measured the dimensions of crystals prepared in bulk with a fixed concentration (60 μg/mL) of each molecule in Figure 4.1. The average aspect ratios listed in Table 4.1 were determined from a minimum of three separate bulk crystallization batches and at least 100 crystals per batch. Growth solutions in the absence of modifier (referred to herein as the control) yield a distribution of crystals with an average aspect ratio of 2.8 ± 0.1 (a representative optical micrograph of COM crystals is provided in Figure C1 in Appendix C). OGMs that increase the aspect ratio relative to the control indicate a preferential binding to COM {010} surfaces, whereas modifiers that decrease the aspect ratio indicate a preferential binding to either the {001} surfaces or the apical tips of COM crystals (i.e., the {12-1} and/or {021} surfaces). Comparison of OGMs in Table 4.1 reveals that an increasing carbon chain length (molecules 2 – 4) leads to a progressive increase in aspect ratio, with a maximum 20% change observed for adipic acid. Averaged value of calculated calcium-to-calcium interionic distance, $d_{Ca\text{-}Ca}$, increases in order (100), $d_{Ca\text{-}Ca}$ = 4.7 Å = (12-1), $d_{Ca\text{-}Ca}$ = 4.7 Å < (021), $d_{Ca\text{-}Ca}$ = 5.5 Å < (010), $d_{Ca\text{-}Ca}$ = 5.7 Å (Figure C2 in Appendix C). This indicates that larger separation distances between the two acid groups on these OGMs promote binding to {010} surfaces of COM crystals. Also, calcium and oxalate do not orient on the same plane in the case of (12-1), (021) and (010) surface where oxalate ions are more protruding compared to calcium. This may facilitate formation of hydrogen bonding between OGMs with hydroxyl groups to the COM crystal surface.

There are only four molecules that reduced COM crystal aspect ratio within statistical certainty that follow the trend (from highest to lowest aspect ratio) **11** > **9** > **10** > **12**. These OGMs have identical carbon chain length but differ in the number and/or

position of alcohol groups along the carbon backbone. It appears as though the placement of an alcohol group at the C3 position (refer to **3** in Figure 4.1) promotes OGM binding to the apical surfaces, resulting in reduced aspect ratio. Placement of an alcohol at the C2 position is less effective, although the simultaneous placement of alcohols at both positions (i.e., hydroxycitrate, **12**) is markedly more effective, suggesting a synergistic effect that promotes OGM – COM interactions (Chung, Granja et al., 2016). In general, the addition of a carboxylic acid group enhances OGM binding to COM surfaces (e.g., comparisons of **8** to **3** and of **13** to **4**). Interestingly, direct comparison of molecules **8** and **9** suggests that the replacement of a carboxylic acid with an alcohol at the C3 position is more effective at promoting OGM – COM interaction at apical surfaces. This seemingly contradicts a prevailing belief that the placement of more acid groups on OGMs results in more effective COM growth inhibition. Previous studies of peptide growth modifiers have suggested that alcohol groups enhance modifier interactions with calcium mineral surfaces (Wang, Qiu et al., 2006). Comparison of OGMs in Figure 4.1 comprised of identical carbon chain length but different number of alcohols (i.e., molecules **2**, **6**, and **7**) indicates that the addition of alcohols in of itself is insufficient to create significant changes in efficacy. To this end, the spatial positioning of alcohols along the carbon backbone, including their relative separation distances, must be taken into consideration.

Table 4.1 Effect of OGMs on the aspect ratio of COM crystals.

	Aspect ratio †
0. Control, C	2.8 ± 0.1
1. Malonic acid, MA	2.60 ± 0.03
2. Succinic acid, SA	2.8 ± 0.2
3. Glutaric acid, GA	3.0 ± 0.1
4. Adipic acid, AA	3.3 ± 0.1
5. Methyl oxalic acid, MOA	2.5 ± 0.2
6. Malic acid, MCA	2.9 ± 0.1
7. Tartaric acid, TTA	2.7 ± 0.2
8. Tricarballylic acid, TCA	2.7 ± 0.1
9. Dimethyl hydroxyglutaric acid, DHGA	2.5 ± 0.1
10. Citric acid, CA	2.4 ± 0.1
11. Isocitric acid, ICA	2.58 ± 0.07
12. Hydroxycitric acid, HCA	1.49 ± 0.08
13. Butanetetracarboxylic acid, BTCA	2.61 ± 0.04

† Aspect ratio of COM crystals (i.e., [001]/[010]) in the absence and in the presence of OGMs are compared to assess the specificity of each OGMs. Data are the average of at least three separate batches of crystals. A concentration of 60 μg/mL is used for all modifiers.

Scanning electron micrographs of COM crystals (Figure 4.2) reveal distinct changes in bulk morphology among three OGMs that differ only by slight variations in their alcohol number and/or position: citrate (CA, Figure 4.2B), isocitrate (ICA, Figure 4.2C), and hydroxycitrate (HCA, Figure 4.2D). It has been reported that CA binds to COM {001} surfaces and blunts the apical tips (Shirane and Kagawa 1993; Qiu, Wierzbicki et al., 2004). We recently showed that HCA binds to both {12-1} and {021} surfaces to generate diamond-shaped crystals (Chung, Granja et al., 2016). The effect of

ICA on COM crystal morphology is unique in that the general shape of the hexagonal platelet is preserved, while the [100] thickness of crystals (Figure C3 in Appendix C) is reduced and there is a decrease in the surface area of apical tips that are clearly visible on micrographs of control crystals (e.g., the (12-1) surface labelled in Figure 4.2A). Visual inspection of electron micrographs suggests that ICA exhibits a different mode of binding to COM crystals than either CA or HCA. This point will be discussed in greater detail in the following section.

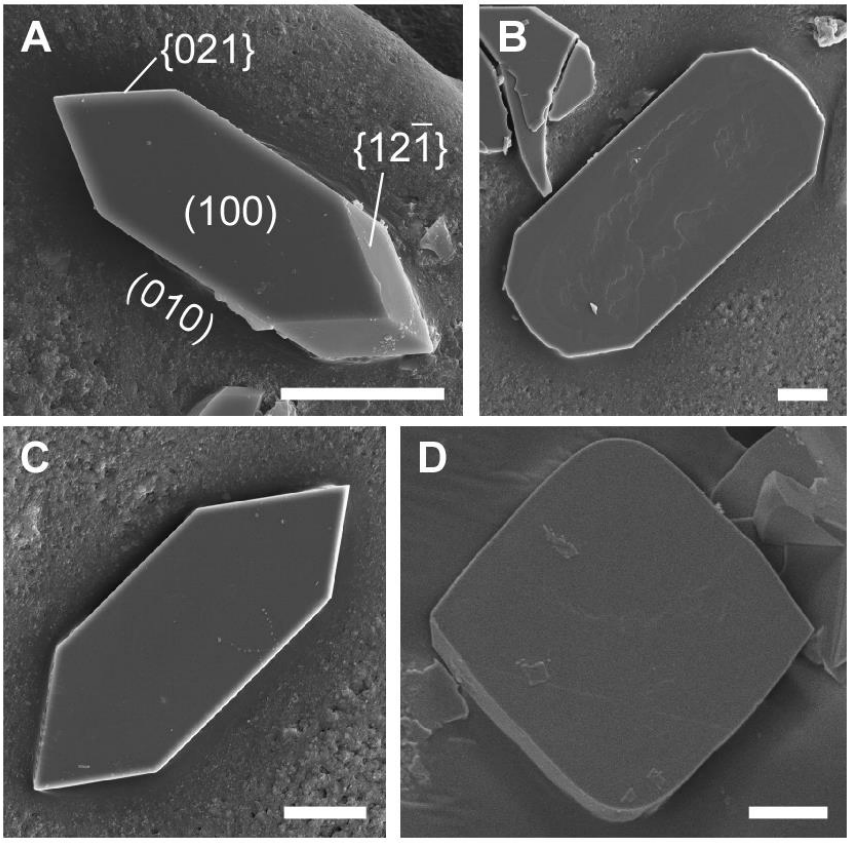

Figure 4.2 Scanning electron micrographs of COM crystals in the absence (A) and in the presence of C_{CA} = 60 μg/mL (B), C_{ICA} = 60 μg/mL (C), and C_{HCA} = 60 μg/mL (D). Scale bars equal 20 μm.

We performed kinetic measurements of COM crystallization in the presence of OGMs according to a previously reported protocol (Farmanesh, Chung et al., 2013; Farmanesh, Chung et al., 2014; Farmanesh, Ramamoorthy et al., 2014; Farmanesh, Alamani et al., 2015; Chung, Granja et al., 2016) using an ion-selective electrode for calcium to track the temporal depletion of solute. Here, we report the relative growth rate (RGR) as a quantitative determinant of modifier efficacy wherein RGR equals the ratio of COM crystal growth rate in the presence of 60 μg/mL OGM to that (under the same conditions) in the absence of OGM. For reference we use the value of CA (i.e., the current therapy administered to COM kidney stone patients) as a benchmark for OGM efficacy. RGR measurements of each OGM are compared in Figure 4.3 with a grey box highlighting the confidence intervals of RGR for CA. The latter results in a RGR of 0.6 (i.e., 40% reduction in the rate of COM crystallization). Any OGM that falls within the grey box has comparable efficacy as CA, whereas those with lower or higher RGR are more or less effective, respectively, than the benchmark. We have previously shown that HCA is a more effective inhibitor of COM growth than CA (Chung, Granja et al., 2016). Here, we find that ICA's inhibitory effect on COM crystallization is nearly identical to that of CA. Two additional modifiers, TTA and BTCA, are moderately effective OGMs, but are less potent than CA. All remaining OGMs with RGR $\geq$ 0.8 have a marginal impact on COM crystallization.

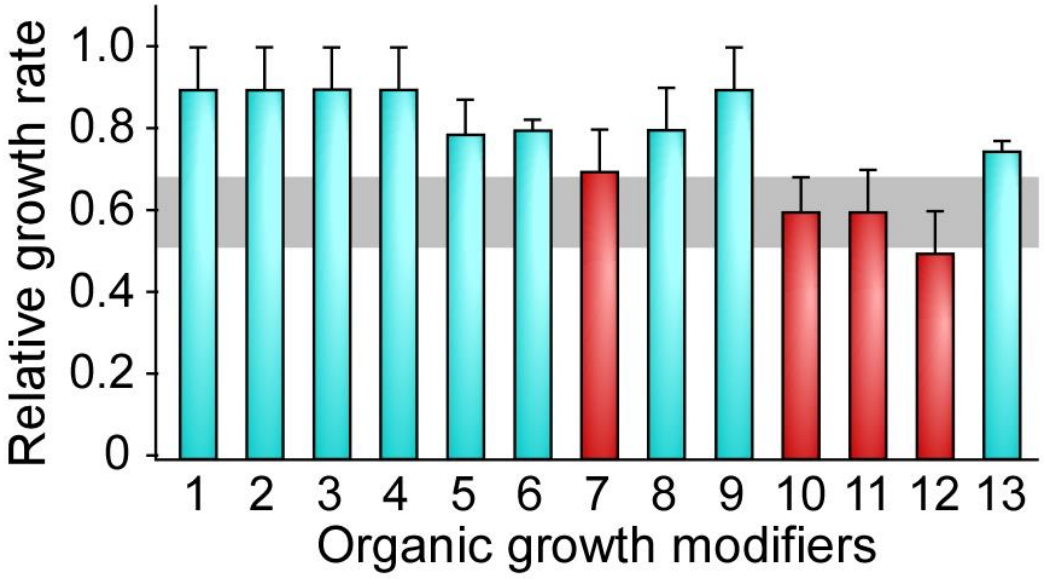

Figure 4.3 The relative growth rate (RGR) was determined by comparing the COM crystallization rate in the presence of C_{OGM} = 60 μg/mL OGM to those in the absence of an OGM. Error bars equal one standard deviation.

There are several trends in RGR that are observed in Figure 4.3. The addition of carboxylic acids to the carbon backbone increases OGM efficacy. There is a slight reduction in RGR between GA (0.9 ± 0.1) and TCA (0.8 ± 0.1) with the insertion of one COOH group. Similarly, the RGR of AA (0.9 ± 0.1) is reduced by nearly 20% with the addition of two COOH groups (i.e., 0.75 ± 0.02 for BTCA). The addition of alcohol groups has a similar impact on OGM efficacy. For instance, a comparison of OGMs with similar carbon chain length reveals a decrease in RGR from molecules with zero to two OH groups as SA (0.9 ± 0.1) > MCA (0.80 ± 0.02) > TTA (0.7 ± 0.1). Likewise, we observe a decrease in RGR for citrate analogues with an increasing number of alcohol groups: TCA (0.8 ± 0.1) > CA (0.60 ± 0.08) ≈ ICA (0.6 ± 0.1) > HCA (0.5 ± 0.1). It is noteworthy that CA and ICA, two modifiers with different modes of binding to COM crystal surfaces, have equivalent efficacy. An additional observation is the impact of

replacing a single carboxylic acid group of oxalate with an ester group (MOA, molecule **5**). Kinetic studies in Figure 4.3 reveal a RGR value (0.79 ± 0.08) that is slightly outside the range of citrate, indicating MOA is less effective of an inhibitor than the benchmark. Interestingly, MOA does have an appreciable effect on the aspect ratio of COM crystals, as shown in Table 4.1, suggesting MOA interacts with the crystal surface(s), but not to an extent that these interactions markedly reduce the overall rate of COM crystallization.

4.2 Inhibitory Mechanisms of Citrate Analogues

Here we provide a molecular description of the interactions between similar modifiers – CA, ICA, and HCA – and COM crystal surfaces using a combination of *in situ* atomic force microscopy (AFM) and density functional theory (DFT). On the basis of modifier-crystal specificity identified in bulk crystallization studies (Figure 4.2 A – D), we selected the COM (100) crystal surface for *in situ* AFM measurements because step advancement on this interface (Figure 4.4) is influenced by all three OGMs. We observe the following trend in growth inhibition: HCA > CA > ICA. Our previous study (Chung, Granja et al., 2016) showed that both HCA and CA are capable of dissolving COM crystals within a specific range of modifier concentration. In Figure 4.4 we compare the effects of OGMs at a single concentration where HCA dissolves the surface (i.e., negative step advancement), CA effectively halts growth, and ICA reduces the rate of step advancement relative to the control. An analysis of the [001] step velocity over a range of ICA concentration (Figure 4.5) reveals that ICA causes a monotonic reduction in step growth, but does not dissolve COM crystals. This finding starkly contrasts that of CA, which induces COM crystal surface dissolution at higher CA concentration. The disparity

in behavior of these two isomers, including their preferential binding to different crystal surfaces, highlights the subtle nuances of modifier performance (i.e., efficacy and specificity) as inhibitors of COM crystallization.

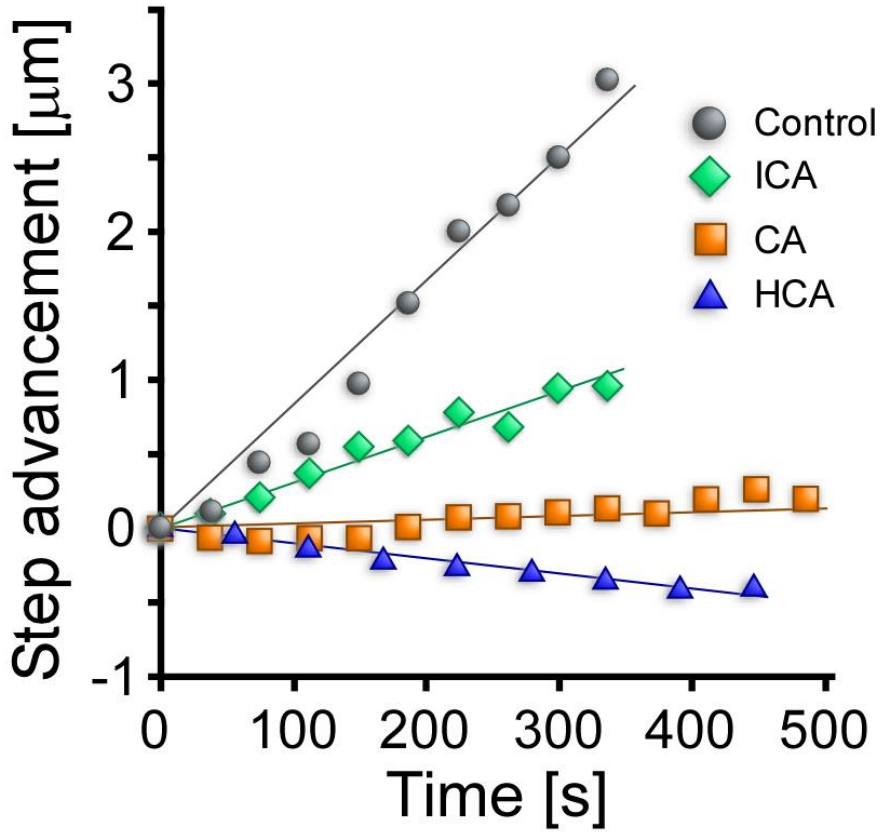

Figure 4.4 *In situ* AFM measurements of step advancement in the c-direction as a function of time in the absence of modifier (grey circles) and with 0.2 μg/mL of ICA (green diamonds), CA (orange squares), and HCA (blue triangles).

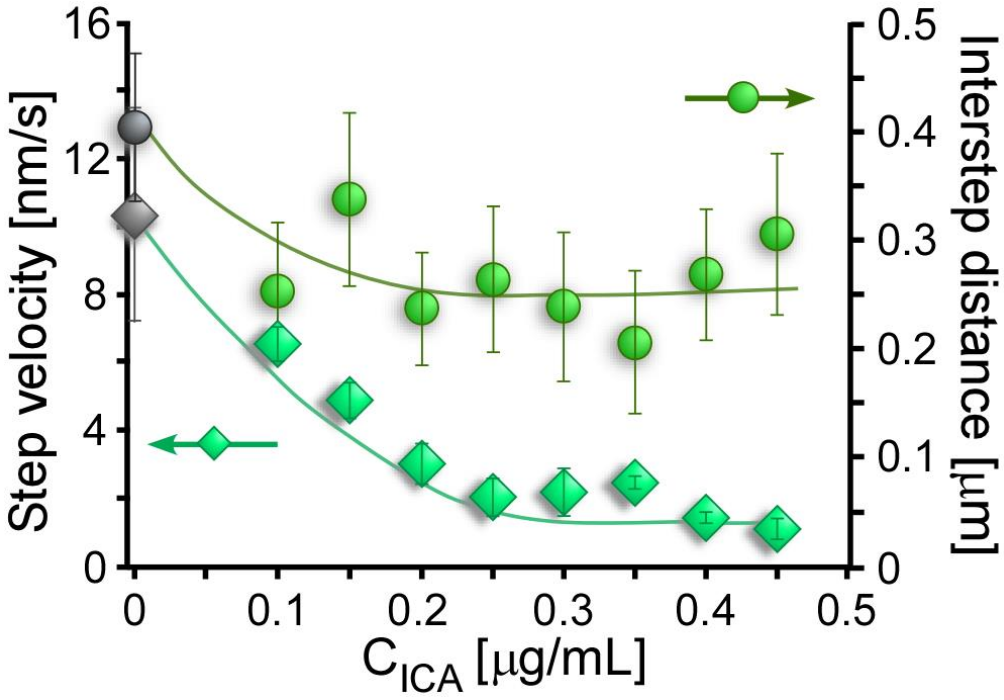

Figure 4.5 Measurements of step velocity (left y-axis) and interstep distance (right y-axis) in the [001] direction as a function of ICA concentration. Symbols are the average of at least five measurements and error bars equal two standard deviations.

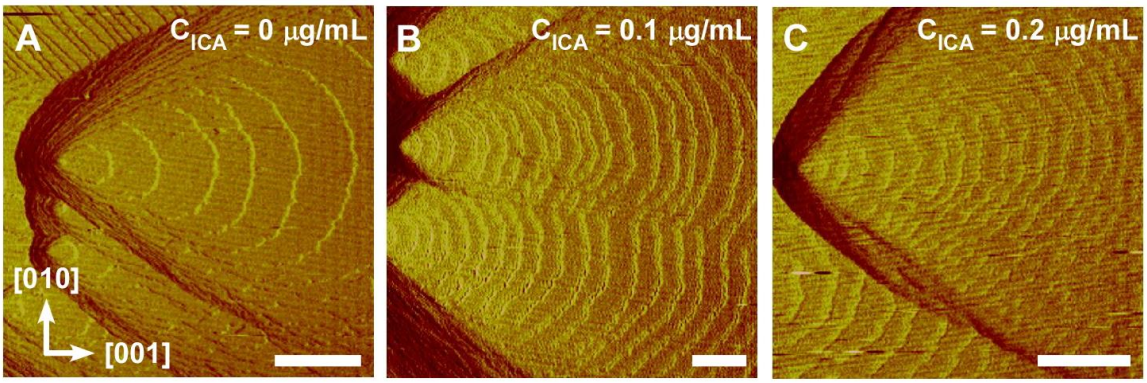

Figure 4.6 Deflection images of a COM (100) crystal surface growing at the following ICA concentrations: (A) 0 μg/mL (control), (B) 0.1 μg/mL, and (C) 0.2 μg/mL. ICA-COM interactions reduce interstep distance and roughen step edges. Scale bars equal 1 μm.

Figure 4.6 shows representative *in situ* AFM snapshots of a COM (100) face wherein triangular hillocks emanating from a dislocation advance across the surface in the c-direction (i.e., spiral dislocation growth mechanism). Time elapsed images of COM crystal surfaces permit the near molecular level assessment of step advancement in the absence (Figure 4.6A) and in the presence of ICA (Figure 4.6 B and C). The interstep distance *h* decreases monotonically with increased ICA concentration (right y-aixs in Figure 4.5). At intermediate ICA concentration, the reduced distance between steps is clearly evident in AFM images (Figure 4.6B). At even higher concentration of ICA (Figure 4.6C), step edges become more jagged (or nonuniform) owing to a mechanism known as step pinning (Cabrera and Vermileya 1958) wherein ICA adsorbs on (100) terraces and impedes the advancement of steps across the surface. There is a well-known theoretical model of spiral growth (Winn and Doherty 2000; Lovette, Browning et al., 2008; Snyder and Doherty 2009) that predicts the rate of crystal growth normal to the surface of imaging, which in this case is referred to the growth in the [100] direction (i.e., the principal determinant of bulk crystal thickness). The normal growth rate equation is

$$G_{[hkl]} = \frac{v \cdot h}{y} = \frac{h}{\tau}, \tag{4.1}$$

where $G_{[hkl]}$ is the rate of crystal growth normal to the (hkl) surface, *h* is the height of steps advancing along the (hkl) plane, *y* is the interstep distance, *v* is the velocity of step advancement, and τ ($= y/v$) is the characteristic time of layers propagating from the screw dislocation. As observed in Figure 4.5, there is a concomitant reduction in step velocity and interstep distance, whereas the average height of the layers is reduced ca. 20% at all ICA concentration. Calculation of τ reveals a reduction in $G_{[100]}$ is primarily due to

increased rotation time of spiral steps (See Figure C3 in Appendix C) and also the decrease in $G_{[100]}$ coincides well with our observation of reduced thickness in COM crystals prepared in the presence of ICA (Figure C4 in Appendix C).

4.3 Density Functional Theory Calculation

We used density functional theory (DFT) calculations to quantify the complexation energy between OGMs and calcium ion (See Figure 4.7) as well as the binding strength of OX, CA, ICA, and HCA on COM (100) and (021) surfaces (Figure 4.8). Complexation energies of HCA-Ca^{2+} is greater than that of other OGMs mostly likely due to the molecular flexibility it exhibits when interacting with calcium ions as shown in previous chapter. CA-Ca^{2+} and ICA-Ca^{2+} show almost identical complexation energy with calcium which is expected since they are isomers and exhibit similar interaction mode with calcium ion, that is neither CA nor ICA display molecular flexibility.

As shown in the previous chapter, HCA exhibits strong binding to both (100) and (021) surface compared to OX with the net difference –31.0 kcal/mol and –94.7 kcal/mol, respectively. Interestingly, CA and ICA also show slightly less but comparable binding energy on (100) and (021) surface. For instance, the net difference in binding energy between CA and OX is –24.2 kcal/mol (BE_{CA} = –80.5 and BE_{OX} = –56.3 kcal/mol), and the corresponding difference on the (021) surface is –65.1 kcal/mol (BE_{CA} = –140.6 and BE_{OX} = –75.5 kcal/mol). Moreover, the net difference in binding energy between ICA and OX on (100) face is even greater than that of HCA and OX, i.e., –38.5 kcal/mol (BE_{ICA} = –94.8 and BE_{OX} = –56.3 kcal/mol), and the corresponding difference on the

(021) surface is less than that of HCA and OX but greater than that of CA and OX, i.e., –77.1 kcal/mol (BE_{ICA} = –152.6 and BE_{OX} = –75.5 kcal/mol).

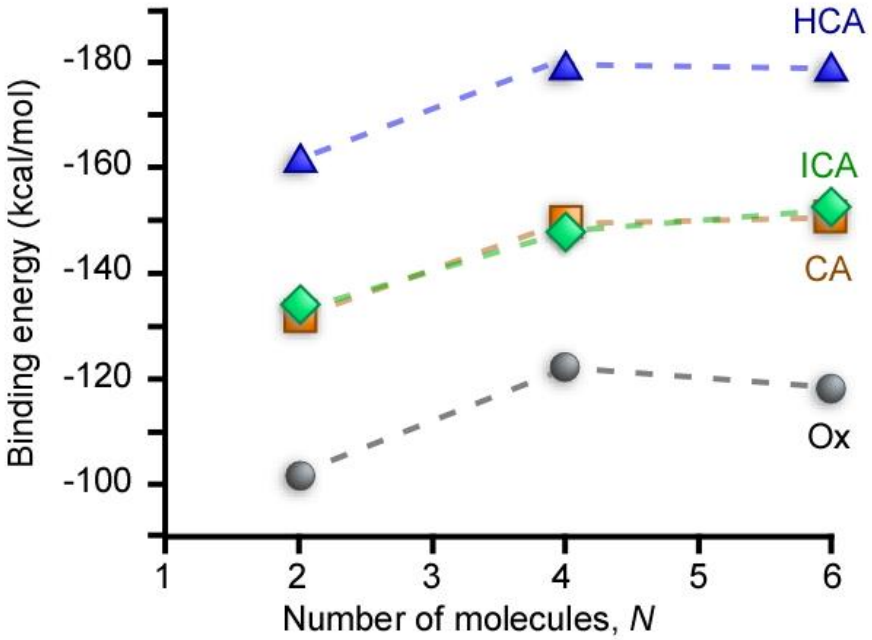

Figure 4.7 DFT-calculated complexation energy of fully dissociated HCA, CA, ICA, and OX molecules with calcium ions are shown.

In order to quantify the change in total energy of surface upon adsorption of modifiers, we compared the surface energy of relaxed crystal surface in the absence and in the presence of fully dissociated modifiers using the following equation:

$$dE_{surf} = dE_{OGM-COMrelaxed} - dE_{COMrelaxed}. \quad (4.2)$$

Adsorption of OGMs on (100) surface imposes strain on crystal lattice in an unfavourable manner which translates to endothermic energy value (i.e., positive values indicate endothermic and energy values correspond to the difference between single point energy calculations of the COM surface without OGMs or pristine) as shown in Table C2 in Appendix C. Absolute magnitude of binding energy to (100) surface decreases in the order of ICA > HCA > CA; however, the change in the total energy of surface upon

adsorption OGMs decreases in the order of HCA > CA > ICA. In the case of (021) surface, the absolute magnitude of binding energy to surface decreases in the order of HCA > ICA > CA and the same trend holds for the change in the total energy of surface upon adsorption OGMs.

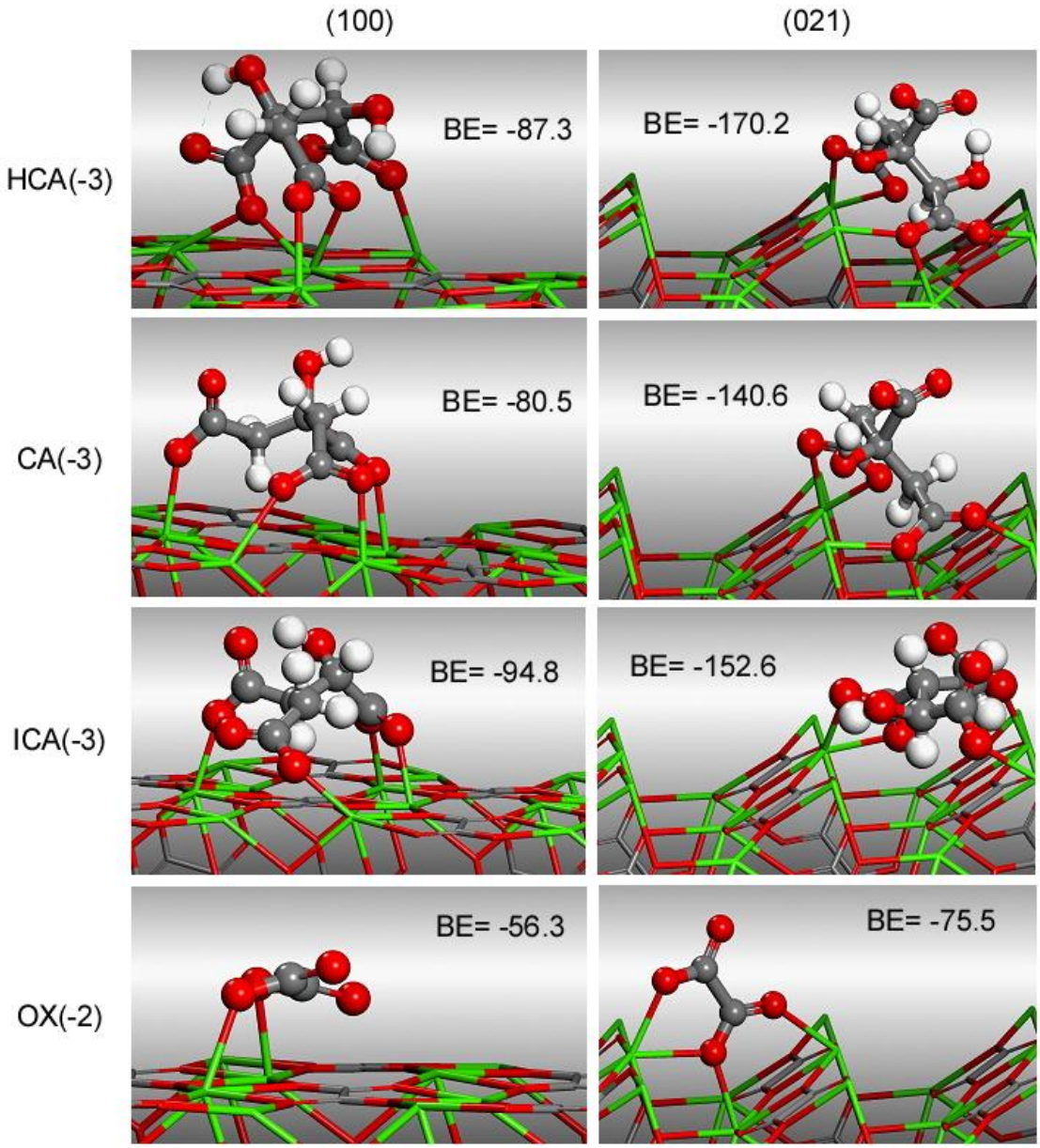

Figure 4.8 Binding energy (BE) of fully dissociated HCA(-3), CA(-3), ICA(-3), and OX(-2) on COM (100) and (021) surface are shown, respectively. BE are presented in units of kcal/mol.

Table 4.2 Denstiy functional theory calculation of binding energy and displacement of lattice.

	$\mathbf{BE_{(021)}/BE_{(100)}}$	$\mathbf{\delta_{(021)}/\delta_{(100)}}$	$\mathbf{\Phi_{(100)}}$	$\mathbf{\Phi_{(021)}}$
HCA(-3) – OX	1.95	2.84	148º	46º
CA(-3) – OX	1.82	2.20	173º	49º
ICA(-3) – OX	1.61	2.04	175º	53º
Pristine OX	1.34	2.24	121º	49º

Here, we quantified crystal lattice strain by employing a geometric comparison between the frozen and relaxed structures of COM surfaces in the absence and the presence of OGMs. We quantified the displacement of relaxed atoms (relative to their frozen state) on COM crystal surfaces by taking the average of the absolute values of the (x,y,z) coordinate displacements wherein the average displacement δ is represented as:

$$\delta = \frac{\sum_{i=1}^{N_{atoms}} \sqrt{(x_{i,frozen} - x_{i,relaxed})^2 + (y_{i,frozen} - y_{i,relaxed})^2 + (z_{i,frozen} - z_{i,relaxed})^2}}{N_{atoms}}. \quad (4.3)$$

We also vectorized the displacement of crystal lattice in the presence of OGMs as depicted in Figure 4.9 where $\omega = \upsilon \times \nu$, χ is the sum of all displacement vectors, $\Phi = \cos^{-1} \frac{\chi \times \omega}{|\chi||\omega|}$ where $\Phi > 90^o$ indicates that the crystal lattice is being pushed down towards crystals and $\Phi < 90^o$ indicates that the crystal lattice is being pull away from the crystal. As listed in Table C3 in Appendix C, all three OGMs imposed similar magnitude of surface displacement, δ, on (100) surface; however, the angle, Φ, to which the displacement occurred was different and adsorption of all OGMs resulted in the crystal lattice to be 'pushed down'. Interestingly, adsorption of HCA on (100) surface exhibited more comparable lattice displacement trajectory than that of CA and ICA and both

isomers acted in a similar manner. Unlike (100) surface, the adsorption of OGMs on (021) surface decreases in the order of HCA > CA > ICA; however, the degree of Φ were comparable and adsorption of all OGMs resulted in the crystal lattice to be 'pulled up' away from the crystal.

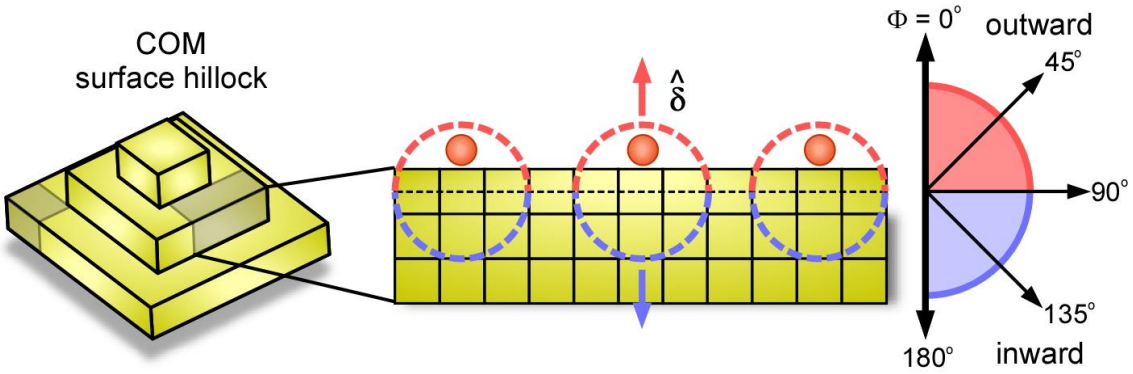

Figure 4.9 Schematic depicting the vectorization of strain $\hat{\delta}$ upon adsorption of modifiers to COM crystal surfaces. Dashed lines are strain fields induced by modifiers pulling calcium/oxalate away from the surface (red) or into the surface (blue) at an angle Φ relative to the crystal plane.

It is worth mentioning that while the binding energy ICA to both (100) and (021) crystal surfaces was greater than that of CA, adsorption of ICA induced less surface energy difference as well as lattice displacement compared to CA. This may be due to the positioning of hydroxyl group in their structure i.e., hydroxyl group in ICA is positioned in C2 whereas that in CA is positioned in C3, and their direction relative to crystal surface. If the hydroxyl group in ICA is facing towards COM crystals, it may enhance the binding energy through additional H-bond interaction. Also, if the hydroxyl group in CA is positioned away from the surface, even though it may not exhibit stronger binding with crystal surface, it may interact with water molecule via H-bonding and exhibit greater lattice displacement.

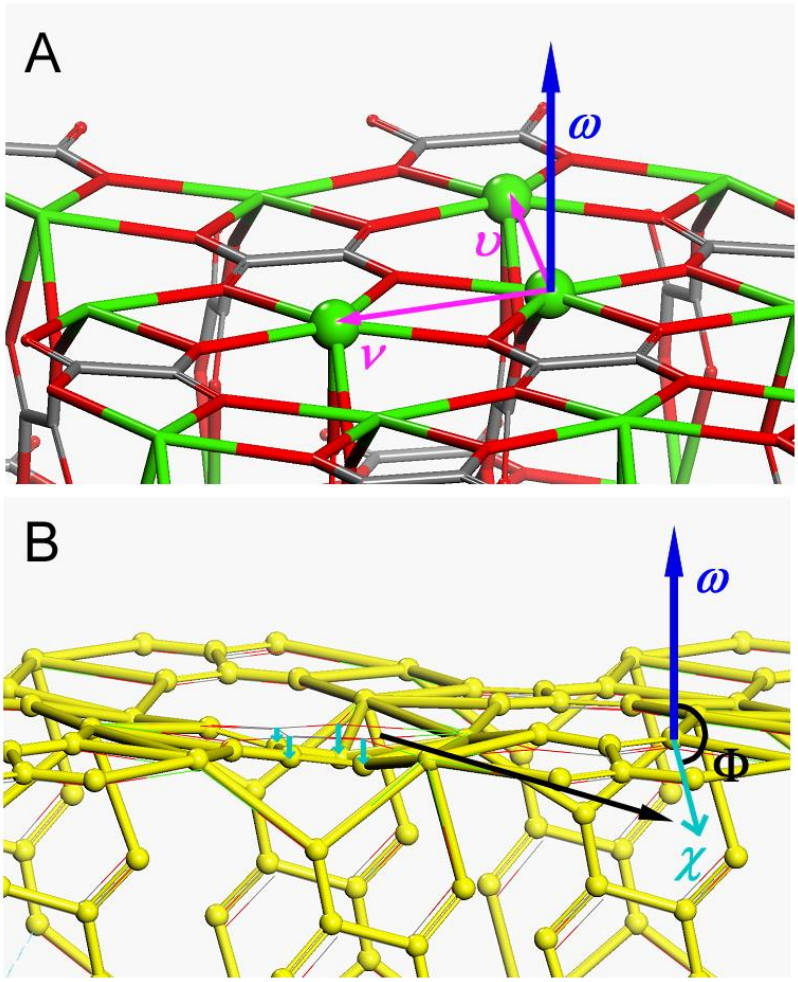

Figure 4.10 Schematic depiction of vectorizing the surface displacement in shown.

4.4 COM Crystallization in Human Urine

COM crystal growth inhibition study was performed in human urine. Eight different urine samples with low citrate level were selected to minimize the inherent effect of natural citrate present in urine. Each urine samples were used to monitor the efficacy of three OGMs, CA, ICA, and HCA and each experiment was compared to its own control urine medium (i.e., no OGM) due to the unique urine chemistry. Figure 4.11 shows a representative curve of the COM crystal growth in the absence and in the presence of OGMs at the concentration of 2 mM. It is clear that HCA is significantly

more effective in inhibiting COM crystal growth. Numerical comparison of the efficacy was performed by calculating the growth rate constants for each experiment for OGMs and directly comparing them to their respective control experiment. Growth rate in the presence of HCA and CA is merely 6% and 40%, respectively, of that in the absence of OGMs (See Table 4.3). P-values were calculated with non-parametric Wilcoxin test.

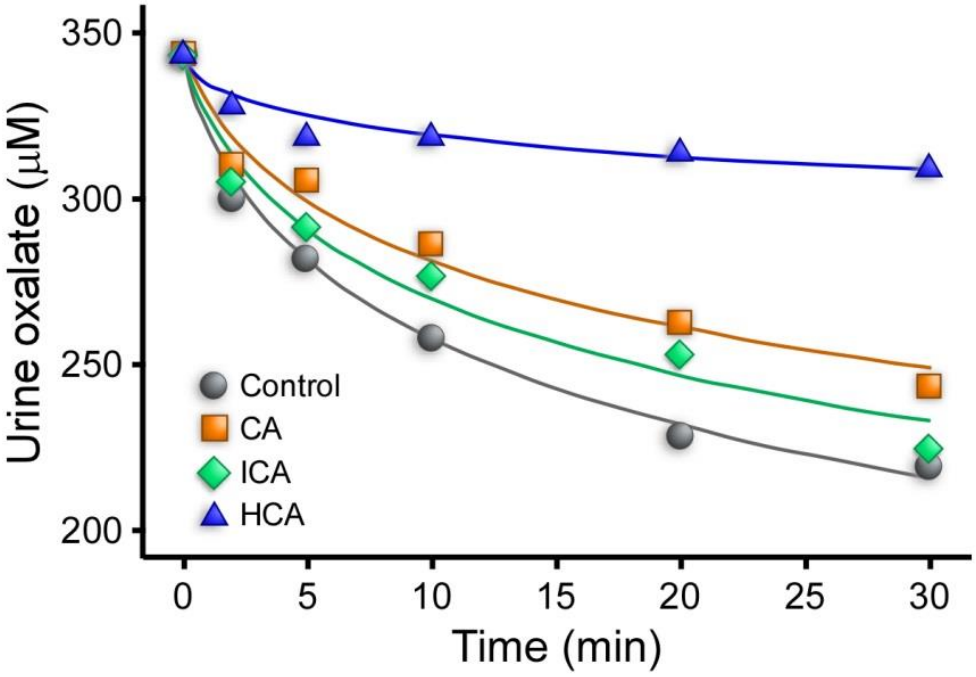

Figure 4.11 Calcium oxalate growth assays in human urine. The reduction in urine oxalate concentration is monitored as a function of time using 2 mM modifier. Urine samples were collected from stone-formers with relatively low citrate levels. Lines are extrapolations to guide the eye.

Table 4.3 Comparison of growth rate constants.

	$k_{OGM}/k_{control}$ x 100
HCA	6 ± 3
CA	40 ± 15[†]
ICA	53 ± 11[†‡]

[†]p = 0.01 compared to that of HCA
[‡]p = 0.05 compared to that of CA

Chapter 5

Elucidating the Effects of Polyprotic Acid Speciation

Molecular modifiers (or more generally, impurities) in crystallization can have a significant influence on the thermodynamics and kinetics of crystal growth. In synthetic crystallization, the use of modifiers has proven to be an effective route to produce materials with tailored physicochemical properties (Olafson, Li et al., 2016) for applications that span from energy to medicine. Modifiers are also utilized in natural and biological crystallization to mediate the formation of crystals or hierarchical structures thereof with exquisite motifs (Arias and Fernandez 2008; Evans 2008). A significant body of literature on this topic has been devoted to calcification (e.g., carbonates, phosphates, and oxalates) pertaining to relevant processes in biomineralization (e.g., nacre, coccoliths) (Meldrum and Colfen 2008), pathological diseases (e.g., cataracts (Pande, Pande et al., 2001), gallstones (Holan, Holzbach et al., 1979), and atherosclerosis (Dorozhkin 2007)), and scale formation in oil/gas recovery (Risthaus, Bosbach et al., 2001). The most effective modifiers of calcium mineralization tend to be polyprotic acids. Examples include proteins or biomolecules (e.g., glycosaminoglycans) that are rich in glutamic and aspartic acids or phosphorylated residues (Asplin, Deganello et al., 1991; Guo, Ward et al., 2002; Wesson, Johnson et al., 2003; Wang, Qiu et al., 2006; Grohe, O'Young et al., 2007; Taller, Grohe et al., 2007; Langdon, Wignall et al., 2009; Weaver, Qiu et al., 2009; Hug, Grohe et al., 2012; Cho, Salter et al., 2013). Moreover, polyprotic organics can be quite effective inhibitors of crystal growth (Ryall, Harnett et al., 1981; Hess, Zipperle et al., 1993; Shirane and Kagawa 1993; Qiu, Wierzbicki et al., 2004; Qiu,

Wierzbicki et al., 2005; Wang, Zhang et al., 2006; Weaver, Qiu et al., 2006; Weaver, Qiu et al., 2007; Grohe, O'Young et al., 2011). In calcium mineralization, most anionic solutes (CO_3^{2-}, PO_4^{3-}, or $C_2O_4^{2-}$) are polyprotic acids that interact with the carboxylates of modifiers via calcium bridges, $-O^-_{(mineral)}\ldots Ca^{2+}\ldots_{(modifier)}{}^-O-$. For such systems where modifier-crystal interactions are governed by electrostatics, a heuristic guideline for selecting an effective modifier is a molecule with multiple charged moieties, which tend to be the most effective inhibitors of calcium mineralization (Jung, Sheng et al., 2004).

In biomineralization, the solute and modifier are typically polyprotic species; therefore, changes in solution pH can have a marked effect on crystal growth and inhibition, respectively. In this study, we investigate the effect of growth solution pH on crystallization using calcium oxalate (CaOx, CaC_2O_4), which was selected as a model system based on its relevance to pathological crystallization in kidney stone disease. Notably, ca. 80% of kidney stones are derived from calcium oxalate and other calcium minerals (e.g., brushite) (Coe, Parks et al., 1992; Dussol, Geider et al., 1995; Pramanik, Asplin et al., 2008). Calcium oxalate monohydrate (COM) is the most thermodynamically-stable hydrate of calcium oxalate, has a monoclinic space group ($P2_1/c$) and unit cell parameters a = 6.3 Å, b = 14.6 Å, and c = 10.1 Å. Indexing of COM crystal face is based on the whewellite crystal notation reported by Tazzoli (Tazzoli and Domeneghetti 1980). COM crystals prepared *in vitro* exhibit a habit (Figure 5.1A, hexagonal platelets) that is similar to the morphology of crystals formed *in vivo* (Ryall, Harnett et al., 1991; Wesson and Ward 2007). The four predominant surfaces of COM crystals are illustrated in Figure 5.1B.

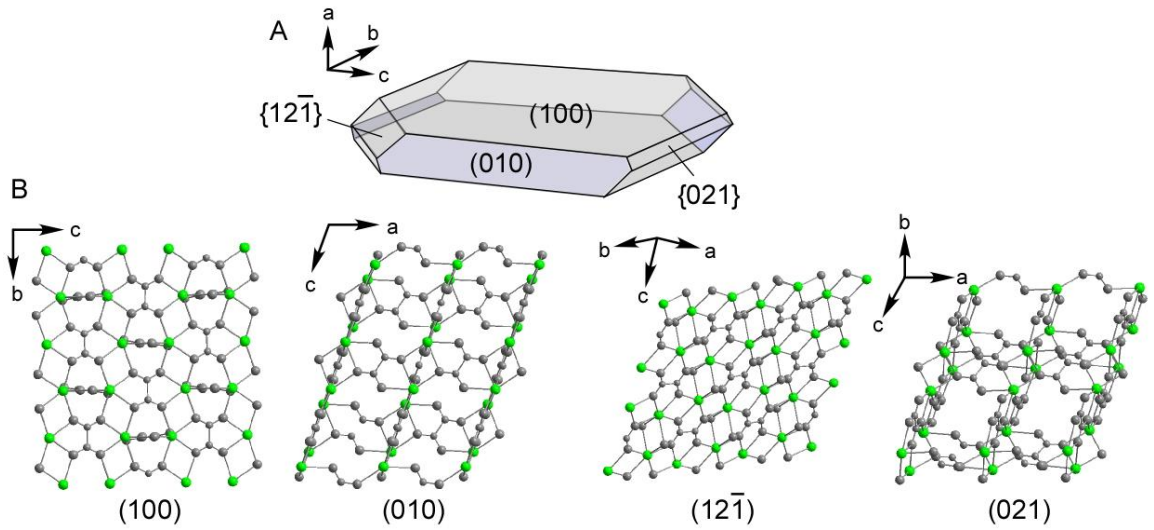

Figure 5.1 A schematic of a single COM crystal with its four crystallographically significant faces labelled as (100), (010), {12-1}, and {021} (A). Top view of cross sectional images normal to the four crystallographic planes (B).

The lifetime incidence rate of kidney stone disease in the United States is approximately 15% and is projected to increase in the next century (Stamatelou, Francis et al., 2003; Brikowski, Lotan et al., 2008) owing to several factors that include an increased sedentary lifestyle, choices of food consumption, obesity, global warming (i.e., dehydration), metabolic syndromes, hypercalciuria (Bushinsky 1998; Scheinman, Cox et al., 2000), and hyperoxaluria (Asplin 2002). Stone formation is governed by several factors that include (but are not limited to) solute supersaturation, urine pH, and the presence of urinary proteins and small organics. The clinical implications of CaOx superstation in urine has been examined since the 1960s (Nordin and Robertson 1966; Robertson 1969). The supersaturation and pH in physiological media can vary significantly from one person to the next, making COM crystallization an interesting model system to evaluate the effects of solution alkalinity on crystallization. For various types of stones, such as uric acid (Sakhaee 2009) and calcium phosphate (Parks,

Worcester et al., 2004), clinical trials show an inverse correlation between urine pH and stone formation. Such observations are intuitively linked to their respective dissociation constants. For example, lower pH leads to higher concentrations of neutral uric acid (pKa_1 = 5.4) (Finlayson and Smith 1974), which promotes its crystallization (Riese and Sakhaee 1992; Sakhaee, Adams-Huet et al., 2002). Likewise, partially-dissociated phosphate groups (e.g., HPO_4^{2-}) are more abundant around pH 6.7 (i.e., close to its pKa). Indeed, patients with uric acid or phosphate stones have a tendency to excrete urine with low and high pH, respectively (Asplin, Parks et al., 1998).

The physiological pH for COM stone formation is generally deemed to have little (if any) effect on crystal growth based on the relevant dissociation constant of oxalate (pKa = 4.3) being lower than the average pH of human urine (5 – 8). A study by Langley reported that the free calcium ion concentration in urine decreases with increasing pH (owing to the increased precipitate in both stone forming and non-stone forming patient samples) (Langley and Fry 1997). Conversely, Verplaetse et al. reported that the solubility of COM crystals is not affected by pH > 5 (Verplaetse, Verbeeck et al., 1986). Changes in solution pH may also impact the speciation of urinary molecules that serve as native inhibitors of COM crystallization, or synthetic molecules such as citrate that are administered as therapeutics of stone disease. Moreover, the negative charge of COM crystals in aqueous media can influence the local concentrations of charged ions and molecules in close proximity to growth sites on crystal surfaces. To our knowledge, the role of solute and modifier speciation on COM crystallization has not been systematically addressed.

Here, we examine the influence of growth solution pH on the charged state of polyprotic acids that constitute both the solute and modifiers of COM crystallization. Using a combination of bulk crystallization assays and speciation models, we show that the rate of crystal growth and its degree of inhibition depend on the concentration of fully dissociated solute and modifier, respectively. Models employed in this study emphasize the importance of local pH changes as a function of distance from COM interfaces owing to the Boltzmann distribution of ionic species surrounding negatively-charged crystal surfaces. Our findings reveal that the role of modifiers as inhibitors and promoters of COM crystal growth can be tuned by changes in solution pH. Moreover, we show that the efficacy of modifiers is strongly correlated to the alkalinity of the growth medium. These findings have implications for understanding how to control the rate of calcium oxalate crystallization; however, our results also provide insight that could help better understand the role of polyprotic modifiers for a broader class of calcium minerals. Moreover, our observations may prove relevant to understanding the influence of pH in pathological COM kidney stone disease.

5.1 Speciation Models of Polyprotic Acids

Table 5.1 lists the equilibrium equations and corresponding dissociation constants (pKa) for the solute and two modifiers selected for this study: oxalate (OX, $C_2H_2O_4$), citrate (CA, $C_6H_8O_7$), and hydroxycitrate (HCA, $C_6H_8O_8$). The molecular structures of these polyprotic acids are provided in Figure 5.2 (A – C, insets). This model system is comprised of OX, the simplest diacid and principal component of COM crystals. The dissociation of OX acid groups is represented by Equations (5.1) and (5.2). CA is a

known inhibitor of COM crystallization that is administered as a therapeutic drug for calcium oxalate kidney stones (Ryall, Harnett et al., 1981; Ettinger, Pak et al., 1997; Qiu, Wierzbicki et al., 2004; Phillips, Hanchanale et al., 2015). CA has three carboxylic acids with corresponding speciation reactions in Equations (5.3) – (5.5). HCA, a structural analogue of CA with one additional hydroxyl group, was recently identified as a potent inhibitor of COM crystallization (Chung, Granja et al., 2016). The three dissociation reactions of HCA are represented in Equations (5.6) – (5.8).

Table 5.1 Speciation reaction and dissociation constants for polyprotic acids.

Equation	Oxalate	p*K*a[†]
(5.1)	$C_2H_2O_4 \leftrightarrow C_2HO_4^- + H^+$	1.25
(5.2)	$C_2HO_4^- \leftrightarrow C_2O_4^{2-} + H^+$	4.30
Equation	Citrate	p*K*a[†]
(5.3)	$C_6H_8O_7 \leftrightarrow C_6H_7O_7^- + H^+$	3.13
(5.4)	$C_6H_7O_7^- \leftrightarrow C_6H_6O_7^{2-} + H^+$	4.76
(5.5)	$C_6H_6O_7^{2-} \leftrightarrow C_6H_5O_7^{3-} + H^+$	6.40
Equation	Hydroxycitrate	p*K*a[‡]
(5.6)	$C_6H_8O_8 \leftrightarrow C_6H_7O_8^- + H^+$	2.90
(5.7)	$C_6H_7O_8^- \leftrightarrow C_6H_6O_8^{2-} + H^+$	4.29
(5.8)	$C_6H_6O_8^{2-} \leftrightarrow C_6H_5O_8^{3-} + H^+$	5.11

[†]Dissociation constants from Martell and Smith
[‡]Dissociation constants from ChemAxon

We calculated the percentage of neutral and charged species as a function of solution pH for OX (Figure 5.2A), CA (Figure 5.2B), and HCA (Figure 5.2C) using a speciation model that is described in greater detail within the Appendix D. For this study, we selected pH 4 – 10 as a range that encompasses the average physiological conditions

of calcium oxalate stone formation (i.e., pH 5 – 8) (Fleming, van Bronswijk et al., 2001). COM crystals grow by the incorporation of divalent oxalate, labelled as OX(-2). The concentration of OX(-2) governs the supersaturation, which is the driving force for COM crystallization. Model results indicate that OX(-2) is the dominant species at pH > 6, below which there is an appreciable rise in the concentrations of OX(-1) and neutral OX. The fully-dissociated form of CA, labelled as CA(-3), is the dominant species at pH > 8, whereas the equivalent form of HCA, labelled as HCA(-3), is prevalent at lower alkalinity (pH > 6.5). Calculations were made using the activity (rather than the concentration) of each species. The activity coefficients γ_i were calculated using the Debye-Hűckel equation

$$\log \gamma_i = \left(\frac{-0.51\, z_i^2 \sqrt{I}}{1+(\alpha_i \sqrt{I}/305)}\right), \quad (9)$$

where z_i is the ion valence, I is the ionic strength ($\mu = 0.5 \sum_i c_i z_i^2$), and α_i is the ion hydrated radius (Table 5.2). The ionic strength was set equal to the experimental condition used to measure COM growth. Notably, growth solutions were prepared with 150 mM NaCl to match the physiological medium of COM crystallization (i.e., the average ionic strength of human urine) (Shirane, Kurokawa et al., 1999).

Table 5.2 Hydrated radius of ions.

Species	α (pm)
Ca^{2+}	600
$C_2O_4^{2-}$	450
Na^{+}	450
Cl^{-}	300

The estimated variations of polyprotic acid speciation in Figure 5.2 raised two questions, which we address herein. The first question pertains to the effect of OX charge on COM crystal growth in view of a common perception within the kidney stone community that pH has little effect on pathological COM crystallization. Models in Figure 5.2A reveal a significant drop in OX(-2) concentration within the lower range of physiological pH that could markedly alter the rate of COM crystallization. A second question, which is based on the observed disparity of CA and HCA speciation in the same pH range, is whether such differences would influence their efficacy as COM growth inhibitors. *In vitro* studies of COM crystallization in literature are typically performed at pH ≈ 6 where the concentration of fully-dissociated modifiers, HCA(-3) and CA(-3), are calculated to be 88 and 27%, respectively. Herein, we examine in greater detail the role of solute and modifier speciation in COM crystal growth and inhibition, respectively.

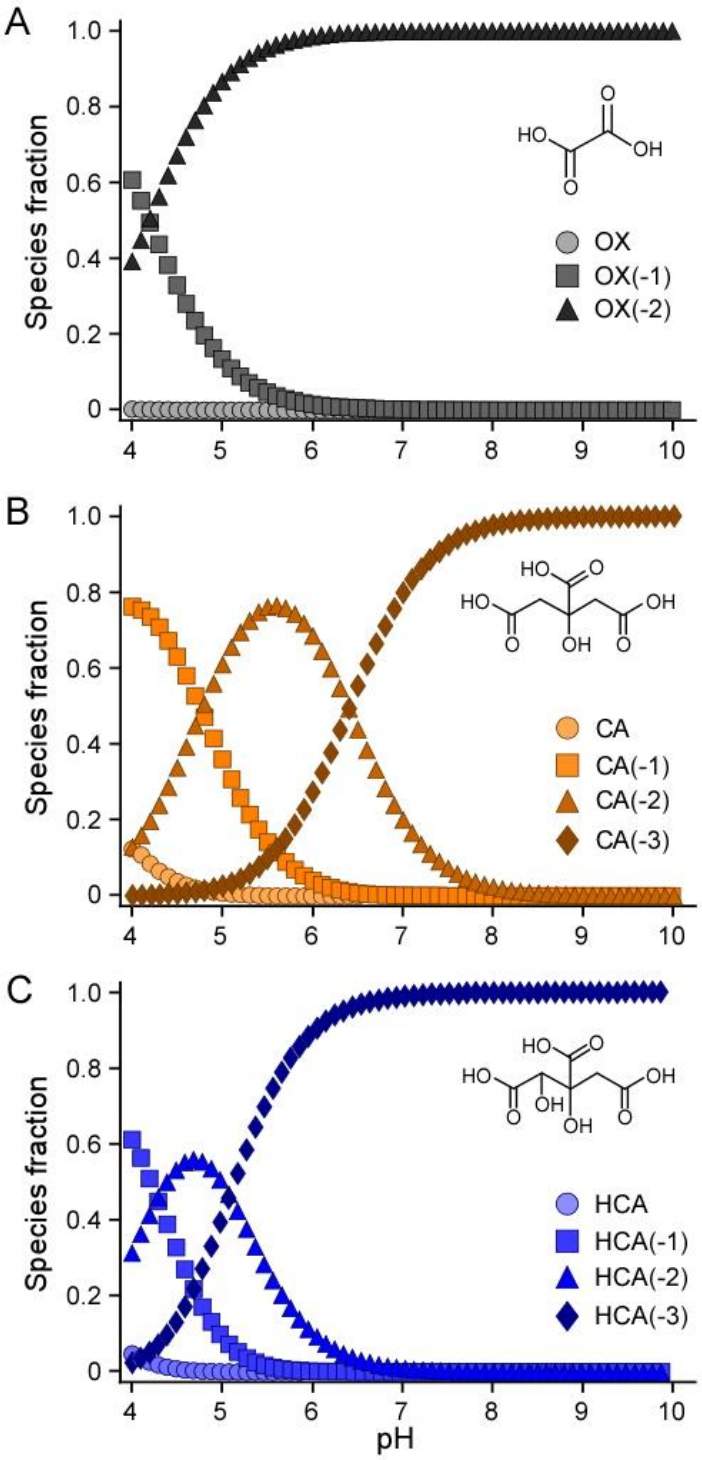

Figure 5.2 Dissociated states of organic acids as a function of pH. The fractions of neutral and charged species for (a) OX, (b) CA, and (c) HCA were calculated with ionic strength 150 mM using a combination of mass balances and speciation reactions.

5.2 Diffuse Double Layer Surrounding Crystals

COM crystals are negatively charged in aqueous solution (Viswanathan, Rimer et al., 2011), which was confirmed by the measurement of zeta potential, owing to the dissociation of calcium ions that generates interfaces largely populated with carboxylic acid groups of terminated oxalates. Crystal growth by the addition of OX(-2) or its inhibition via interactions with modifiers (HCA or CA) occur through the formation of calcium bridges (Figure 5.3B) between the carboxylic acids of OX on the COM surface and that of the acid in solution, $_{(COM)}$–COO^{-}…Ca^{2+}…^{-}OOC–$_{(acid)}$. The schematic in Figure 5.3A depicts the electrostatic potential ψ as a function of distance *x* from a charged surface. The ions surrounding the negatively-charged interface occupy several distinct regions. The immediate Stern layer comprised of counterions (e.g., Ca^{2+}) can be subdivided into Helmholtz layers (inner and outer) based on the degree of ion hydration. At longer distances from the surface, ions account for the diffuse layer with a thickness estimated by the Debye length, κ^{-1},

$$\kappa^{-1} = \left[\left(\frac{1000e^2N_A}{\varepsilon_0\varepsilon_r k_B T}\right)\sum z_i^2 M_i\right]^{-1/2}, \tag{5.10}$$

where e is the charge of an electron, N_A is Avogadro's number, ε_0 is the permittivity of free space, ε_r is the relative dielectric constant, k_B is the Boltzmann constant, T is the temperature, z_i is the ion valence, and M_i is the molar concentration of ions in solution. The electrostatic potential of a COM crystal surface and surrounding double layer was calculated using the linearized Poisson-Boltzmann equation,

$$\psi(x) = \psi_0 \exp(-x/\kappa^{-1}), \tag{5.11}$$

where the equation was established under the assumption that the surface potential ψ_0 (at x = 0) is low (i.e., $|\psi_0| < 25$ mV). Here, we estimate the surface potential using an experimentally measured zeta potential ζ of COM crystals, which is the charge near the outer Helmholtz layer (labelled in Figure 5.3B).

The concentration of ions in the diffuse double layer surrounding COM crystal surfaces exhibit a monotonic dependence on the electrostatic potential $\psi(x)$ that is governed by the Boltzmann distribution (Hiemenz and Rajagopalan 1997), represented here for H^+,

$$[H^+] = [H^+]_\infty \exp(-e\psi(x)/k_B T), \tag{5.12}$$

where $[H^+]_\infty$ is the bulk concentration measured experimentally with a pH meter. It is important to point out that the pH near a charged surface (at x = 0) is different than that of the bulk (at $x = \infty$). These local variations in pH can influence crystal growth/inhibition based on changes in molecule speciation. As illustrated in Figure 5.3C, there is a monotonic increase in $[H^+]$ near the crystal surface, leading to lower pH in the region surrounding crystal growth sites that concomitantly alters acid speciation. We approximated the fraction of neutral and charged organic acids as a function of distance from a COM surface using a combination of mass balances (described in Appendix D), speciation models (Table 5.1), and colloidal relationships for charged interfaces (Equations 5.10 – 5.12). Profiles of OX species are shown in Figure 5.4 at three bulk pH values, while similar plots of CA and HCA speciation are provided in Appendix D. At pH 4 (Figure 5.4), the percentage of fully dissociated oxalate, OX(-2), drops from 40% in the bulk to 20% at the crystal surface. The difference between bulk and surface OX

concentration narrows as the pH increases. At pH 6 (Figure 5.4), oxalate in the bulk is fully dissociated compared to 96% of OX species near the crystal surface.

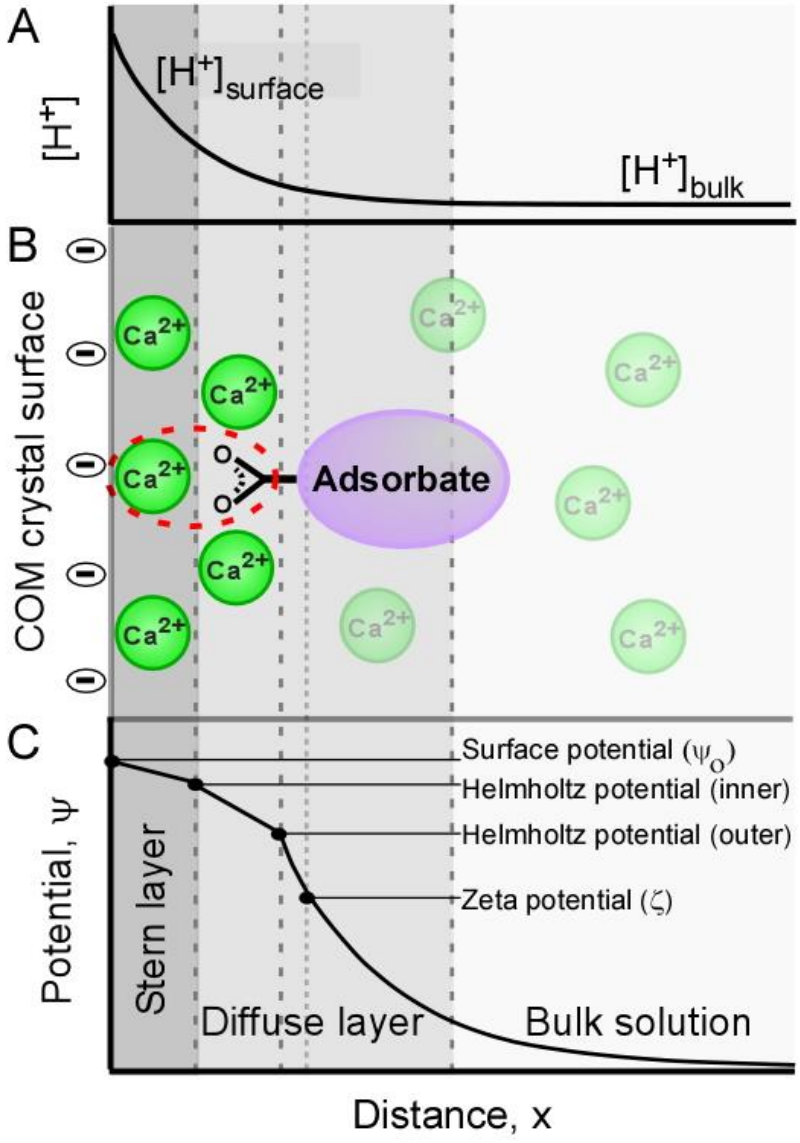

Figure 5.3 Electrostatic potential decaying with increased distance from crystal surface (A) and a schematic of adsorbate–COM crystal surface interaction (B). Exponential decay of $[H^+]$ as a function of distance from the negatively charged surface.

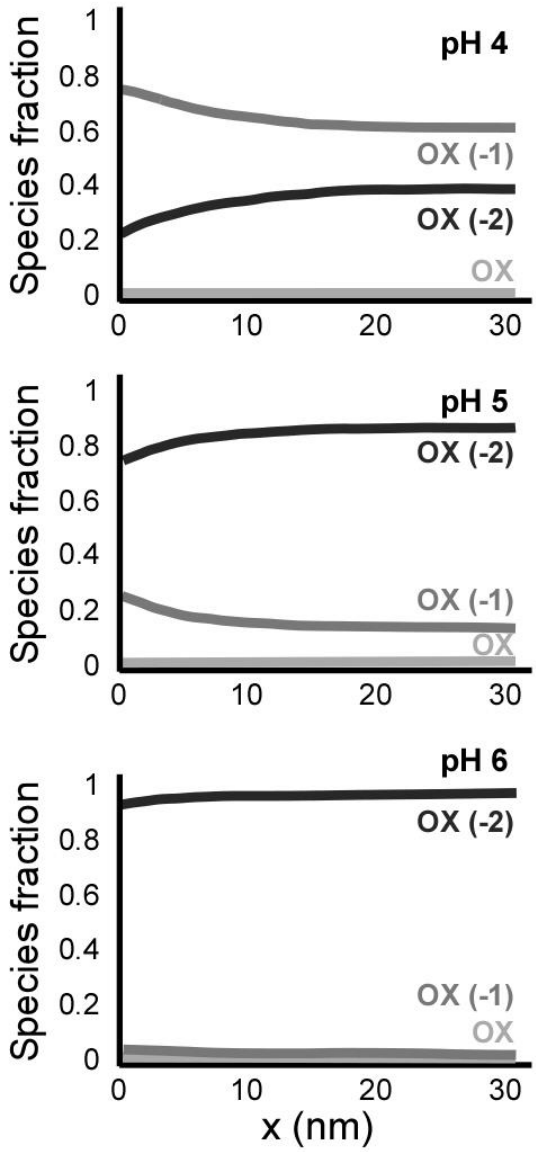

Figure 5.4 Species fraction of oxalate in its neutral, monovalent, and divalent state was calculated for pH 4 – 6 as a function of distance from the COM crystal surface.

5.3 Kinetic Rate of COM Crystallization

We used an ion-selective electrode (ISE) to track the temporal depletion of free Ca^{2+} ions in a supersaturated calcium oxalate (CaOx) growth solution. The slope of ISE curves, corresponding to changes in Ca^{2+} concentration as a function of time, represents

the rate of COM crystallization (analogous to previous methods reported by Farmanesh et al., (Farmanesh, Ramamoorthy et al., 2014)). These measurements were made in solutions with pH ranging between 4 and 10 to assess the effect of organic acid speciation. Herein, we report the relative growth rate (RGR), which is the rate of COM crystallization at a specific pH scaled by a reference value measured in the absence of modifier at pH 6. Using calcium oxalate (CaOx) solutions with fixed concentration C_{CaOx} = 0.5 mM, measurements in the absence of modifier reveal changes in the RGR (Figure 5.5, grey circles) that directly correlate to changes in the OX(-2) concentration. The rate of crystal growth *r* is determined by the following relationship,

$$r \propto k(C - C_e), \tag{5.13}$$

where k is a kinetic rate constant, *C* is the concentration of OX (i.e., $C = C_{Ox^{2-}}$), and C_e is equilibrium concentration of CaOx based on the solubility of COM crystals. The latter is expressed as,

$$C_e = \sqrt{K_{sp}\gamma_{Ca}^{-1}\gamma_{Ox}^{-1}}, \tag{5.14}$$

where K_{sp} is the solubility product (1.66 x 10^{-9} mol^2/L^2 at 25˚C) (Tomazic and Nancollas 1979) corresponding to the following reaction,

$$COM_{(s)} \overset{K_{sp}}{\longleftrightarrow} Ca^{2+}_{(aq)} + Ox^{2-}_{(aq)}. \tag{5.15}$$

As shown in Figure 4, there is a rapid decrease in the concentration of OX(-2) at pH < 6 with a commensurate reduction in the RGR of COM crystallization.

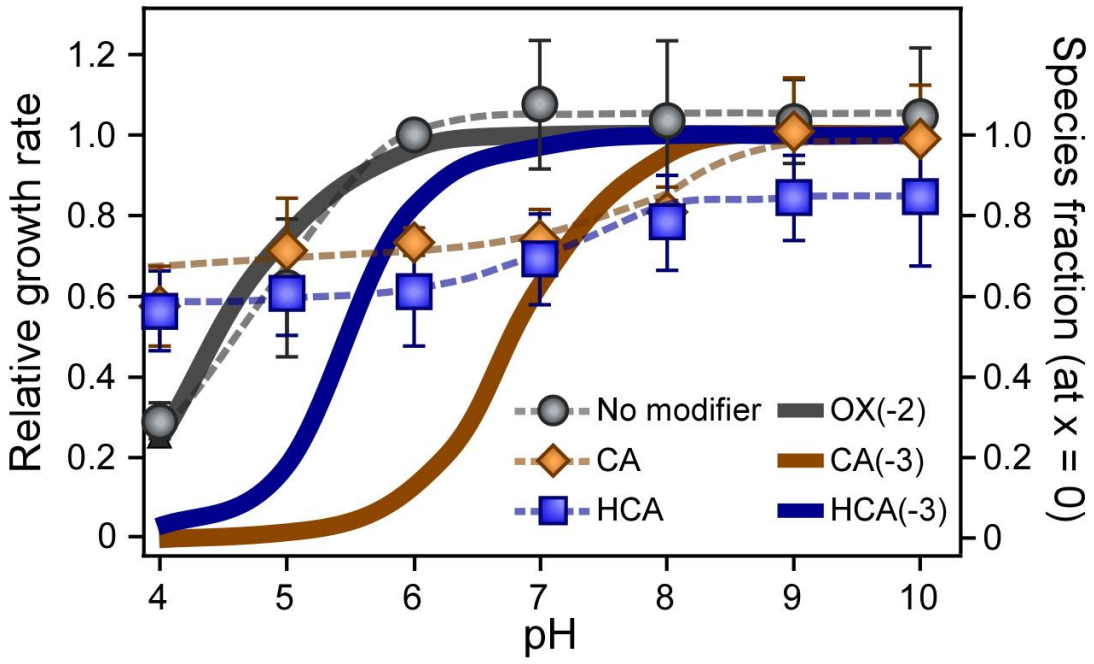

Figure 5.5 Relative growth rate at pH values 4 – 10 in the absence and in the presence of C_{CA} = 20 μg/mL and C_{HCA} = 20 μg/mL, respectively and species fraction of fully dissociated OX, CA, and HCA are plotted. Error bars indicate two standard deviations.

The speciation profiles in Figure 5.5 account for the change in pH at COM crystal surfaces by substituting $[H^+]_{x=\infty}$ with $[H^+]_{x=0}$ in model equations. When comparing pH-dependent profiles of acid speciation in bulk solution (Figure 5.2) to the surface of COM crystals (Figure 5.5), the latter are slightly shifted to higher pH. The net positive shifts in pH for the profiles of OX(-2), CA(-3), and HCA(-3) are approximately 0.3, 0.4, and 0.3, respectively. General trends in both RGR and speciation for all polyprotic acids are sigmoidal with an approximate inflection point that occurs at a pH value corresponding to the increase in the fraction of fully-dissociated acid: HCA(-3) and CA(-3). In a previous study (Chung, Granja et al., 2016), we reported that HCA is a more effective inhibitor of COM crystallization than CA at pH 6.2; however, as the pH of the

growth solution is increased, differences in RGR between the two inhibitors narrows, such that their efficacy at the upper limit of physiological conditions (pH 8) is nearly identical. Interestingly, further increase in pH leads to a marked reduction in CA efficacy (i.e., RGR approaches that of solutions without modifier). Possible explanations for the quiescent shift of CA are provided later. In Figure 5.5, we also observe that HCA exhibits a loss in efficacy with increased pH (from RGR = 0.6 to 0.8); however, HCA retains its ability to inhibit COM crystal growth.

Bulk crystallization measurements in acidic media (i.e., pH < 6) reveal a crossover in the behavior of CA and HCA from COM growth inhibitors (at high pH) to promoters (at low pH). The effect of crystal growth promotion has been observed previously for COM (Farmanesh, Chung et al., 2014) as well as other calcium minerals (Nielsen, De Yoreo et al., 2013). It is posited that the enhanced rate of crystal growth is the result of two possible mechanisms, both of which facilitate the attachment of solute to growth sites on crystal surfaces: (1) promoters may disrupt solvent structuring in the Stern layer, thereby decreasing the barrier(s) for solute diffusion from solution to the crystal surface; and (2) promoters may increase the local supersaturation (calcium or oxalate ions) near the crystal surface. We observe that CA and HCA promotion of COM growth leads to an increase in the RGR by 99 and 95%, respectively. The exact mechanism of growth promotion at low alkalinity is unknown and remains a topic of ongoing investigation. It is interesting to point out that the rate of COM growth at pH 4 is negligible (RGR = 0.3) owing to only 39% of oxalate being fully dissociated. Under these conditions, it would seem that any process leading to a marginal increase in OX(-2)

concentration near COM crystal surfaces could have a notable impact on the rate of growth.

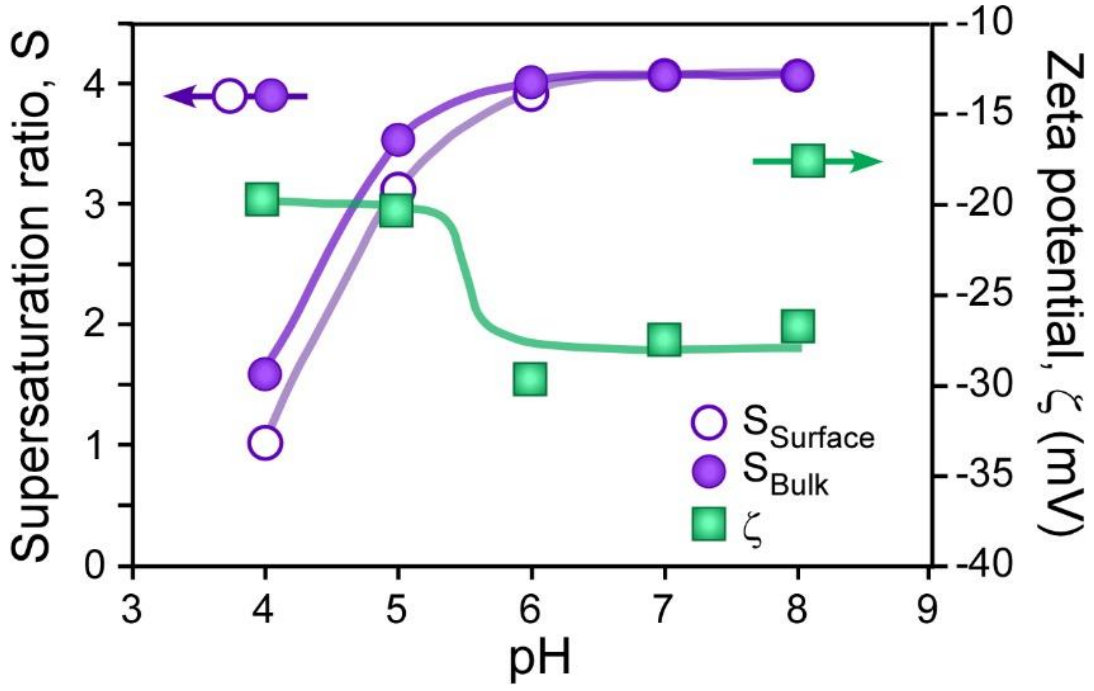

Figure 5.6 Supersaturation ratio, S at COM crystal surface and at bulk was calculated according to species fraction at pH 4 – 8 (left axis). Zeta potential, ζ of COM crystals was measured from pH 4 – 8 (right axis).

In Figure 5.6 we compare the supersaturation ratio S in bulk solution and at COM surfaces as a function of solution pH (where $S = C/C_e$ and $C = C_{OX(-2)}$). Comparisons are made between the concentration of solute in the bulk solution (S_{Bulk}, $x = \infty$) and at the crystal interface ($S_{Surface}$, $x = 0$). In acidic media, the differences between S_{Bulk} and $S_{Surface}$ are more pronounced due to the reduced concentration of OX(-2) species near the crystal surface (see Figure 5.4). The difference becomes large enough that the supersaturation near the crystal surface at pH 4 is close to equilibrium (i.e., S = 1 or $C \approx C_e$). The fact that COM crystals still grow at this condition while the speciation model predicts no growth may reflect inaccuracies in the reported pKa value for oxalate (Chung, Granja et

al., 2016) owing to the ionic strength dependency of the dissociation constant (Martell and Smith 1982). On this basis, the species fractions of solute (and modifiers) in Figure 5.2 could potentially be shifted to lower pH, resulting in a larger fraction of fully dissociated OX at lower alkalinity. It is also feasible that changes in surface potential could impact model calculations. We measured the zeta potential ζ of COM crystals to approximate the surface potential ψ_0. As shown in Figure 5.6, there is an increase in the magnitude of surface charge $|\zeta|$ with increasing pH (from ζ = –20 to –25 mV), suggesting an increased fraction of fully dissociated oxalates on COM surfaces. In the speciation model calculations, we used an average surface charge; thus, the slight reduction in ζ at lower pH could explain the disparity between model predictions and bulk crystallization measurements of COM growth around pH 4. However, there is overall good agreement between the experimental results and model predictions across the full range of growth solution pH.

We measured the zeta potential ζ of COM crystals in order to approximate the surface potential ψ_0 for speciation models. Zeta potential of COM crystals were measured using Zetasizer Nanoseries (Malvern Instruments) at room temperature. Samples were prepared by adding ca. 1 μg seed COM crystals to 10 mL of a 0.15 mM saturated calcium oxalate solution. Measurements were performed in the absence and presence of 50 μg/mL growth modifiers at pH 4 to 8 (pH 9 and 10 were not measured due to electrode stability issue in the cell). Prior to measurement, sample solutions were stirred for approximately one hour to allow sufficient time for modifier to interact with COM crystal surfaces. Universal ‘dip’ cell kit (ZEN 1002, Malvern Instruments) was

submerged into 1 mL volume of each sample solution to measure the electrophoretic mobility of COM crystals which was calculated using Smoluchowski equation.

On the basis of electrostatics, the increased net negative charge of COM crystals at higher alkalinity may explain the loss of modifier efficacy at pH > 8; that is, the concentration of fully-dissociated acids, CA(-3) and HCA(-3), is reduced near crystal surfaces according to the Boltzmann distribution. This is a reasonable explanation for the slight decrease in HCA efficacy, but it is seemingly insufficient to explain the complete loss of CA efficacy. An additional factor may be the concentration of OH^- ions at higher alkalinity. For instance, the hydroxide ion concentration at pH 10 is 0.1 mM, which is comparable to the concentrations of solute (C_{CaOx} = 0.5 mM) and modifier (e.g., C_{CA} = 0.07 mM). At pH 6, the concentration of hydroxide ions is much lower (10^{-5} mM). Competitive binding of polyprotic acids and OH^- ions with crystal surfaces may impede CA – COM interactions. If this is true, however, it would also imply that HCA – COM interactions are unaffected by OH^- concentration, which likewise implies that HCA binds more favorably to COM surfaces than CA. Although the latter is consistent with prior density functional theory calculations (Chung, Granja et al., 2016), yet more detailed studies are required to fully resolve the loss of CA efficacy in highly alkaline solutions.

5.4 COM Bulk Crystal Properties

Here we quantify the effects of solution pH on COM crystal size and shape by comparing the *c/b* aspect ratio of crystals (Figure 5.7) measured along the [001] and [010] dimensions (refer to Figure 5.1A). Bulk crystallization assays were performed in the absence and presence of modifiers at fixed supersaturation and modifier concentration

(C_{CA} = C_{HCA} = 20 μg/mL). Crystal growth in the absence of modifier results in a slight elongation of crystals in the *c* direction (i.e., higher aspect ratio) with increased pH. This change is attributed to the increased length of crystals in the [001] direction, whereas the width is approximately constant with varying pH (see Figure 5.9). In acidic media, modifiers have little to no effect on the crystal aspect ratio, which can be attributed to the low concentration of trivalent CA and HCA species. The preferential binding of CA to {001} surfaces, which is well documented (Qiu, Wierzbicki et al., 2004; De Yoreo, Qiu et al., 2006; Wang, Zhang et al., 2006; Grohe, O'Young et al., 2011), results in the blunting of apical tips at higher pH, thereby resulting in rectangular-shaped COM crystals (Figure 5.8). CA reduces the aspect ratio of crystals relative to crystals grown in the absence of modifier, leading to a relatively flat *c/b* profile over the entire pH range. Conversely, HCA binds to the apical tips of COM crystals, or the {12-1} and {021} surfaces (Chung, Granja et al., 2016), leading to the diamond-shaped habit observed in optical micrographs (Figure 5.8). The effect of HCA on the *c/b* aspect ratio reaches a plateau at pH > 6 with no appreciable change in crystal morphology at higher alkalinity; however, we do observe that the presence of HCA at high pH leads to more rounded edges of diamond-shaped COM crystals.

Our previous study (Chung, Granja et al., 2016) showed that both CA and HCA reduce the number of COM crystals by as much as 50% at pH 6. We posited that both modifiers act as inhibitors of crystal nucleation. Here, we observe the same trends for COM crystallization over a broader range of growth solution pH (see Figure 5.10). At pH 5 and 6, modifiers have nearly the same effect on the number of crystals produced in bulk assays. At pH 7 – 9, modifiers inhibit COM nucleation, but to a lesser extent.

Interestingly, the most acidic (pH 4) and basic (pH 10) growth solutions resulted in a higher number of COM crystals in the presence of both modifiers. Notably, at pH 4 there is ca. 70% and 48% increase in the number of crystals with CA and HCA, respectively. At pH 10, there is ca. 45% and 61% increases for CA and HCA, respectively). These observations suggest that CA and HCA promote nucleation under specific growth solution conditions. The promotion of nucleation at lower pH is qualitatively consistent with our observation of crystal growth promotion; however, it is not well understood what causes a switch in the mode of action at pH 10.

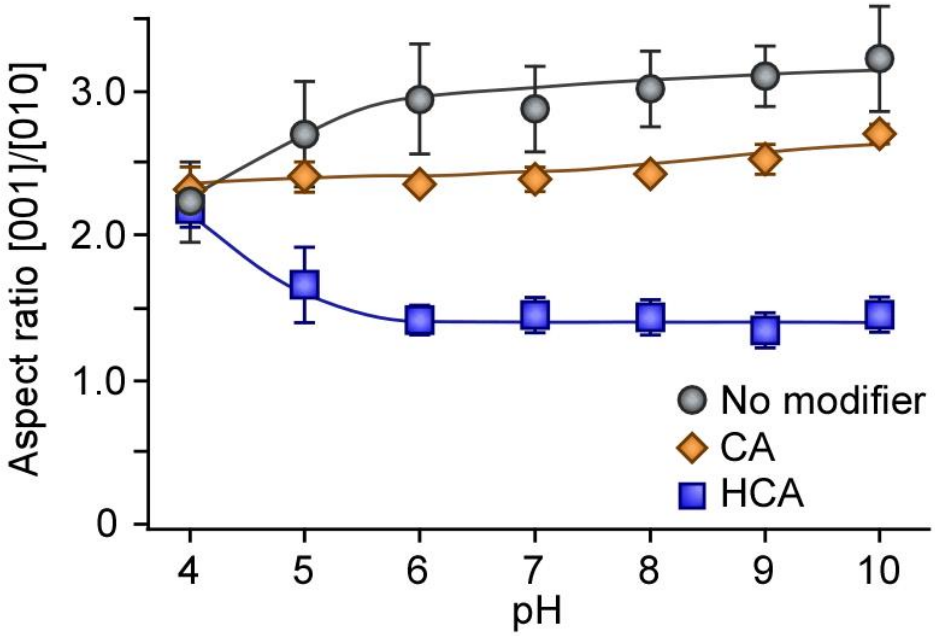

Figure 5.7 Influence of pH on bulk COM crystal habit was analyzed by comparing the aspect ratio of crystals from pH 4 to 10 in the absence and in the presence of C_{CA} = 20 μg/mL and C_{HCA} = 20 μg/mL, respectively. Error bars indicate one standard deviation.

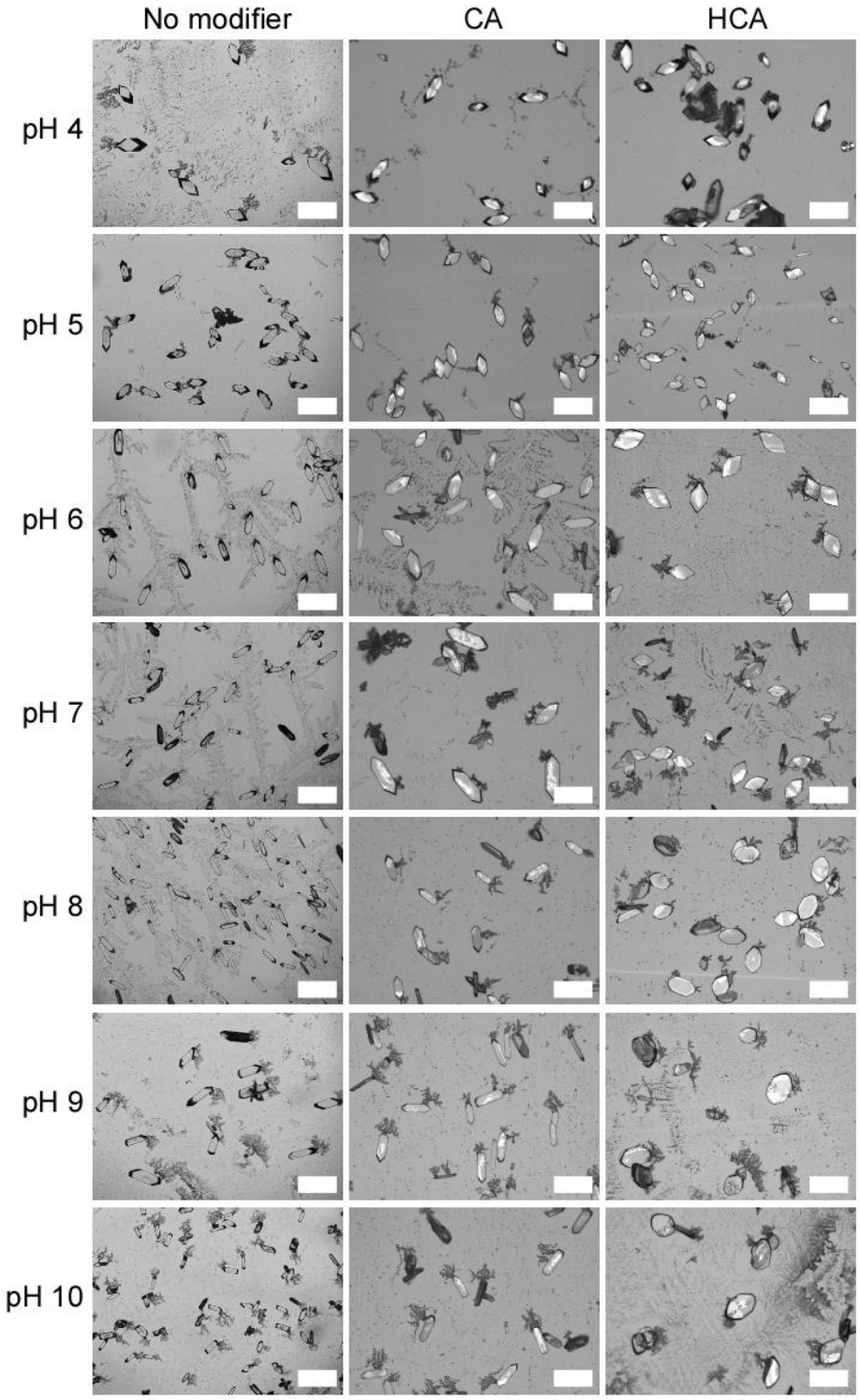

Figure 5.8 Optical micrographs of COM crystals prepared in the absence (left) and in the presence of C_{CA} = 20 μg/mL (middle) and C_{HCA} = 20 μg/mL (right), respectively, at pH values 4 – 10.

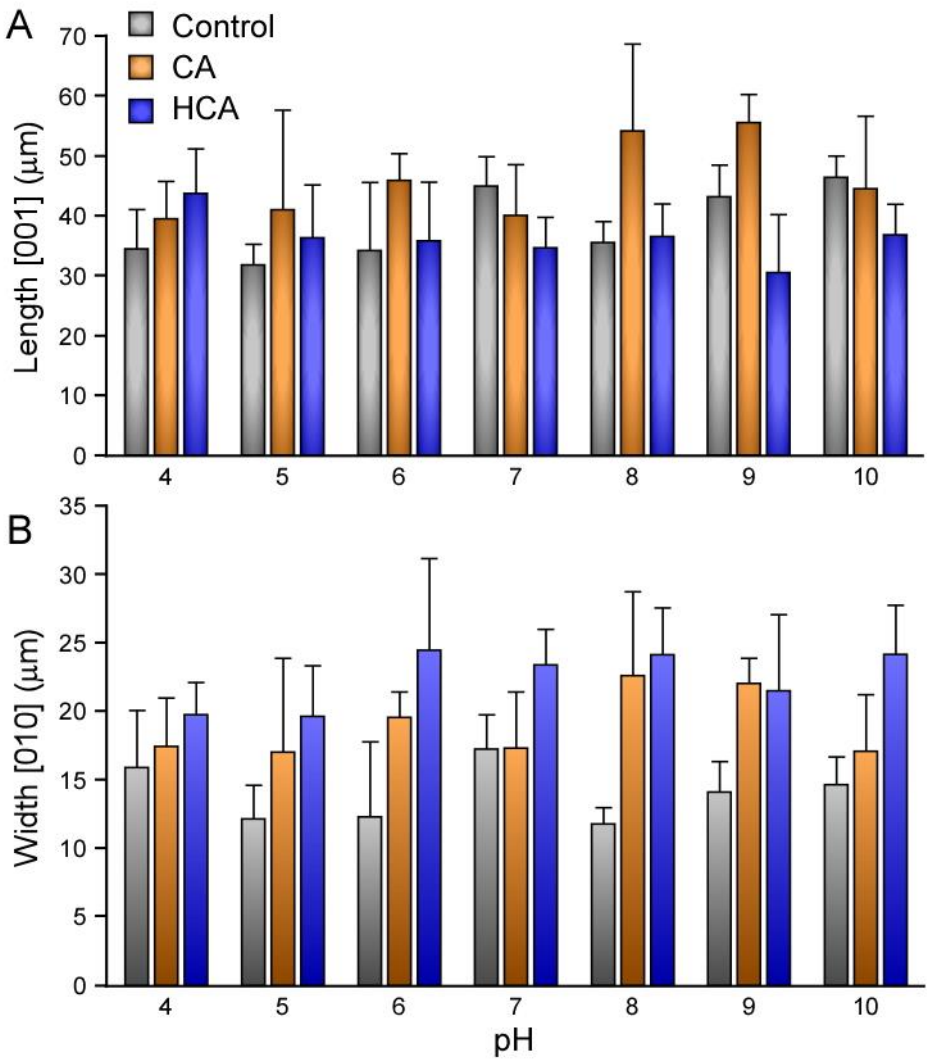

Figure 5.9 Influence of pH on the length (A) and width (B) of crystals from pH 4 to 10 in the absence (i.e., control) and in the presence of C_{CA} = 20 μg/mL and C_{HCA} = 20 μg/mL, respectively. Error bars indicate one standard deviation.

In Figure 5.9 we compare the distributions of COM crystal length and width (refer to Figure 5.1A). Crystals were prepared at pH 4 – 10 in the absence and presence of modifiers (20 μg/mL). The relatively large standard deviation of data reflects the polydispersity of crystal size. At pH 4, the presence of modifiers leads to a marginal increase in crystal dimensions (*c* and *b*), though the aspect ratio (*c/b*) is unaffected (refer

to Figure 5.7). As the solution alkalinity is increased (pH > 6), the length of COM crystals is increased in the absence and in the presence of CA; however, HCA has little effect on the length of COM crystals, most likely because HCA is fully dissociated at pH > 6. For a similar reason, the presence of fully dissociated CA at pH > 8 leads to a more dramatic increase in the length of COM crystals. The width of COM crystals is relatively constant in the absence of modifiers, which results in a net increase in the *c/b* aspect ratio. HCA increases the width of COM crystals owing to its preference for binding to {12-1} and {021} surfaces, rendering growth in the [010] direction more dominant than in the [001] direction.

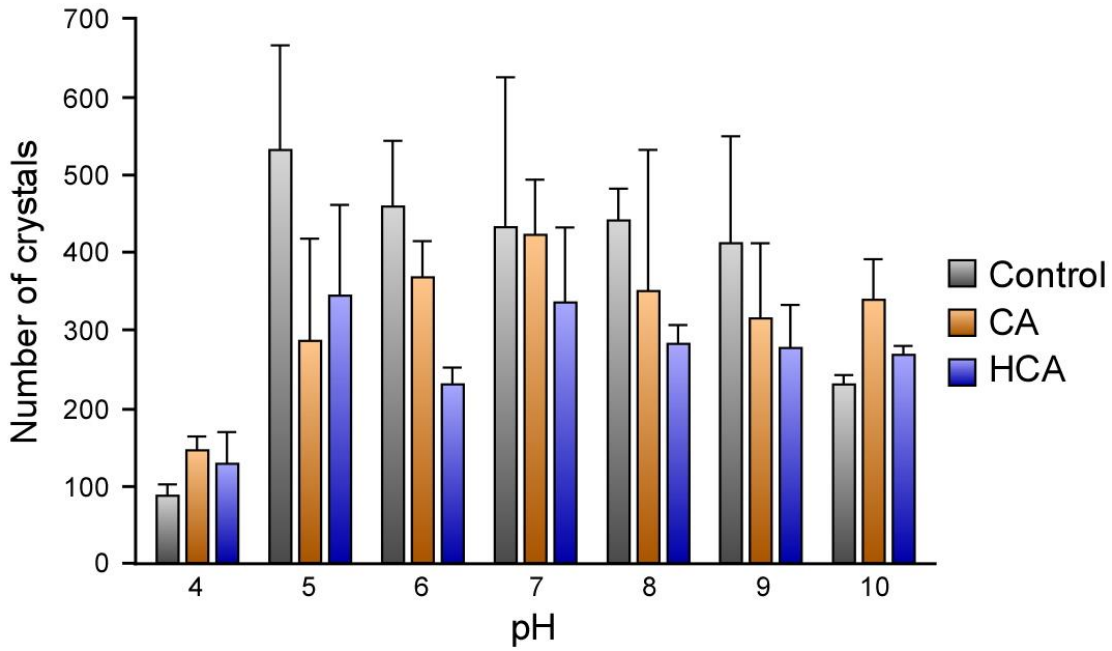

Figure 5.10 The number of COM crystals collected prior to bulk crystallization was measured in the absence (i.e., control) and in the presence of C_{CA} = 20 μg/mL and C_{HCA} = 20 μg/mL, respectively, at pH values 4 – 10. Error bars indicate one standard deviation.

In Figure 5.10 we compare the number of COM crystals (N_{COM}) formed in the absence and presence of modifiers (20 μg/mL). N_{COM} was measured by counting the

crystals collected on the glass substrate used in bulk crystallization assays. Sixteen optical micrographs (each micrograph area equals 647 μm × 484 μm) were obtained from different regions of the substrate and three separate batches were analyzed. At pH 4, N_{COM} is significantly reduced due to the lack of fully dissociated oxalate, OX(-3), in the growth solution. This leads to a dramatic reduction in COM nucleation. Interestingly, the presence of CA and HCA increase N_{COM}, which is consistent with our kinetic study revealing modifiers to be growth promoters at low pH (refer to Figure 5.5). At pH 5, approximately 80% of OX is fully dissociated in bulk solution and there is a marked increase in N_{COM}. At pH ≥ 5, modifiers reduce N_{COM} relative to the control, with the exception of pH 10 where N_{COM} is again higher for modifiers than for the control. The overall trend for N_{COM} is consistent in the absence and presence of modifiers, i.e., N_{COM} increases with increasing pH as the fully-dissociated species of solute and modifier become more prominent. Once the fully dissociated states are reached, N_{COM} decreases with further increase in solution pH. For instance, CA-containing growth solutions exhibit an increase in N_{COM} with increasing pH until reaching pH 7 where additional increases in alkalinity result in a notable reduction in N_{COM}. A similar trend is observed for HCA where the switch to decreasing N_{COM} occurs at pH 5. The effects of modifiers at pH 10 are not well understood.

5.5 Conclusions

In summary, we studied the effect of pH on COM crystal growth in the absence and in the presence of CA and HCA by a combination of theoretical calculations, kinetic studies, and bulk crystallization assays to understand the importance of solute and

modifier speciation. Model calculations of OX, CA, and HCA speciation were performed to determine how the populations of charged species are influenced by changes in the pH of the growth medium. These calculations incorporated the effects of crystal surface charge and the corresponding Boltzmann distribution of ionic species as a function of distance from negatively-charged COM crystal surfaces. We found that the kinetic rate of COM crystallization parallels trends in OX(-2) concentration. Similarly, the efficacy of modifiers exhibits a sigmoidal behavior with increasing pH that mimics the profiles of fully-dissociated polyprotic acids. In acidic growth media, there is a loss of COM crystal growth owing to the reduction in OX(-2) concentration. At these conditions, the inhibitory effects of CA and HCA on COM growth also decrease as the concentrations of trivalent modifier is reduced. Interestingly, we observe that both modifiers switch from growth inhibitors to promoters at lower pH.

Our findings reveal that the lower range of physiological pH does impact the rate of calcium oxalate crystallization. Indeed, the observed decrease in COM growth rate at lower pH may have implications for interpreting/understanding human kidney stone formation; however, as is often the case with interpreting *in vivo* data, there are likely multiple factors that influence stone formation with changing pH in the complex environment of pathological crystallization. For instance, changes in pH can potentially affect metabolic processes, the interaction of biomolecules with COM crystal surfaces, and/or the formation of other pathological crystals. To this end, the results presented here offer insight on how to control COM crystallization through the judicious selection of growth conditions wherein the interplay of polyprotic acid dissociation among solute and modifiers can yield a wide range of effects on crystallization. Trends gleaned from this

study may serve as a platform for designing therapeutics of calcium oxalate kidney stone disease. Given the ubiquitous use of polyprotic acids in biomineralization, our findings may also provide heuristic guidelines for tailoring modifiers of other calcium crystals.

Chapter 6

Summary and Future Outlook

Crystalline materials play a crucial role in the function of living organisms; however, it can be an undesirable process associated with human diseases which is targeted to be inhibited. A common mechanism that regulates crystal growth of biogenic, natural, and synthetic materials is the action of growth modifiers, which range from small ions and molecules to large macromolecules. Upon adsorbing on crystal surfaces, the growth modifiers impede the addition of solute and subsequently reduce the rate of growth. Understanding the molecular recognition of modifier to crystal surface sites and the energetics of interaction between modifier and crystal surface are critical in order to manipulated biomineralization process; however, it remains a challenge to elucidate complex inhibitor-crystal (or organic-inorganic) interactions.

Pathological biomineralization such as formation of kidney stone has been extensively researched both clinically and in benchscale studies with the focus on understanding the effect of natural macromolecule that are present in human urine. Calcium oxalate monohydrate (COM) is the most predominant crystalline species in human kidney stones. COM crystallization may be inhibited by the adsorption of urinary constituents that are rich in negatively-charged moieties in their structure (e.g., aspartic acid and glutamic acid). In aqueous solutions, calcium ions on COM crystal surface dissociate and leave a negatively-charged surface where molecules with negatively-charged moieties may adsorb on the surface by mimicking the oxalate vacancies on the crystal surface.

Previous studies reported by others and our own group reveal that subtle changes in the sequence of peptides and proteins have pronounced impact on their specificity and efficacy in inhibiting COM crystallization. Using this logic, we have selected a library of polyprotic organic acids to observe the impact of subtle differences in their molecular structure such as the length of carbon backbone chain, number of carboxylic acid groups, and number and positioning of hydroxyl groups, and their performance. Citrate, a current therapeutic for COM kidney stone disease, was used as a benchmark to determine the growth modifiers effectiveness. Bulk crystallization assays were employed to quantify the specificity of modifiers and kinetics of COM crystallization was monitored to determine the effectiveness of modifiers. *In situ* atomic force microscopy was utilized to observe the surface growth phenomena in the presence of modifiers in real time.

Two molecular modifiers, citrate and hydroxycitrate which has one additional hydroxyl group to its structure compared to citrate, exhibited a unique mode of inhibitory action that differed from that of others wherein crystal surface dissolution was induced upon adsorption of modifiers. This phenomenon was observed in real time via *in situ* atomic force microscopy which occurred under supersaturated solutions where the concentration of modifiers was three orders of magnitude less than that of the solute. This negates the argument that modifiers were thermodynamically inhibiting the crystal growth by lowering the supersaturation ratio. Combination of results from *in situ* atomic force microscopy studies and density functional theory calculations support our hypothesis that strong interaction between modifier and crystal imparted a localized strain on the crystal lattice which subsequently led to continuous surface dissolution.

Furthermore, preliminary results from human urine studies reveal that hydroxycitrate is capable of increasing the upper metastability limit of human urine to crystalize COM stones which delays nucleation. Also, it was found that hydroxycitrate can be excreted through urine when orally administered which proves its bioavailability. Collectively, these findings support further exploration of the clinical potential of hydroxycitrate as a treatment for calcium oxalate nephrolithiasis.

We also examined the role of solute and modifier speciation on COM crystallization. As previously stated, putative growth modifiers of COM crystallization used in this study and studied by others are rich in negatively charged groups in their structure which invokes the question of the role of solution alkalinity in tuning the deprotonated states for those moieties. By observing the Boltzmann distribution of proton concentration near the negatively-charged COM crystal surface, we calculated and compared the species fraction of oxalate and two potent growth modifiers used in previous studies at the crystal surface and at bulk medium. At the low limit of physiological condition, there is a discrepancy between local supersaturation at the surface of COM and at bulk which dramatically decreases the growth rate. Also, both citrate and hydroxycitrate showed enhancement of growth rate at low pH which may be attributed to disruption of solvent structure by modifiers or their influence on local supersaturation near crystal surface; however, the phenomena remains elusive and further investigation is required. At higher pH that is outside of physiological condition i.e., pH > 8, we observed that modifiers, especially citrate, lose their efficacy in inhibiting COM crystal growth which may be due to crowding effect from increasing concentration of hydroxide ions near the crystal surface; however, it is not well understood at this point.

It is unfortunate and even puzzling to know how little the therapeutics for stone disease have advanced over the last few decades. Developing new drugs and regimen for any disease clinically is time consuming and very costly. Benchscale studies can serve as a fast screening stage and can also provide more systematic results even though they are not always pertinent to physiological settings. Still, I strongly believe that it is important to keep the communication forward between the two disciplines which can only be synergistic.

As mentioned throughout my thesis, the methods used to examine crystal growth and inhibition of crystal growth in this thesis is such a flexible platform that can be applied to many different crystalline systems. In the near future, this platform will be appropriately modified and employed to study the growth and growth inhibition of two other constituents of kidney stone, brushite and ammonium urate. Benchscale studies try to mimic the conditions that are more relevant to physiological condition, such as supersaturation, pH, and ionic strength. However, improvement can be made to the methods, especially on the time scale of the experiments, such as how long the modifiers can come in contact with the stones and what degree of effectiveness is required to inhibit crystal growth in the physiologically relevant time frame. Microfluidic devices with transparent chambers may provide more insights on how modifier and flow of the media affect crystal growth inhibition.

Finally, we believe that these findings invoke further clinical investigation of modifiers used in this study and their role in inhibiting calcium oxalate stone disease *in vivo*. Also, this platform may serve as a heuristic guideline to modify crystallization for

not only other pathological biominerals but also for various organic and inorganic crystalline materials.

References

Abboud, I. A. (2008). "Concentration Effect of Trace Metals in Jordanian Patients of Urinary Calculi." Environmental Geochemistry and Health **30**(1): 11-20.

Ahlrichs, R., M. Bar, M. Haser, H. Horn and C. Kolmel (1989). "Electronic-Structure Calculations on Workstation Computers- the Program System Turbomole." Chemical Physics Letters **162**(3): 165-169.

An, Z. H., S. Lee, H. Oppenheimer, J. A. Wesson and M. D. Ward (2010). "Attachment of Calcium Oxalate Monohydrate Crystals on Patterned Surfaces of Proteins and Lipid Bilayers." Journal of the American Chemical Society **132**(38): 13188-13190.

Arias, J. L. and M. S. Fernandez (2008). "Polysaccharides and Proteoglycans in Calcium Carbonate-Based Biomineralization." Chemical Reviews **108**(11): 4475-4482.

Asplin, J., S. Deganello, Y. N. Nakagawa and F. L. Coe (1991). "Evidence That Nephrocalcin and Urine Inhibit Nucleation of Calcium Oxalate Monohydrate Crystals." American Journal of Physiology **261**(5): F824-F830.

Asplin, J., J. Parks, J. Lingeman, R. Kahnoski, H. Mardis, S. Lacey, D. Goldfarb, M. Grasso and F. Coe (1998). "Supersaturation and Stone Composition in a Network of Dispersed Treatment Sites." Journal of Urology **159**(6): 1821-1825.

Asplin, J. R. (2002). "Hyperoxaluric Calcium Nephrolithiasis." Endocrinology and Metabolism Clinics of North America **31**(4): 927.

Asplin, J. R. (2008). "Evaluation of the Kidney Stone Patient." Seminars in Nephrology **28**(2): 99-110.

Asplin, J. R., J. H. Parks, M. S. Chen, J. C. Lieske, F. G. Toback, S. N. Pillay, Y. Nakagawa and F. L. Coe (1999). "Reduced Crystallization Inhibition by Urine from Men with Nephrolithiasis." Kidney International **56**(4): 1505-1516.

Becke, A. D. (1988). "Density-Functional Exchange-Energy Approximation with Correct Asymptotic Behavior." Physical Review A **38**(6): 3098-3100.

Boll, M., E. Sorensen and E. Balieu (1969). "Natually Occurring Lactones and Lactames-3. Absolute Configuration of Hydroxycitric Acid Lactones- Hibiscus Acid and Garcinia Acid." Acta Chemica Scandinavica **23**(1): 286.

Borghi, L., T. Meschi, F. Amato, A. Briganti, A. Novarini and A. Giannini (1996). "Urinary Volume, Water and Recurrences in Idiopathic Calcium Nephrolithiasis: A 5-Year Randomized Prospective Study." Journal of Urology **155**(3): 839-843.

Boyce, W. H. and J. S. King (1963). "1. Some Special Aspects of Metabolic Dysfunction-Present Concepts Concerning Origin of Matrix and Stones." Annals of the New York Academy of Sciences **104**(2): 563.

Brikowski, T. H., Y. Lotan and M. S. Pearle (2008). "Climate-Related Increase in the Prevalence of Urolithiasis in the United States." Proceedings of the National Academy of Sciences of the United States of America **105**(28): 9841-9846.

Burton, W. K., N. Cabrera and F. F. C. (1951). "The Growth of Crystals and the Equilibrium Structure of Their Surfaces." Philosophical Transactions of the Royal Society of London. Series A, Mathematical and Physical Sciences **243**(866): 299-358.

Burton, W. K., N. Cabrera and F. C. Frank (1951). "The Growth of Crystals and the Equilibrium Structure of Their Surfaces." Philosophical Transactions of the Royal Society of London **243**(A866): 299-360.

Bushinsky, D. A. (1998). "Nephrolithiasis." Journal of the American Society of Nephrology **9**(5): 917-924.

Cabrera, N. and D. A. Vermileya (1958). Growth of Crystals from Solution. Growth and Perfection of Crystals. D. R.H., R. B.W. and T. D. New York, Wiley**:** 393-410.

Cahn, J. W. and F. Larche (1982). "Surface Stress and the Chemical Equilibrium of Small Crystals - Ll. Solid Particles Embedded in a Solid Matrix." Acta Metallurgica **30**(1): 51-56.

Canales, B. K., L. Anderson, L. Higgins, J. Slaton, K. P. Roberts, N. T. Liu and M. Monga (2008). "Comprehensive Proteomic Analysis of Human Calcium Oxalate Monohydrate Kidney Stone Matrix." Journal of Endourology **22**(6): 1161-1167.

Chan, B. P. H., K. Vincent, G. A. Lajoie, H. A. Goldberg, B. Grohe and G. K. Hunter (2012). "On the Catalysis of Calcium Oxalate Dihydrate Formation by Osteopontin Peptides." Colloids and Surfaces B-Biointerfaces **96**: 22-28.

ChemAxon. "Hydroxycitric Acid." from http://www.chemicalize.org/structure/#!mol=hydroxycitrate&source=fp.

Chen, C. L., J. H. Qi, R. N. Zuckermann and J. J. DeYoreo (2011). "Engineered Biomimetic Polymers as Tunable Agents for Controlling Caco3 Mineralization." Journal of the American Chemical Society **133**(14): 5214-5217.

Chen, L., A. Xie, R. Jia, Y. Shen, W. Tang and C. Li (2007). "Influence of Bacillus Subtilis on the Growth of Calcium Oxalate." Crystal Research and Technology **42**(9): 881-885.

Chernov, A. A. (1989). "Formation of Crystals in Solutions." Contemporary Physics **30**(4): 251-276.

Cho, K. R., E. A. Salter, J. J. De Yoreo, A. Wierzbicki, S. Elhadj, Y. Huang and S. R. Qiu (2013). "Growth Inhibition of Calcium Oxalate Monohydrate Crystal by Linear Aspartic Acid Enantiomers Investigated by in Situ Atomic Force Microscopy." Crystengcomm **15**(1): 54-64.

Chou, T. C. (2006). "Theoretical Basis, Experimental Design, and Computerized Simulation of Synergism and Antagonism in Drug Combination Studies." Pharmacological Reviews **58**(3): 621-681.

Chung, J. and I. W. Kim (2011). "Effects of Some Polymeric Additives on the Cocrystallization of Caffeine." Journal of Crystal Growth **335**(1): 106-109.

Chung, J. H., I. Granja, M. G. Taylor, G. Mpourmpakis, J. R. Asplin and J. D. Rimer (2016). "Molecular Modifiers Reveal a Mechanism of Pathological Crystal Growth Inhibition." Nature **536**(7617): 446-+.

Coe, F. L. and J. R. Asplin (2010). "Stopping the Stones." Science **330**(6002): 325-326.

Coe, F. L., J. H. Parks and J. R. Asplin (1992). "Medical Progress- the Pathogenesis and Treatment of Kidney Stones." New England Journal of Medicine **327**(16): 1141-1152.

Coe, F. L., J. H. Parks and J. R. Asplin (1992). "Medical Progress - the Pathogenesis and Treatment of Kidney-Stones." New England Journal of Medicine **327**(16): 1141-1152.

Cook, A. F., P. K. Grover and R. L. Ryall (2009). "Face-Specific Binding of Prothrombin Fragment 1 and Human Serum Albumin to Inorganic and Urinary Calcium Oxalate Monohydrate Crystals." Bju International **103**(6): 826-835.

Davis, K. J., P. M. Dove and J. J. De Yoreo (2000). "The Role of Mg2+ as an Impurity in Calcite Growth." Science **290**(5494): 1134-1137.

De Yoreo, J. J., S. R. Qiu and J. R. Hoyer (2006). "Molecular Modulation of Calcium Oxalate Crystallization." American Journal of Physiology-Renal Physiology **291**(6): F1123-F1131.

De Yoreo, J. J. and P. G. Vekilov (2003). Principles of Crystal Nucleation and Growth. Biomineralization. P. M. Dove, J. J. De Yoreo and S. Weiner, Mineralogical Soc. America, Washington, DC. **54:** 57-93.

Deganello, S. and O. E. Piro (1981). "The Crystal Structure of Calcium Oxalate Monohydrate (Whewellite)." Neues Jahrbuch Fur Mineralogie-Monatshefte(2): 81-88.

Dey, A., G. de With and N. Sommerdijk (2010). "In Situ Techniques in Biomimetic Mineralization Studies of Calcium Carbonate." Chemical Society Reviews **39**(2): 397-409.

Dorozhkin, S. V. (2007). "Calcium Orthophosphates." Journal of Materials Science **42**(4): 1061-1095.

Dove, P. and J. De Yoreo (2004). Inhibition of Caco3 Crystallization by Small Molecules: The Magnesium Example. Nanoscale Structure and Assembly at Solid-Fluid Interfaces. X. Liu and J. De Yoreo, Kluwer Academic Publishers. **II**.

Dunlop, J. W. C. and P. Fratzl (2010). "Biological Composites." Annual Review of Materials Research **40**: 1-24.

Dussol, B., S. Geider, A. Lilova, F. Leonetti, P. Dupuy, M. Daudon, Y. Berland, J. C. Dagorn and J. M. Verdier (1995). "Analysis of the Soluble Organic Matrix of 5 Morphologically Different Kidney-Stones - Evidence for a Specific Role of Albumin in the Constitution of the Stone Protein Matrix." Urological Research **23**(1): 45-51.

Dyer, R. and B. E. C. Nordin (1967). "Urinary Crystals and Their Relation to Stone Formation." Nature **215**(5102): 751.

Elhadj, S., J. J. De Yoreo, J. R. Hoyer and P. M. Dove (2006). "Role of Molecular Charge and Hydrophilicity in Regulating the Kinetics of Crystal Growth." Proceedings of the National Academy of Sciences of the United States of America **103**(51): 19237-19242.

Elliot, J. S. and E. Eusebio (1967). "Calcium Oxalate Solubility: The Effect of Trace Metals." Investigative urology **4**(5): 428-430.

Elliot, J. S. and I. N. Rabinowitz (1980). "Calcium-Oxalate Crystalluria - Crystal Size in Urine." Journal of Urology **123**(3): 324-327.

Ettinger, B., C. Y. C. Pak, J. T. Citron, C. Thomas, B. AdamsHuet and A. Vangessel (1997). "Potassium-Magnesium Citrate Is an Effective Prophylaxis against Recurrent Calcium Oxalate Nephrolithiasis." Journal of Urology **158**(6): 2069-2073.

Evan, A. P., L. R. Willis, J. E. Lingeman and J. A. McAteer (1998). "Renal Trauma and the Risk of Long-Term Complications in Shock Wave Lithotripsy." Nephron **78**(1): 1-8.

Evans, J. S. (2008). ""Tuning in" to Mollusk Shell Nacre- and Prismatic-Associated Protein Terminal Sequences. Implications for Biomineralization and the Construction of High Performance Inorganic-Organic Composites." Chemical Reviews **108**(11): 4455-4462.

Falini, G., S. Albeck, S. Weiner and L. Addadi (1996). "Control of Aragonite or Calcite Polymorphism by Mollusk Shell Macromolecules." Science **271**(5245): 67-69.

Farmanesh, S., B. G. Alamani and J. D. Rimer (2015). "Identifying Alkali Metal Inhibitors of Crystal Growth: A Selection Criterion Based on Ion Pair Hydration Energy." Chemical Communications **51**(73): 13964-13967.

Farmanesh, S., J. Chung, D. Chandra, R. D. Sosa, P. Karande and J. D. Rimer (2013). "High-Throughput Platform for Design and Screening of Peptides as Inhibitors of Calcium Oxalate Monohydrate Crystallization." Journal of Crystal Growth **373**: 13-19.

Farmanesh, S., J. Chung, R. D. Sosa, J. H. Kwak, P. Karande and J. D. Rimer (2014). "Natural Promoters of Calcium Oxalate Monohydrate Crystallization." Journal of the American Chemical Society **136**(36): 12648-12657.

Farmanesh, S., S. Ramamoorthy, J. Chung, J. R. Asplin, P. Karande and J. D. Rimer (2014). "Specificity of Growth Inhibitors and Their Cooperative Effects in Calcium Oxalate Monohydrate Crystallization." Journal of the American Chemical Society **136**(1): 367-376.

Feyereisen, M., G. Fitzgerald and A. Komornicki (1993). "Use of Approximate Integrals in Ab Initio Theory- an Application in Mp2 Enegry Calculations." Chemical Physics Letters **208**(5-6): 359-363.

Finlayson, B. and A. Smith (1974). "Stability of First Dissociable Proton of Uric-Acid." Journal of Chemical and Engineering Data **19**(1): 94-97.

Fleming, D. E., W. van Bronswijk and R. L. Ryall (2001). "A Comparative Study of the Adsorption of Amino Acids on to Calcium Minerals Found in Renal Calculi." Clinical Science **101**(2): 159-168.

Frank, F. C. (1949). "The Influence of Dislocations on Crystal Growth." Discussions of the Faraday Society **5**: 48-54.

Frank, F. C. (1952). "Crystal Growth and Dislocations." Advanced Physics **1**(1): 91-109.

Friddle, R. W., M. L. Weaver, S. R. Qiu, A. Wierzbicki, W. H. Casey and J. J. De Yoreo (2010). "Subnanometer Atomic Force Microscopy of Peptide-Mineral Interactions Links Clustering and Competition to Acceleration and Catastrophe." Proceedings of the National Academy of Sciences of the United States of America **107**(1): 11-15.

Fu, G., S. R. Qiu, C. A. Orme, D. E. Morse and J. J. De Yoreo (2005). "Acceleration of Calcite Kinetics by Abalone Nacre Proteins." Advanced Materials **17**(22): 2678-+.

Gilmer, G. H., R. Ghez and N. Cabrera (1971). "Analysis of Combined Surface and Volume Diffusion Processes in Crystal Growth." Journal of Crystal Growth **8**(1): 79.

Graether, S. P., M. J. Kuiper, S. M. Gagne, V. K. Walker, Z. C. Jia, B. D. Sykes and P. L. Davies (2000). "Beta-Helix Structure and Ice-Binding Properties of a Hyperactive Antifreeze Protein from an Insect." Nature **406**(6793): 325-328.

Grimme, S., J. Antony, S. Ehrlich and H. Krieg (2010). "A Consistent and Accurate Ab Initio Parametrization of Density Functional Dispersion Correction (Dft-D) for the 94 Elements H-Pu." Journal of Chemical Physics **132**(15).

Grohe, B., B. P. H. Chan, E. S. Sorensen, G. Lajoie, H. A. Goldberg and G. K. Hunter (2011). "Cooperation of Phosphates and Carboxylates Controls Calcium Oxalate Crystallization in Ultrafiltered Urine." Urological Research **39**(5): 327-338.

Grohe, B., J. O'Young, D. A. Ionescu, G. Lajoie, K. A. Rogers, M. Karttunen, H. A. Goldberg and G. K. Hunter (2007). "Control of Calcium Oxalate Crystal Growth by Face-Specific Adsorption of an Osteopontin Phosphopeptide." Journal of the American Chemical Society **129**(48): 14946-14951.

Grohe, B., J. O'Young, A. Langdon, M. Karttunen, H. A. Goldberg and G. K. Hunter (2011). "Citrate Modulates Calcium Oxalate Crystal Growth by Face-Specific Interactions." Cells Tissues Organs **194**(2-4): 176-181.

Guo, S. W., M. D. Ward and J. A. Wesson (2002). "Direct Visualization of Calcium Oxalate Monohydrate Crystallization and Dissolution with Atomic Force Microscopy and the Role of Polymeric Additives." Langmuir **18**(11): 4284-4291.

Gvozdev, N. V., E. V. Petrova, T. G. Chernevich, O. A. Shustin and L. N. Rashkovich (2004). "Atomic Force Microscopy of Growth and Dissolution of Calcium Oxalate Monohydrate (Com) Crystals." Journal of Crystal Growth **261**(4): 539-548.

Hallson, P. C. and G. A. Rose (1979). "Uromucoids and Urinary Stone Formation." Lancet **1**(8124): 1000-1002.

Hess, B., Y. Nakagawa, J. H. Parks and F. L. Coe (1991). "Molecular Abnormality of Tamm-Horsfall Glycoprotein in Calcium Oxalate Nephrolithiasis." American Journal of Physiology **260**(4): F569-F578.

Hess, B., L. Zipperle and P. Jaeger (1993). "Citrate and Calcium Effects on Tamm-Horsfall Glycoprotein as a Modifier of Calcium Oxalate Crystal Aggregation." American Journal of Physiology **265**(6): F784-F791.

Hida, H., T. Yamada and Y. Yamada (2006). "Absolute Configuration of Hydroxycitric Acid Produced by Microorganisms." Bioscience Biotechnology and Biochemistry **70**(8): 1972-1974.

Hiemenz, P. C. and R. Rajagopalan (1997). Principles of Colloid and Surface Chemistry. New York.

Hofbauer, J., I. Steffan, K. Hobarth, G. Vujicic, H. Schwetz, G. Reich and O. Zechner (1991). "Trace-Elements and Urinary Stone Formation: New Aspects of the Pathological Mechanism of Urinary Stone Formation." Journal of Urology **145**(1): 93-96.

Holan, K. R., R. T. Holzbach, R. E. Hermann, A. M. Cooperman and W. J. Claffey (1979). "Nucleation Time- Key Factor in the Pathogenesis of Cholesterol Gallstone Disease." Gastroenterology **77**(4): 611-617.

Hottenhuis, M. H. J. and C. B. Lucasius (1989). "The Influence of Internal Crystal Structure on Surface Morphology: In Situ Observations of Potassium Hydrogen Phthalate (010)." Journal of Crystal Growth **94**(3): 708-720.

Hoyer, J. R., J. R. Asplin and L. Otvos (2001). "Phosphorylated Osteopontin Peptides Suppress Crystallization by Inhibiting the Growth of Calcium Oxalate Crystals." Kidney International **60**(1): 77-82.

Huang, M. L., D. Ehre, Q. Jiang, C. H. Hu, K. Kirshenbaum and M. D. Ward (2012). "Biomimetic Peptoid Oligomers as Dual-Action Antifreeze Agents." Proceedings of the National Academy of Sciences of the United States of America **109**(49): 19922-19927.

Hug, S., B. Grohe, J. Jalkanen, B. Chan, B. Galarreta, K. Vincent, F. Lagugne-Labarthet, G. Lajoie, H. A. Goldberg, M. Karttunen and G. K. Hunter (2012). "Mechanism of Inhibition of Calcium Oxalate Crystal Growth by an Osteopontin Phosphopeptide." Soft Matter **8**(4): 1226-1233.

Jung, T., X. X. Sheng, C. K. Choi, W. S. Kim, J. A. Wesson and M. D. Ward (2004). "Probing Crystallization of Calcium Oxalate Monohydrate and the Role of Macromolecule Additives with in Situ Atomic Force Microscopy." Langmuir **20**(20): 8587-8596.

Killian, C. E., R. A. Metzler, Y. U. T. Gong, I. C. Olson, J. Aizenberg, Y. Politi, F. H. Wilt, A. Scholl, A. Young, A. Doran, M. Kunz, N. Tamura, S. N. Coppersmith and P. Gilbert (2009). "Mechanism of Calcite Co-Orientation in the Sea Urchin Tooth." Journal of the American Chemical Society **131**(51): 18404-18409.

Klamt, A. and G. Schuurmann (1993). "Cosmo- a New Approach to Dielectric Screening in Solvents with Explicit Expressions for the Screening Energy and Its Gradient." Journal of the Chemical Society, Perkin Transactions 2(5): 799-805.

Knorle, R., P. Schnierle, A. Koch, N. P. Buchholz, F. Hering, H. Seiler, T. Ackermann and G. Rutishauser (1994). "Tamm-Horsfall Glycoprotein- Role in Inhibition and Promotion of Renal Calcium Oxalate Stone Formation Studied with Fourier-Transform Infrared Spectroscopy." Clinical Chemistry **40**(9): 1739-1743.

Krishnamurty, K. V. and G. M. Harris (1961). Chemical Reviews **61**(3).

Langdon, A., G. R. Wignall, K. Rogers, E. S. Sorensen, J. Denstedt, B. Grohe, H. A. Goldberg and G. K. Hunter (2009). "Kinetics of Calcium Oxalate Crystal Growth in the Presence of Osteopontin Isoforms: An Analysis by Scanning Confocal Interference Microcopy." Calcified Tissue International **84**(3): 240-248.

Langley, S. E. M. and C. H. Fry (1997). "The Influence of Ph on Urinary Ionized Ca2+ : Differences between Urinary Tract Stone Formers and Normal Subjects." British Journal of Urology **79**(1): 8-14.

Levinson, A. A., M. Nosal, M. Davidman, E. L. Prien and R. G. Stenvenson (1978). "Trace Elements in Kidney Stones from Three Areas in the United States." Investigative urology **15**(4): 270-274.

Lewis, Y. and S. Neelakantan (1965). "(-)-Hydroxycitric Acid - the Principal Acid in the Fruits of *Garcinia Cambogia*." Phytochemistry **4**: 619-625.

Linnikov, O. D. (2000). "Investigation of the Initial Period of Sulphate Scale Formation - Part 3. Variations of Calcium Sulphate Crystal Growth Rates at Its Crystallization on a Heat-Exchange Surface." Desalination **128**(1): 47-55.

Loe, Y. C. C., N. Bergeron, N. Rodriguez and J. M. Schwarz (2001). "Gas Chromatography/Mass Spectrometry Method to Quantify Blood Hydroxycitrate Concentration." Analytical Biochemistry **292**(1): 148-154.

Lovette, M. A., A. R. Browning, D. W. Griffin, J. P. Sizemore, R. C. Snyder and M. F. Doherty (2008). "Crystal Shape Engineering." Industrial & Engineering Chemistry Research **47**(24): 9812-9833.

Lupulescu, A. I. and J. D. Rimer (2014). "In Situ Imaging of Silicalite-1 Surface Growth Reveals the Mechanism of Crystallization." Science **344**(6185): 729-732.

Lutsko, J. F., N. Gonzalez-Segredo, M. A. Duran-Olivencia, D. Maes, A. E. S. Van Driessche and M. Sleutel (2014). "Crystal Growth Cessation Revisited: The Physical Basis of Step Pinning." Crystal Growth & Design **14**(11): 6129-6134.

Madsen, H. E. L. (2008). "Influence of Foreign Metal Ions on Crystal Growth and Morphology of Brushite (Cahpo4, 2h(2)O) and Its Transformation to Octacalcium Phosphate and Apatite." Journal of Crystal Growth **310**(10): 2602-2612.

Makarov, V. A., B. K. Andrews, P. E. Smith and B. M. Pettitt (2000). "Residence Times of Water Molecules in the Hydration Sites of Myoglobin." Biophysical Journal **79**(6): 2966-2974.

Malivuk, D. A., A. A. Zekic, M. M. Mitrovic and B. M. Misailovic (2013). "Dissolution of Sodium Chlorate Crystals in Supersaturated Solutions." Journal of Crystal Growth **377**: 164-169.

Markov, I. V. (2003). Crystal Growth for Beginners: Fundamentals of Nucleation, Crystal Growth, and Epitaxy. Singapore, World Scientific.

Martell, A. E. and R. M. Smith (1982). Tricarboxylic Acids. Critical Stability Constants New York, Plenum Press. **5:** 329-330.

Meldrum, F. C. (2003). "Calcium Carbonate in Biomineralisation and Biomimetic Chemistry." International Materials Reviews **48**(3): 187-224.

Meldrum, F. C. and H. Colfen (2008). "Controlling Mineral Morphologies and Structures in Biological and Synthetic Systems." Chemical Reviews **108**(11): 4332-4432.

Meyer, J. L. and W. C. Thomas (1982). "Trace Metal-Citric Acid Complexes as Inhibitors of Calcification and Crystal Growth. Ii. Efects of Fe(Iii), Cr(Iii) and Al(Iii) Complexes on Calicum Oxalate Crystal Growth." Journal of Urology **128**(6): 1376-1378.

Millan, A. (2001). "Crystal Growth Shape of Whehellite Polymorphs: Influence of Structure Distorrions on Crystal Shape." Crystal Growth & Design **1**(3): 245-254.

Millan, A. (2001). "Crystal Growth Shape of Whewellite Polymorphs: Influence of Structure Distortions on Crystal Shape." Crystal Growth & Design **1**(3): 245-254.

Millan, A., O. Sohnel and F. Grases (1997). "The Influence of Crystal Morphology on the Kinetics of Growth of Calcium Oxalate Monohydrate." Journal of Crystal Growth **179**(1-2): 231-239.

Mo, L., L. Liaw, A. P. Evan, A. J. Sommer, J. C. Lieske and X. R. Wu (2007). "Renal Calcinosis and Stone Formation in Mice Lacking Osteopontin, Tamm-Horsfall Protein, or Both." American Journal of Physiology-Renal Physiology **293**(6): F1935-F1943.

Moe, O. W. (2006). "Kidney Stones: Pathophysiology and Medical Management." Lancet **367**(9507): 333-344.

Moe, O. W., M. S. Pearle and K. Sakhaee (2011). "Pharmacotherapy of Urolithiasis: Evidence from Clinical Trials." Kidney International **79**(4): 385-392.

Mpourmpakis, G., S. Caratzoulas and D. G. Vlachos (2010). "What Controls Au Nanoparticle Dispersity During Growth?" Nano Letters **10**(9): 3408-3413.

Munoz, J. A. and M. Valiente (2005). "Effects of Trace Metals on the Inhibition of Calcium Oxalate Crystallization." Urological Research **33**(4): 267-272.

Nancollas, G. H. and G. L. Gardner (1974). "Kinetics of Crystal-Growth of Calcium-Oxalate Monohydrate." Journal of Crystal Growth **21**(2): 267-276.

Nielsen, L. C., J. J. De Yoreo and D. J. DePaolo (2013). "General Model for Calcite Growth Kinetics in the Presence of Impurity Ions." Geochimica Et Cosmochimica Acta **115**: 100-114.

Nordin, B. E. C. and W. G. Robertson (1966). "Calcium Phosphate and Oxalate Ion Products in Normal and Stone-Forming Urines." Bmj-British Medical Journal **1**(5485): 450-453.

Olafson, K. N., M. A. Ketchum, J. D. Rimer and P. G. Vekilov (2015). "Mechanisms of Hematin Crystallization and Inhibition by the Antimalarial Drug Chloroquine." Proceedings of the National Academy of Sciences of the United States of America **112**(16): 4946-4951.

Olafson, K. N., R. Li, B. G. Alamani and J. D. Rimer (2016). "Engineering Crystal Modifiers: Bridging Classical and Nonclassical Crystallization." Chemistry of Materials **28**(23): 8453-8465.

Orme, C. A., A. Noy, A. Wierzbicki, M. T. McBride, M. Grantham, H. H. Teng, P. M. Dove and J. J. DeYoreo (2001). "Formation of Chiral Morphologies through Selective Binding of Amino Acids to Calcite Surface Steps." Nature **411**(6839): 775-779.

Pak, C. Y. C. (1994). "Citrate and Renal Calculi: An Update." Mineral and Electrolyte Metabolism **20**(6): 371-377.

Pak, C. Y. C., K. Sakhaee, C. Crowther and L. Brinkley (1980). "Evidence Justifying a High Fluid Intake in Treatment of Nephrolothiasis." Annals of Internal Medicine **93**(1): 36-39.

Pande, A., J. Pande, N. Asherie, A. Lomakin, O. Ogun, J. King and G. B. Benedek (2001). "Crystal Cataracts: Human Genetic Cataract Caused by Protein Crystallization." Proceedings of the National Academy of Sciences of the United States of America **98**(11): 6116-6120.

Parks, J. H., E. M. Worcester, F. L. Coe, A. P. Evan and J. E. Lingeman (2004). "Clinical Implications of Abundant Calcium Phosphate in Routinely Analyzed Kidney Stones." Kidney International **66**(2): 777-785.

Pearle, M. S., E. A. Calhoun, G. C. Curhan and P. Urologic Diseases of America (2005). "Urologic Diseases in America Project: Urolithiasis." Journal of Urology **173**(3): 848-857.

Perdew, J. P. (1986). "Density-Functional Approximation for the Correlation Energy of the Inhomogeneous Electron Gas." Physical Review B **33**(12): 8822-8824.

Petrova, E. V., N. V. Gvozdev and L. N. Rashkovich (2004). "Growth and Dissolution of Calcium Oxalate Monohydrate (Com) Crystals." Journal of Optoelectronics and Advanced Materials **6**(1): 261-268.

Phillips, R., V. S. Hanchanale, A. Myatt, B. Somani, G. Nabi and C. S. Biyani (2015). "Citrate Salts for Preventing and Treating Calcium Containing Kidney Stones in Adults." The Cochrane database of systematic reviews **10**: CD010057-CD010057.

Pragasam, V., P. Kalaiselvi, B. Subashini, K. Sumitra and P. Varalakshmi (2005). "Structural and Functional Modification of Thp on Nitration: Comparison with Stone Formers Thp." Nephron. Physiology **99**(1): p28-34.

Pramanik, R., J. R. Asplin, M. E. Jackson and J. C. Williams (2008). "Protein Content of Human Apatite and Brushite Kidney Stones: Significant Correlation with Morphologic Measures." Urological Research **36**(5): 251-258.

Qiu, S. R. and C. A. Orme (2008). "Dynamics of Biomineral Formation at the near-Molecular Level." Chemical Reviews **108**(11): 4784-4822.

Qiu, S. R., A. Wierzbicki, C. A. Orme, A. M. Cody, J. R. Hoyer, G. H. Nancollas, S. Zepeda and J. J. De Yoreo (2004). "Molecular Modulation of Calcium Oxalate Crystallization by Osteopontin and Citrate." Proceedings of the National Academy of Sciences of the United States of America **101**(7): 1811-1815.

Qiu, S. R., A. Wierzbicki, E. A. Salter, S. Zepeda, C. A. Orme, J. R. Hoyer, G. H. Nancollas, A. M. Cody and J. J. De Yoreo (2005). "Modulation of Calcium Oxalate Monohydrate Crystallization by Citrate through Selective Binding to Atomic Steps." Journal of the American Chemical Society **127**(25): 9036-9044.

Riese, R. J. and K. Sakhaee (1992). "Uric Acid Nephrolithiasis- Pathogenesis and Treatment." Journal of Urology **148**(3): 765-771.

Rimer, J. D., Z. An, Z. Zhu, M. H. Lee, D. S. Goldfarb, J. A. Wesson and M. D. Ward (2010). "Crystal Growth Inhibitors for the Prevention of L-Cystine Kidney Stones through Molecular Design." Science **330**(6002): 337-341.

Rimer, J. D., Z. H. An, Z. N. Zhu, M. H. Lee, D. S. Goldfarb, J. A. Wesson and M. D. Ward (2010). "Crystal Growth Inhibitors for the Prevention of L-Cystine Kidney Stones through Molecular Design." Science **330**(6002): 337-341.

Risthaus, P., D. Bosbach, U. Becker and A. Putnis (2001). "Barite Scale Formation and Dissolution at High Ionic Strength Studied with Atomic Force Microscopy." Colloids and Surfaces a-Physicochemical and Engineering Aspects **191**(3): 201-214.

Ristic, R. I., J. N. Sherwood and K. Wojciechowski (1988). "Assessment of the Strain in Small Sodium-Chlorate Crystals and Its Relation to Growth Rate Dispersion." Journal of Crystal Growth **91**(1-2): 163-168.

Robertson, W. G. (1969). "Measurement of Ionized Calcium in Biological Fluids." Clinica Chimica Acta **24**(1): 149-157.

Ronco, P., M. Brunisholz, M. Geniteau-Legendre, F. Chatelet, P. Verroust and G. Richet (1987). "Physiopathologic Aspects of Tamm-Horsfall Protein: A Phylogenetically Conserved Marker of the Thick Ascending Limb of Henle's Loop." Advances in nephrology from the Necker Hospital **16**: 231-249.

Rosenberger, F. (1986). "Inorganic and Protein Crystal Growth: Similarities and Differences." Journal of Crystal Growth **76**(3): 618-636.

Ryall, R. L., R. M. Harnett, C. M. Hibberd, K. A. Edyvane and V. R. Marshall (1991). "Effects of Chondroitin Sulfate, Human Serum-Albumin and Tamm-Horsfall Mucoprotein on Calcium-Oxalate Crystallization in Undiluted Human Urine." Urological Research **19**(3): 181-188.

Ryall, R. L., R. M. Harnett and V. R. Marshall (1981). "The Effect of Urine, Pyrophosphate, Citrate, Magnesium and Glycosaminoglycans on the Growth and Aggregation of Calcium-Oxalate Crystals Invitro." Clinica Chimica Acta **112**(3): 349-356.

Sakhaee, K. (2009). "Recent Advances in the Pathophysiology of Nephrolithiasis." Kidney International **75**(6): 585-595.

Sakhaee, K., B. Adams-Huet, O. W. Moe and C. Y. C. Pak (2002). "Pathophysiologic Basis for Normouricosuric Uric Acid Nephrolithiasis." Kidney International **62**(3): 971-979.

Sayan, P., S. T. Sargut and B. Kiran (2009). "Calcium Oxalate Crystallization in the Presence of Amino Acids, Proteins and Carboxylic Acids." Crystal Research and Technology **44**(8): 807-817.

Scales, C. D. J., A. C. Smith, J. M. Hanley and C. S. Saigal (2012). "Prevalence of Kidney Stones in the United States." European Urology **62**(1): 160-165.

Scheinman, S. J., J. P. D. Cox, S. E. Lloyd, S. H. S. Pearce, P. V. Salenger, R. R. Hoopes, D. A. Bushinsky, O. Wrong, J. R. Asplin, C. B. Langman, A. G. W. Norden and R. V. Thakker (2000). "Isolated Hypercalciuria with Mutation in Clcn5: Relevance to Idiopathic Hypercalciuria." Kidney International **57**(1): 232-239.

Scurr, D. S. and W. G. Robertson (1986). "Modifiers of Calcium Oxalate Crystallization Found in Urine. 3. Studies on the Role of Tamm-Horsfall Mucoprotein and of Ionic Strength." Journal of Urology **136**(2): 505-507.

Sheng, X. X., T. S. Jung, J. A. Wesson and M. D. Ward (2005). "Adhesion at Calcium Oxalate Crystal Surfaces and the Effect of Urinary Constituents." Proceedings of the National Academy of Sciences of the United States of America **102**(2): 267-272.

Shirane, Y. and S. Kagawa (1993). "Scanning Electron Microscopic Study of the Effect of Citrate and Pyrophosphate on Calcium Oxalate Crystal Morphology." Journal of Urology **150**(6): 1980-1983.

Shirane, Y., Y. Kurokawa, S. Miyashita, H. Komatsu and S. Kagawa (1999). "Study of Inhibition Mechanisms of Glycosaminoglycans on Calcium Oxalate Monohydrate Crystals by Atomic Force Microscopy." Urological Research **27**(6): 426-431.

Sizemore, J. P. and M. F. Doherty (2009). "A New Model for the Effect of Molecular Imposters on the Shape of Faceted Molecular Crystals." Crystal Growth & Design **9**(6): 2637-2645.

Snyder, R. C. and M. F. Doherty (2009). "Predicting Crystal Growth by Spiral Motion." Proceedings of the Royal Society A: Mathematical, Physical and Engineering Sciences **465**(2104): 1145-1171.

Stamatelou, K. K., M. E. Francis, C. A. Jones, L. M. Nyberg and G. C. Curhan (2003). "Time Trends in Reported Prevalence of Kidney Stones in the United States: 1976-1994." Kidney International **63**(5): 1817-1823.

Stephenson, A. E., J. L. Hunter, N. Han, J. J. DeYoreo and P. M. Dove (2011). "Effect of Ionic Strength on the Mg Content of Calcite: Toward a Physical Basis for Minor Element Uptake During Step Growth." Geochimica Et Cosmochimica Acta **75**(15): 4340-4350.

Streit, J., L. C. Tran-Ho and E. Konigsberger (1998). "Solubility of the Three Calcium Oxalate Hydrates in Sodium Chloride Solutions and Urine-Like Liquors." Monatshefte Fur Chemie **129**(12): 1225-1236.

Taller, A., B. Grohe, K. A. Rogers, H. A. Goldberg and G. K. Hunter (2007). "Specific Adsorption of Osteopontin and Synthetic Polypeptides to Calcium Oxalate Monohydrate Crystals." Biophysical Journal **93**(5): 1768-1777.

Tazzoli, V. and C. Domeneghetti (1980). "The Crystal-Structures of Whewellite and Weddellite - Reexamination and Comparison." American Mineralogist **65**(3-4): 327-334.

Tazzoli, V. and C. Domeneghetti (1980). "The Crystal Structures of Whewellite and Weddellite- Reexamination and Comparison." American Mineralogist **65**(3-4): 327-334.

Tomazic, B. B. and G. H. Nancollas (1979). "A Study of the Phase-Transformation of Calcium Oxalate Trihydrate-Monohydrate." Investigative Urology **16**(5): 329-335.

van der Heijden, A. E. D. M. and J. P. van der Eerden (1992). "Growth Rate Dispersion: The Role of Lattice Strain." Journal of Crystal Growth **118**: 14-26.

van Enckevort, W. J. P. and J. H. Los (2008). ""Tailor-Made" Inhibitors in Crystal Growth: A Monte Carlo Simulation Study." Journal of Physical Chemistry C **112**(16): 6380-6389.

van Loon, L. J. C., J. J. M. Van Rooijen, B. Niesen, H. Verhagen, W. H. M. Saris and A. J. M. Wagenmakers (2000). "Effects of Acute (-)-Hydroxycitrate Supplementation on Substrate Metabolism at Rest and During Exercise in Humans." American Journal of Clinical Nutrition **72**(6): 1445-1450.

Verplaetse, H., R. M. H. Verbeeck, A. Verbaeys and W. Oosterlinck (1986). "Solubility of Calcium-Oxalate Monohydrate and Hydroxyapatite in Edta Solutions." Journal of Urology **135**(3): 608-611.

Viswanathan, P., J. D. Rimer, A. M. Kolbach, M. D. Ward, J. G. Kleinman and J. A. Wesson (2011). "Calcium Oxalate Monohydrate Aggregation Induced by Aggregation of Desialylated Tamm-Horsfall Protein." Urological Research **39**(4): 269-282.

Voronkov, V. V. and L. N. Rashkovich (1994). "Step Kinetics in the Presence of Mobile Adsorbed Impurity." Journal of Crystal Growth **144**(1-2): 107-115.

Wandt, M. A. E. and M. A. B. Pougnet (1986). "Simultaneous Determination of Major and Trace-Elements in Urinary Calculi by Microwave-Assisted Digestion and Inductively Coupled Plasma Atomic Emission Spectrometirc Analysis." Analyst **111**(11): 1249-1253.

Wandt, M. A. E. and L. G. Underhill (1988). "Covariance Biplot Analysis of Trace-Element Concentrations in Urinary Stones." British Journal of Urology **61**(6): 474-481.

Wang, L. and G. H. Nancollas (2008). "Calcium Orthophosphates: Crystallization and Dissolution." Chemical Reviews **108**(11): 4628-4669.

Wang, L. J., J. J. De Yoreo, X. Y. Guan, S. R. Qiu, J. R. Hoyer and G. H. Nancollas (2006). "Constant Composition Studies Verify the Utility of the Cabrera-Vermilyea (C-V) Model in Explaining Mechanisms of Calcium Oxalate Monohydrate Crystallization." Crystal Growth & Design **6**(8): 1769-1775.

Wang, L. J., X. Y. Guan, R. K. Tang, J. R. Hoyer, A. Wierzbicki, J. J. De Yoreo and G. H. Nancollas (2008). "Phosphorylation of Osteopontin Is Required for Inhibition of Calcium Oxalate Crystallization." Journal of Physical Chemistry B **112**(30): 9151-9157.

Wang, L. J., S. R. Qiu, W. Zachowicz, X. Y. Guan, J. J. DeYoreo, G. H. Nancollas and J. R. Hoyer (2006). "Modulation of Calcium Oxalate Crystallization by Linear Aspartic Acid-Rich Peptides." Langmuir **22**(17): 7279-7285.

Wang, L. J., W. Zhang, S. R. Qiu, W. J. Zachowicz, X. Y. Guan, R. K. Tang, J. R. Hoyer, J. J. De Yoreo and G. H. Nancollas (2006). "Inhibition of Calcium Oxalate Monohydrate Crystallization by the Combination of Citrate and Osteopontin." Journal of Crystal Growth **291**(1): 160-165.

Weaver, M. L., S. R. Qiu, J. R. Hoyer, W. H. Casey, G. H. Nancollas and J. J. De Yoreo (2006). "Improved Model for Inhibition of Pathological Mineralization Based on Citrate-Calcium Oxalate Monohydrate Interaction." Chemphyschem **7**(10): 2081-2084.

Weaver, M. L., S. R. Qiu, J. R. Hoyer, W. H. Casey, G. H. Nancollas and J. J. De Yoreo (2007). "Inhibition of Calcium Oxalate Monohydrate Growth by Citrate and the Effect of the Background Electrolyte." Journal of Crystal Growth **306**(1): 135-145.

Weaver, M. L., S. R. Qiu, J. R. Hoyer, W. H. Casey, G. H. Nancollas and J. J. De Yoreo (2009). "Surface Aggregation of Urinary Proteins and Aspartic Acid-Rich Peptides on the Faces of Calcium Oxalate Monohydrate Investigated by in Situ Force Microscopy." Calcified Tissue International **84**(6): 462-473.

Weigend, F. and M. Haser (1997). "Ri-Mp2: First Derivatives and Global Consistency." Theoretical Chemistry Accounts **97**(1-4): 331-340.

Weigend, F., M. Haser, H. Patzelt and R. Ahlrichs (1998). "Ri-Mp2: Optimized Auxiliary Basis Sets and Demonstration of Efficiency." Chemical Physics Letters **294**(1-3): 143-152.

Weissbuch, I., L. Addadi, M. Lahav and L. Leiserowitz (1991). "Molecular Recognition at Crystal Interfaces." Science **253**(5020): 637-645.

Weissbuch, I., M. Lahav and L. Leiserowitz (2003). "Toward Stereochentical Control, Monitoring, and Understanding of Crystal Nucleation." Crystal Growth & Design **3**(2): 125-150.

Weissbuch, I. and L. Leiserowitz (2008). "Interplay between Malaria, Crystalline Hemozoin Formation, and Antimalarial Drug Action and Design." Chemical Reviews **108**(11): 4899-4914.

Wesson, J. A., R. J. Johnson, M. Mazzali, A. M. Beshensky, S. Stietz, C. Giachelli, L. Liaw, C. E. Alpers, W. G. Couser, J. G. Kleinman and J. Hughes (2003). "Osteopontin Is a Critical Inhibitor of Calcium Oxalate Crystal Formation and Retention in Renal Tubules." Journal of the American Society of Nephrology **14**(1): 139-147.

Wesson, J. A. and M. D. Ward (2007). "Pathological Biomineralization of Kidney Stones." Elements **3**(6): 415-421.

Winn, D. and M. F. Doherty (2000). "Modeling Crystal Shapes of Organic Materials Grown from Solution." American Institue of Chemical Engineers Journal **46**(7): 1348-1367.

Yachantha, C., R. Z. Hossain, K. Yamakawa, K. Sugaya, P. Tosukhowong, Y. Ogawa and S. Saito (2009). "Effect of Potassium Depletion on Urinary Stone Risk Factors in Wistar Rats." Urological Research **37**(6): 311-316.

Young, J. R., J. M. Didymus, P. R. Bown, B. Prins and S. Mann (1992). "Crystal Assembly and Phylogenetic Evolution in Heterococcoliths." Nature **356**(6369): 516-518.

Appendix A

Chapter 1 Supplementary Information

A1. Calcium oxalate monohydrate crystal system

There are different crystal index systems for COM crystals reported in the literature. $P2_1/c$ space group was reported by Tazzoli and Domeneghetti (Tazzoli and Domeneghetti 1980) with unit cell parameter a = 6.290 Å, b = 14.580 Å, and c = 10.116 Å (β= 109.46^o) and $P2_1/n$ space group was reported by Deganello and Piro (Deganello and Piro 1981) with unit cell parameter a = 9.978 Å, b = 14.5884 Å, and c = 6.2913 Å (β= 107.05^o). This thesis consistently used index system reported by Tazzoli.

Table A1 COM crystal face indices.

Tazzoli	Deganello	Goldschmidt
{100}	{-101}	e {-101}
{101}	{010}	b {010}
{001}	{100}	c {001}
{10-1}	{001}	a {100}
{011}	{110}	y {021}
{11-1}	{011}	r {210}
{10-2}	{101}	μ {101}
{021}	{120}	x {011}
{121}	{22-1}	Φ {112}
{12-1}	{021}	m {110}
{112}	{31-1}	p {21-6}
{013}	{310}	w {061}
{031}	{130}	I {032}
{131}	{23-1}	{23-4}
{13-1}	{031}	n {230}
{12-3}	{221}	f {112}
{140}	{14-1}	δ {121}
{14-1}	{041}	u {120}
{15-1}	{26-1}	d {250}
{161}	{26-1}	s {13-2}

{16-1} {061} l {130}

A2. Stone treatment

Table A2 COM stone treatment.

Diagnostic Evaluation	Interventions/Recommendations
Stone analysis, if possible	- Appropriate protein intake (< 30% of total caloric intake) - Calcium supplements (calcium citrate if also desire to raise urine citrate level) - Check serum 25-hydroxyvitamin D levels (low limit < 30 ng/mL or 74.88 nM) - Take > 250 mg/dose, or total calcium > 850 mg/day with meals - Thiazide diuretics (e.g., hydrochlorothiazide) 25 to 50 mg/day - Vitamin D increases intestinal calcium absorption and renal calcium and phosphate absroption
24-hour urine oxalate: upper level > 40 mg/day	- Diet with moderate amount of fruits and vegetables (do not restrict calcium) - Consider magnesium potassium citrate supplementation - Moderate vitamin C intake by dietary sources rather than supplements - Restrict high oxalate foods (more than 6 mg/serving), such as beans, spinach, rhubarb, chocolate, wheat, nuts, and berries - Magnesium potassium citrate: two tablets three times/day with meals
24-hour urine calcium (mg calcium/g creatinine): upper level > 210 for adult men, > 275 for adult women	- Sodium restriction of 2 g/day or less - Do not restrict calcium intake below recommendations - Avoid foods high in salt and do not add salt to food
24-hour urine magnesium: lower level < 70 mg/day	- Increase dietary sources of magnesium - Consider magnesium potassium citrate supplementation - Eat fish, nuts, grains, yogurt

	- Magnesium potassium citrate: two tablets three times/day with meals
24-hour urine citrate: lower level < 450 mg/day for adult men, < 550 mg/day for adult women	- Citrate supplementation - Add lemon or lime juice in water - Potassium citrate 10 to 20 mEq orally with meals - Calcium citrate: two 500 mg tablets/day with meals

Appendix B

Chapter 3 Supplementary Information

B1. Citrate and hydroxycitrate speciation

The pH of crystallization media impacts the net charge of the modifier. Both citrate (CA) and hydroxycitrate (HCA) have three dissociation constants corresponding to each of their carboxylic acid groups. In physiologically relevant environments, such as the kidney, the pH of urine varies between 5 and 8 (Asplin 2008). *In vitro* COM crystallization assays are performed at approximately neutral pH. For instance, the growth solutions employed in this study are pH = 6.2 ± 0.2, which is identical to previous *in vitro* assays published by Rimer and coworkers (Farmanesh, Chung et al., 2013; Farmanesh, Chung et al., 2014; Farmanesh, Ramamoorthy et al., 2014; Farmanesh, Alamani et al., 2015). As shown in Figure B1, equilibrium calculations at pH 6.2 predict HCA is predominantly in the fully dissociated state (i.e., net charge = –3) while approximately 40% of CA species are in the fully dissociated state, labeled as CA(-3) or $C_6H_5O_7^{3-}$. The acid-base speciation reactions for CA along with the respective dissociation constants, pKa_i, are the following:

$$C_6H_8O_7 \overset{pKa_1}{\longleftrightarrow} C_6H_7O_7^- + H^+, \quad pKa_1 = 3.13, \tag{B1}$$

$$C_6H_7O_7^- \overset{pKa_2}{\longleftrightarrow} C_6H_6O_7^{2-} + H^+, \ pKa_2 = 4.76, \text{ and} \tag{B2}$$

$$C_6H_6O_7^{2-} \overset{pKa_3}{\longleftrightarrow} C_6H_5O_7^{3-} + H^+, \ pKa_3 = 6.40. \tag{B3}$$

The speciation reactions and corresponding equilibrium dissociation constants for HCA are the following (ChemAxon):

$$C_6H_8O_8 \overset{pKa_1}{\longleftrightarrow} C_6H_7O_8^- + H^+, \quad pKa_1 = 2.90, \tag{B4}$$

$$C_6H_7O_8^- \overset{pKa_2}{\longleftrightarrow} C_6H_6O_8^{2-} + H^+, \quad pKa_2 = 4.29, \text{ and} \tag{B5}$$

$$C_6H_6O_8^{2-} \overset{pKa_3}{\longleftrightarrow} C_6H_5O_8^{3-} + H^+, \quad pKa_3 = 5.11. \tag{B6}$$

As shown in Figure B1, the percentage of fully dissociated HCA (labeled as HCA(-3) or $C_6H_5O_8^{3-}$) at pH 6.2 is 92%. At pH 8.0 (i.e., the upper limit of urine), the percentage of HCA(-3) is nearly 100%. As such, DFT calculations in Chapter 3 were performed using the dominant species, HCA(-3).

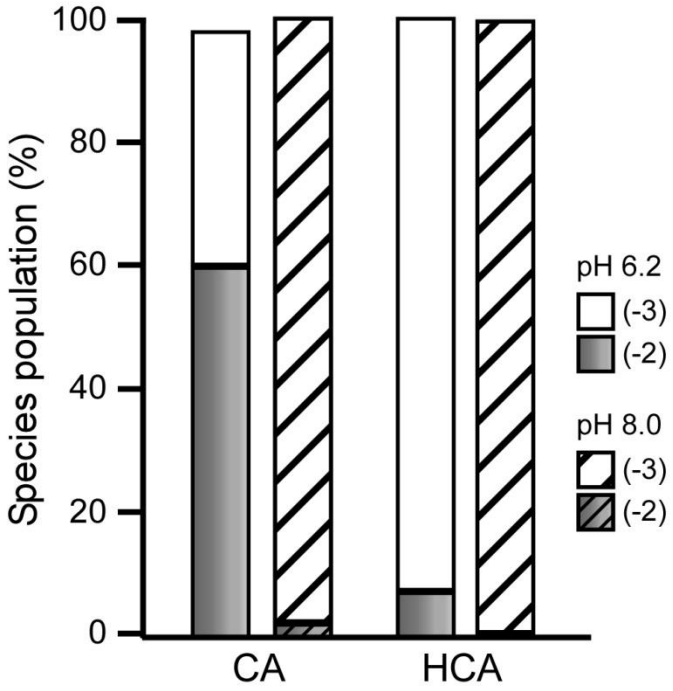

Figure B1 Percentage of deprotonated CA and HCA species, calculated from equations (B1) – (B6). Fully dissociated species (charge -3) are represented by white bars and partially dissociated species (charge -2) are represented by grey bars.

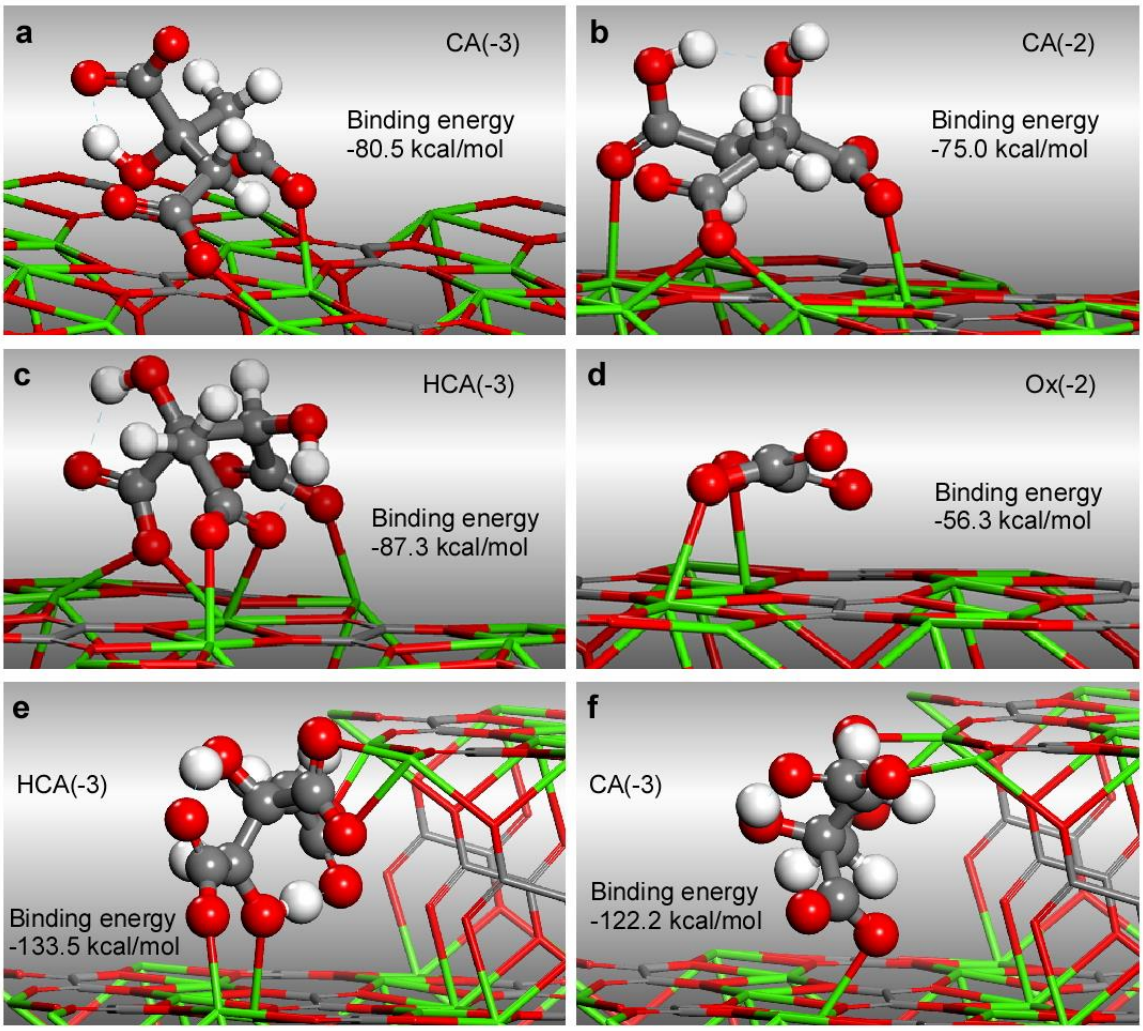

Figure B2 DFT calculations showing the adsorption configuration and binding energy of CA(-3) (a), CA(-2) (b), HCA(-3) (c) and Ox(-2) (d) on the COM (100) surface and of HCA(-3) (e) and CA(-3) (f) binding to a (001) step on the COM (100) surface.

The reported pKa values were obtained from Martell and Smith (Martell and Smith 1982). There are discrepancies in the reported $pKa,_3$ value due to the ionic strength dependency of the dissociation constant. For instance, some references report $pKa,_3$ = 5.66 when the ionic strength is 100 mM (Martell and Smith 1982), which is less than the ionic strength of CaOx solutions used in ISE and bulk crystallization assays. On this basis, it is likely that the dominant species in CaOx growth solutions is CA(-3).

DFT calculations of CA-crystal interactions and CA-calcium ion complexes in the manuscript were performed using CA(-3); however, equivalent DFT calculations were performed with CA(-2). The results of these calculations, which are presented in Figure B2, reveal that the conclusions reached in Chapter 3 are not altered by CA charge. Atoms are colored as follows: hydrogen (white), carbon (grey), oxygen (red) and calcium (green).

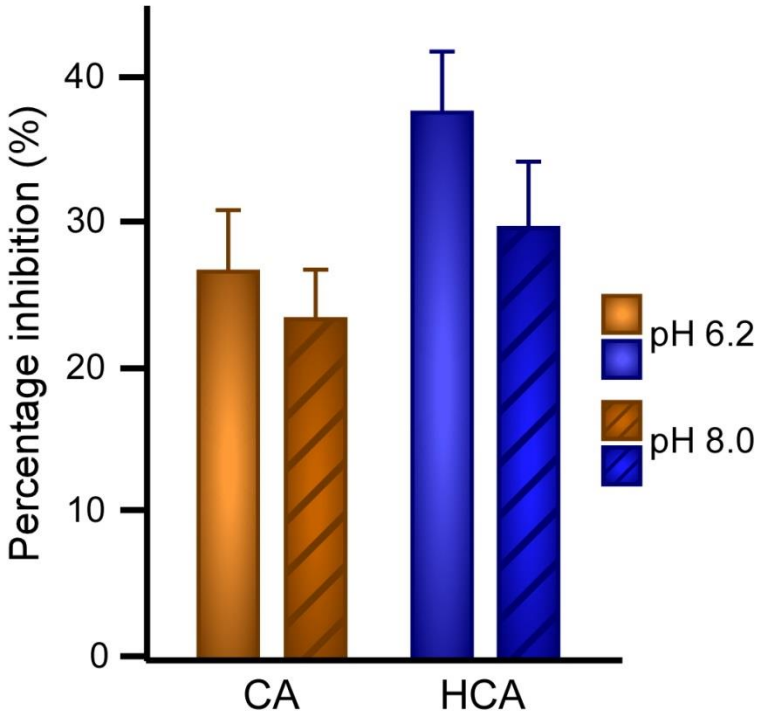

Figure B3 Kinetic study of COM crystallization in the presence of C_{CA} = 20 μg/mL and C_{HCA} = 20 μg/mL at pH 6.2 and 8 are shown. Error bars equal one standard deviation.

Moreover, we conducted bulk crystallization, ISE, and *in situ* AFM measurements in growth solutions at pH 6.2 (nominal condition) and pH 8.0 to assess the influence of CA charge on its efficacy as a COM crystal modifier. At pH 8.0, approximately 99.8% of CA species are in the fully dissociated state (neglecting the effect of ionic strength). Bulk

crystallization assays reveal approximately no change in crystal morphology and size at these two pH values. Similarly, *in situ* AFM measurements at pH 6.2 and 8.0 at C_{CA} = 0.1 μg/mL showed no apparent change in etch pit formation on COM (100) surfaces. ISE experiments at pH 6.2 and 8.0 reveal subtle differences in the percent inhibition of COM growth at $C_{CA} = C_{HCA}$ = 20 μg/mL (Figure B3). The percent inhibition of COM growth is slightly reduced at higher pH, but HCA is the most effective modifier irrespective of solution alkalinity ($P < 0.05$ comparing HCA to CA at both levels of pH).

B2. COM (100) surface dissolution in the presence of citrate and hydroxycitrate

In Figure B4 we provide a detailed analysis of etch pit formation on a COM (100) surface in the presence of C_{HCA} = 0.25 μg/mL. Time-resolved *in situ* AFM images at periodic times reveal the formation and growth of etch pits (Figure B4a – c). For each dashed line in the AFM image, the corresponding height profiles are provided in Figure B4d – f, respectively. The nominal growth of hillocks on the (100) surface in the absence of modifier (Figure B4d) occurs by the advancement of single steps. Each step has an average height of 0.4 nm, which is the approximate size of the unit cell parameter in the *a* direction. Upon the addition of HCA, etch pits monotonically evolve in both depth (Figure B4g) and width (Figure B4h) with imaging time. The concentration of modifier in this study is approximately three orders of magnitude less than the concentration of Ca^{2+} ions in supersaturated solution, indicating the effect of etch pit formation is not solely attributed to reduced calcium oxalate supersaturation as a result of modifier-calcium ion complexation.

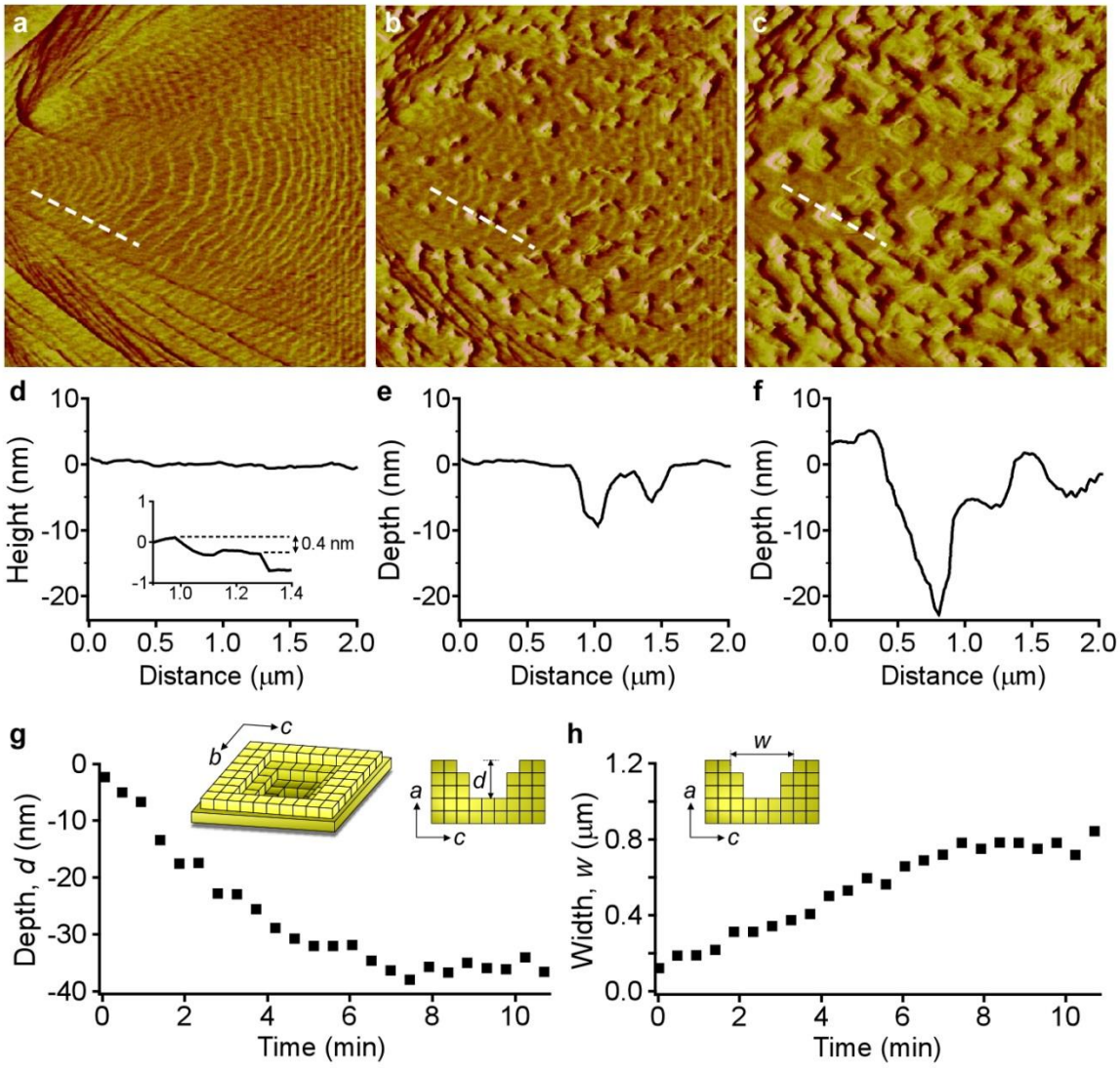

Figure B4 Snapshots of *in situ* AFM study on COM (100) surface in the presence of C_{HCA} = 0.25 μg/mL (a – c) and corresponding surface profiles (d – f) are shown. Etch pit evolution in depth (g) and width (h) was monitored over time.

B3. Mechanism of HCA-induced dissolution of COM crystals

Common mechanisms of crystal growth inhibition include step pinning and kink blocking (Boll, Sorensen et al., 1969). The former involves the adsorption of modifiers on terraces or step edges, which impede the advancement of steps. Modifiers adsorbed with their average adsorbate-to-adsorbate spacing comparable to the critical radius of

curvature, r_c, for the step (i.e., high surface coverage at high modifier concentration) impedes step advancement, leading to reduced step velocity and ultimately suppressed growth when the step radius approaches r_c (Cabrera and Vermileya 1958; Voronkov and Rashkovich 1994). The mode of action for HCA on COM crystallization at low modifier concentration, as inferred from time-resolved AFM images of the COM (010) surface, does not appear to be step pinning due to the absence of protrusions on steps (i.e., a characteristic trait of modifiers that operate by a step pinning mode of action(Cabrera and Vermileya 1958)). AFM measurements of COM (100) surface growth at high concentration of either CA or HCA revealed the formation of irregular-shaped steps, which may indicate that modifiers bind to step edges on this surface (consistent with a previously proposed mechanism for CA inhibition by Qiu et al., (Qiu, Wierzbicki et al., 2004)).

Kink blocking is commonly observed when the crystal grows by a screw dislocation mechanism (Frank 1949; Burton, Cabrera et al., 1951) wherein modifiers adsorb to kink sites and reduce the kink density and extend the critical length of the step (Sizemore and Doherty 2009). The net result is a decreased rate of step advancement within the plane of measurement, as well as reduced growth of hillocks in the direction normal to this plane. AFM studies of COM growth have shown that steps emanating from screw dislocations on the (100) and (010) surfaces advance across the crystal plane. Burton, Cabrera, and Frank (BCF) derived a theoretical model of spiral growth predicting the rate of crystal growth normal to the basal face, $G_{[hkl]}$, as

$$G_{[100]} = \frac{(v_i)_{hkl} h_{hkl}}{(y_i)_{hkl}} = \frac{h}{\tau}, \tag{B7}$$

where h_{hkl} is the height of (hkl) steps advancing along the COM (100) plane, y_i is the interstep distance, and v_i is the velocity of step advancement (Winn and Doherty 2000; Lovette, Browning et al., 2008; Snyder and Doherty 2009). The subscript refers to the *i*th edge of growth hillocks, which advance across the surface in spiral patterns with a characteristic rotation time τ. Observations of decreased COM [100] thickness in Figure 3.2B are qualitatively consistent with this theoretical equation.

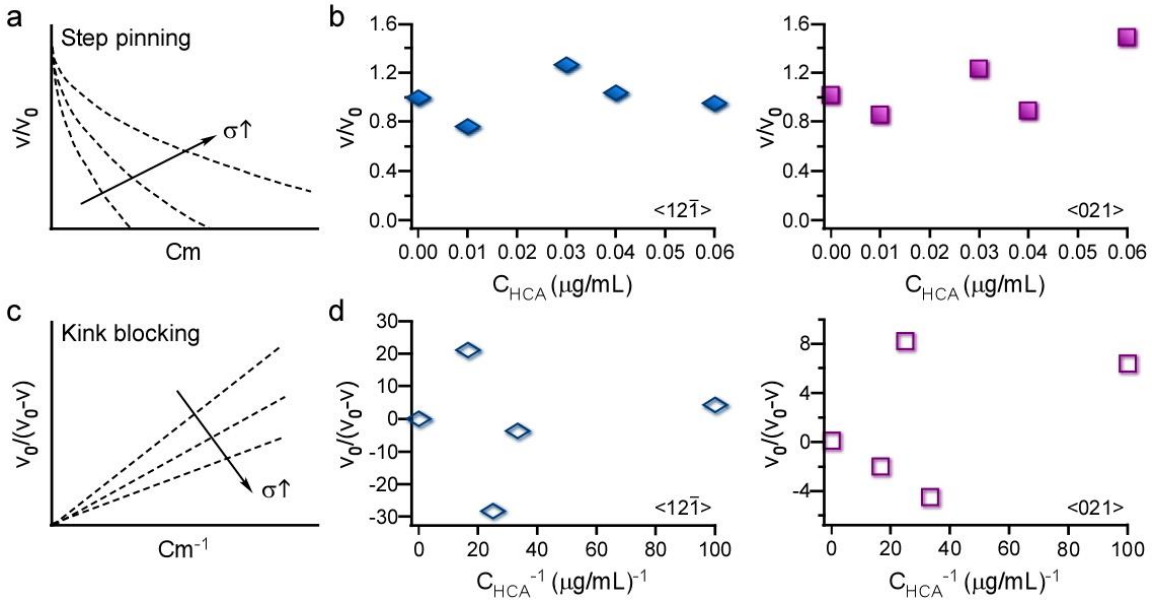

Figure B5 Representative velocity profiles indicating step pinning (a) and kink blocking (c). Plots generated for steps in <12-1> and <021> direction in COM (010) surface in the presence of HCA (b and d).

It is energetically more favorable when modifiers adsorb on kink sites rather than on step edges or terraces. Both modes of action can alter the shape of crystals due to specific modifier-step and/or modifier-kink interactions. In our studies of COM crystallization, the mode of action for CA and HCA at low modifier concentration inferred from *in situ* AFM images does not appear to be kink blocking. To quantitatively analyze AFM data, we constructed Bliznakov plots, which represent the relationship

between relative step velocity and modifier concentration. In Figure B5a we plot a hypothetical v/v_0 trend with increasing modifier concentration as a function of CaOx supersaturation where v and v_0 are step velocities in the presence and absence of modifier, respectively. For the step pinning mode of action, this plot should exhibit a monotonic decrease in v/v_0 with increasing modifier concentration (for example, see Olafson et al., (Olafson, Ketchum et al., 2015)). Plots for HCA (Figure B5b) deviate from this trend, suggesting that HCA does not bind to the (010) surface. For modifiers that operate in a kink blocking mode of action, a plot of $v_0/(v_0 - v)$ with increasing inverse modifier concentration should produce a linear trend as shown in Figure B5c; however, plots for HCA exhibit no apparent trend (Figure B5d), which leads us to believe that HCA preferentially binds to steps, as illustrated in Figure 3.10C. Note that the plateau region for v (Figure 3.8B) observed at low modifier concentration (C_{HCA} < 0.04 μg/mL) has also been reported by others examining the effects of proteins and polyamino acids on COM (010) and (100) step advancement (Wesson and Ward 2007). In these studies, it was suggested that the size of the step relative to the size of the modifier can lead to complex sorbate-crystal binding (including the possibility of cooperative effects among multiple HCA molecules at step sites).

Modifier complexation of free calcium ions in solution reduces the rate of COM growth by lowering the supersaturation. The solubility of COM crystals C_s (i.e., equilibrium concentration of solute) is as follows,

$$C_s = \sqrt{K_{sp}\gamma_{Ca}^{-1}\gamma_{Ox}^{-1}}, \tag{B8}$$

where K_{sp} is the solubility product (1.66 x 10^{-9} mol^2L^{-2} at 25°C) (Moe 2006) and γ_i is the activity coefficient (i = Ca or OX). For the equimolar growth solutions used in this study (C_{Ca} = C_{OX}), the activity coefficients for calcium and oxalate are calculated using the expression

$$\gamma = exp\left(-\left(\frac{0.51z^2\sqrt{I}}{1+\sqrt{I}} - 0.3I\right)\right), \quad \text{(B9)}$$

where z is ion valence and I is ionic strength. The addition of either HCA or CA to a calcium oxalate growth solution lowers supersaturation by (i) forming complexes with free calcium ions to reduce C_{Ca}, and (ii) increasing the ionic strength, which alters the activity coefficients, thereby increasing the solubility of COM crystals. Modifier concentrations used in AFM experiments (ca. 3 μM) are insufficient to reduce supersaturation by complexation (i.e., Ca^{2+}/HCA ≈ 10^3), and impose only minor changes in solubility due to activity effects (i.e., C_s increases by ca. 0.05 %). If the modifier concentration in bulk crystallization is increased to values that are commensurate with supersaturation, the effects of complexation and activity are significant. For example, we performed bulk crystallization in the presence of ca. 0.3 mM HCA (or 100 μg/mL) and observed few COM crystals, indicating almost complete suppression of COM crystallization.

In literature, alternative mechanisms have been proposed to describe the potential effects of modifiers (or impurities) on crystal solubility. At low supersaturation, it is suggested that modifiers can increase local solubility at crystal interfaces, potentially inducing dissolution when the mother liquor is close to saturation (Linnikov 2000). Under similar conditions, it is also possible to observe the effects of Ostwald ripening

where small crystals dissolve at the expense of larger particles that grow based on the Gibbs-Thompson effect (Malivuk, Zekic et al., 2013). Others have proposed that changes in surface free energy can be caused by the site occupancy in crystal lattices with embedded solid particles or impurities (Cahn and Larche 1982), which induce stress on the crystal (analogous to the simulations by Lutsko et al., described in Figure 3.10A) (Lutsko, Gonzalez-Segredo et al., 2014). Additionally, the formation of defects on crystal surfaces (e.g., vacancies or dislocations) can induce stress on the crystal lattice, leading to reduced rates of growth under supersaturated conditions (van der Heijden and van der Eerden 1992).

B4. In vitro assays of COM crystallization in human urine

The upper limit of metastability (ULM) was measured using a modified version of the method described by Asplin et al., (Asplin, Parks et al., 1999). Urine aliquots were obtained over a 24-hour urine collection period from eight patients with kidney stones. All urine samples were brought to a pH of 5.7 by the addition of KOH or HCl as needed. Each urine sample was studied with no additive or with either CA or HCA added to increase their concentration by 2 mM. For each sample, 200 μL of urine was added to 12 wells of a 96 well microliter plate. Solutions of increasing concentration of oxalate (OX) were pipetted into the urine aliquots in the wells. The plate was placed on a shaker for 3 hours at 37°C and then the turbidity of solutions in each well were measured at 620 nm wavelength using a VMax kinetic ELISA microplate reader (Molecular Devices, Sunnyvale, CA). The well at which turbidity increased determined the point of crystallization and the oxalate concentration at this point is the amount of oxalate in the urine measured at baseline plus the amount of oxalate added to the urine in the well

showing increased turbidity. The results are presented as the calcium oxalate concentration product (used as a surrogate of supersaturation) at the point of crystallization (see Figure 3.14). In addition to their crystal inhibition activity, both citrate and HCA complex calcium in solution, lowering the concentration of ionized calcium. Both mechanisms should contribute to changes in the ULM relative to the control, indicative of an inhibition of nucleation. Each urine sample was run in duplicate and the results were averaged. Statistical comparison was performed using the non-parametric Wilcoxon test.

B5. Human trials of hydroxycitrate bioavailability

There were no prior reports of measurements of HCA in human urine in people not consuming HCA supplement. We tested the hypothesis that HCA is not a normal constituent of human urine by measuring the concentration of HCA in random urine samples from five healthy subjects (Protocol #1061857 Western Institutional Review Board).

The hypothesis of the human trial study was that HCA, when orally administered, will be excreted in urine. To test this hypothesis, we assessed urinary excretion to confirm the bioavailability of HCA through oral administration. The protocol was approved by the University of Houston Internal Review Board (case 15176-01). Recruitment was limited to subjects between 21 and 65 years of age. Pregnant women and subjects with known severe chronic kidney disease (stage 4 or 5) were excluded.

The supplement used in the human trial was Super CitriMax Clinical Strength Garcinia Cambogia Extract. The active ingredient, hydroxycitrate, is an modifier of ATP citrate lyase and is presumed to reduce lipogenesis as its mechanism of action for

inducing weight loss (van Loon, Van Rooijen et al., 2000). Each serving (2 capsules) contained 1.5 g *garcinia cambogia* extract with 900 mg active ingredient. The subjects were asked to take *garcinia cambogia* extract for three days at the dose recommended by the manufacturer (i.e., two capsules three times a day). On the third day of *garcinia cambogia* treatment, the subjects collected a 24-hour urine. The urine was collected unrefrigerated using an antimicrobial preservative.

Hydroxycitrate concentration was measured by ion chromatography using an ICS-2000 system (Dionex Corp, Sunnyvale, CA) with AS11 guard and analytic columns, potassium hydroxide (KOH) eluent, and a conductivity detection system (Figure B6). Because isocitrate co-elutes with HCA on this system, urine samples were pre-treated with isocitrate dehydrogenase to remove isocitrate interference. Hydroxycitric acid calcium salt, (-)-(P), purchased from ChromaDex Inc. (Irvine, CA) was used as a standard.

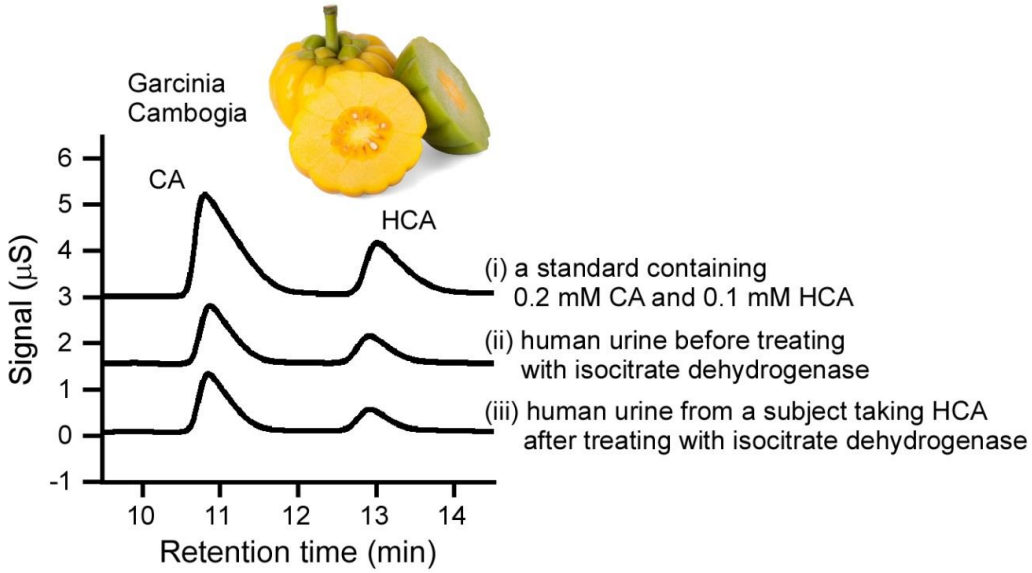

Figure B6 Ion chromatography of a standard (i), human urine before (ii), and after (iii) treatment is shown. Data are shifted in y axis for visual clarity. The inset shows an image of the fruit garcinia cambogia, which contains HCA.

Appendix C

Chapter 4 Supplementary Information

C1. Dissociation constants of organic growth modifiers

Table C1 Dissociation constants of organic growth modifiers.

	pKa_1	pKa_2	pKa_3	pKa_4
0. Oxalic acid, OA	1.25	4.3		
1. Malonic acid, MA	2.85	5.70		
2. Succinic acid, SA	4.21	5.64		
3. Glutaric acid, GA	4.33	5.42		
4. Adipic acid, AA	4.42	5.42		
5. Methyl oxalic acid, MOA	2.01			
6. Malic acid, MCA	3.46	5.10		
7. Tartaric acid, TTA	3.04	4.37		
8. Tricarballylic acid, TCA	3.67	4.87	6.38	
9. Dimethyl hydroxyglutaric acid, DHGA	-	-		
10. Citric acid, CA	3.13	4.76	6.40	
11. Isocitric acid, ICA	3.29	4.71	6.40	
12. Hydroxycitric acid, HCA	2.90	4.29	5.11	
13. Butanetetracarboxylic acid, BTCA	3.23	4.62	5.2	5.8

C2. Bulk crystal assays

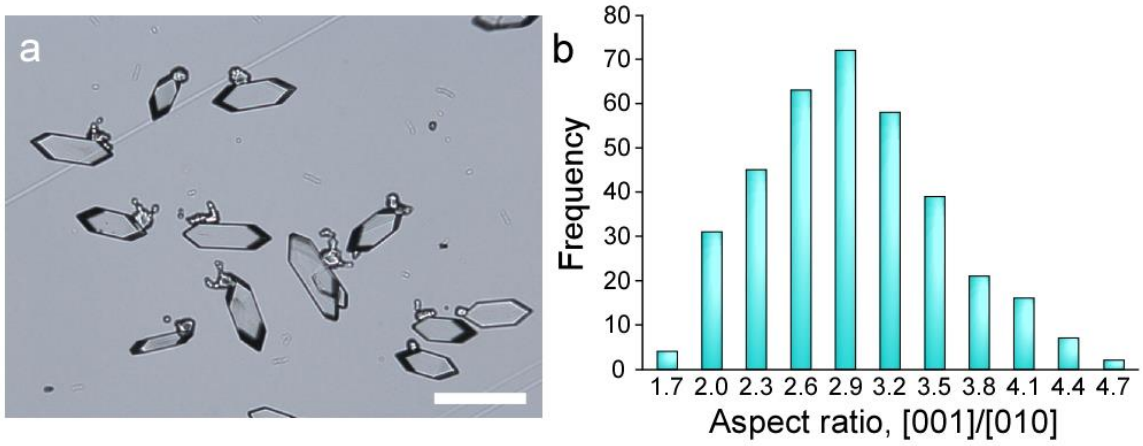

Figure C1 A representative optical micrograph of COM crystals prepared in the absence of modifier (A and a quantitative analysis was performed for the distribution of aspect ratio of COM crystals (B) are shown. Scale bar equals 50 μm.

C3. Interionic distances on COM crystal surfaces

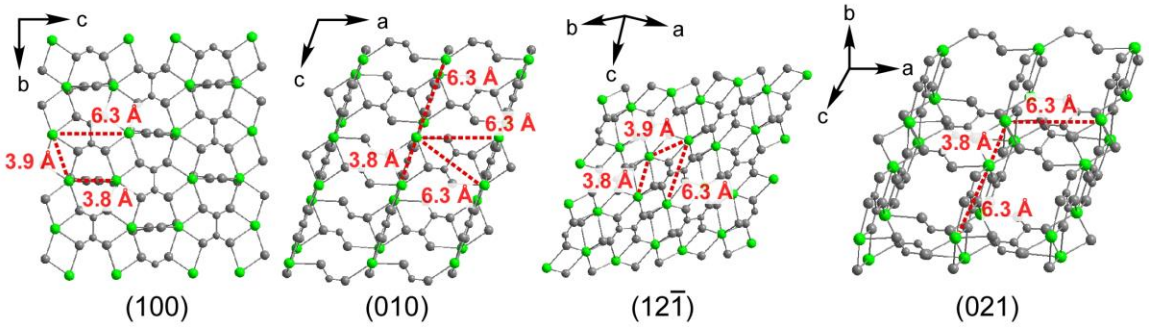

Figure C2 Cross-sectional images of four crystallographic plane of COM crystal viewed normal to each surface are shown. Red dashed lines indicate the calcium-to-calcium interionic distance.

C4. Calculation of rotation time and normal growth rate of spiral hillock growth

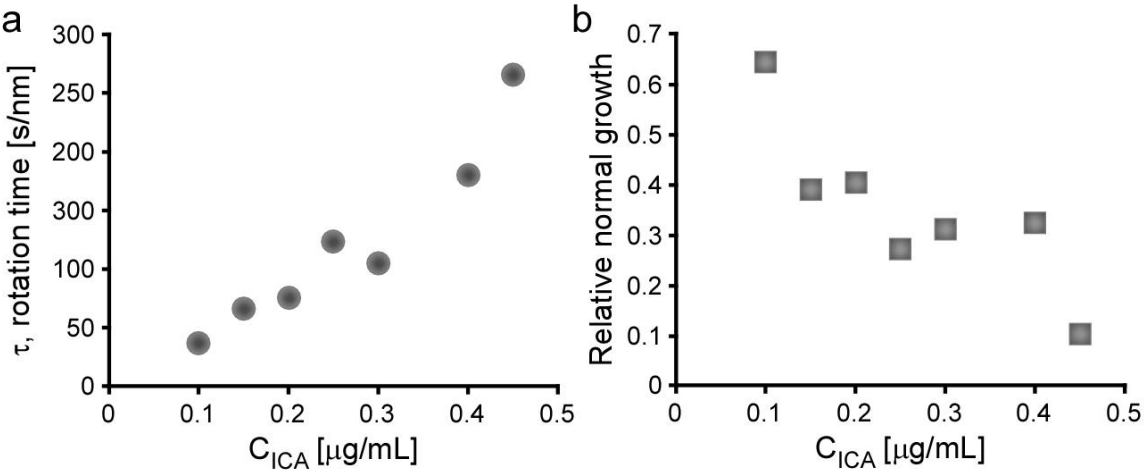

Figure C3 Characteristic rotation time τ (a) and relative normal growth i.e., ratio of G_{ICA} to $G_{control}$ (b) was calculated using equation (1). Rotation time monotonically increases with increase C_{ICA} resulting in a decrease of relative normal growth with increasing C_{ICA}.

C5. Thickness of COM crystals in the presence of ICA

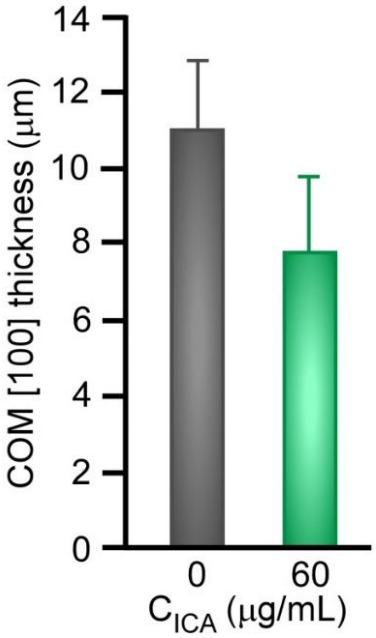

Figure C4 Thickness of COM crystals prepared in the absence (gray) and with 60 μg/mL of ICA (green) is compared. Measurements were performed from three separate batches with a minimum of 20 crystals per batch. Error bars equal one standard deviation.

C6. Limitations of original Cabrera-Vermilyea (C-V) model for step pinning

Inhibition mechanism of growth modifiers can be determined by observing the quantifying the advancement of steps in the presence of modifiers. Step pinning model of Cabrera-Vermilyea is based on the Gibbs-Thomson effect that relates the differences in free energy of steps and solution to advancing step curvature. However, there have been reports of discrepancies between theoretical C-V models and experimental data. For instance, Weaver et al., reported that the original C-V model cannot fully account for the effect of citrate on COM crystallization and stated that the traditional C-V model does not account for adsorption dynamics and assumes the surface coverage of modifiers is proportional to modifier concentration (Weaver, Qiu et al., 2006).

C7. Density functional theory calculations of modifier binding energy

Table C2 Surface binding energy of OGMs on frozen and relaxed surface.

(100) surface		
	Binding energy (kcal/mol)	**dE_{surf} with OGMs (kcal/mol)**
HCA(-3) – OX	-87.3	+18.8
CA(-3) – OX	-80.5	+14.2
ICA(-3) – OX	-94.8	+10.1
(021) surface		
	Binding energy (kcal/mol)	**dE_{surf} with OGMs (kcal/mol)**
HCA(-3) – OX	-170.2	+28.1
CA(-3) – OX	-146.6	+25.7
ICA(-3) – OX	-152.6	-

Table C3 Surface relaxation vectorization.

(100) surface			
	Length (Å)	**Average surface displacement, δ (Å)**	**Φ**
HCA(-3) – OX	2.42	0.25	148º
CA(-3) – OX	3.17	0.25	173º
ICA(-3) – OX	2.53	0.23	175º
Pristine OX	1.40	0.17	121º
(021) surface			
	Length (Å)	**Average surface displacement, δ (Å)**	**Φ**
HCA(-3) – OX	8.41	0.71	46º
CA(-3) – OX	5.40	0.55	49º
ICA(-3) – OX	4.46	0.47	53º
Pristine OX	5.11	0.38	49º

C8. Combination study of OGMs

We conducted a preliminary study to assess the combination effect of OGMs where they would exhibit synergism, addictiveness, or antagonism. Three selected OGMs, tricarballyic acid (TCA), citrate (CA), and hydroxycitrate (HCA) were selected for this study where the efficacy of individual OGMs were compared to that of a binary mixture of OGMs i.e., binary mixture of TCA and CA, TCA and HCA, and CA and HCA, respectively. Comparison of these OGMs are particularly of interest due to their disparate binding affinity to COM crystal surfaces as well as their moderate to high efficacy in inhibiting COM crystallization. This study of cooperative effects of OGMs

was motivated by our previous work of investigating the combination effect of proteins described in section 1.5.2.2.

Herein, we assessed the combined effect of OGMs on the kinetics of COM crystallization using ion selective electrode (ISE) measurement. We present the effect of individual OGMs on COM crystallization at varying concentrations (20, 40, 60, 80, and 100 μg/mL) as well as the effect of binary mixtures at 20 μg/mL: 80 μg/mL, 50 μg/mL: 50 μg/mL, and 80 μg/mL: 20 μg/mL which results in a total of 100 μg/mL OGMs. For instance, in Figure C5, the y-axis shows the percent inhibition (%) of COM crystallization in the presence of either TCA (top x-axis) or CA (bottom x-axis) or the combination of 20 μg/mL CA and 80 μg/mL TCA, 50 μg/mL CA and 50 μg/mL TCA, or 80 μg/mL CA and 20 μg/mL TCA marked by the dual symbols. It revealed that the effects of all three cases of CA-TCA binary mixtures are comparable to that of CA at its individual concentration. At 20 μg/mL CA and 80 μg/mL TCA, the efficacy is 21% which is similar to CA (27%) than TCA (38%) and TCA appears to have little impact even when the concentration of TCA is a factor of four higher than that of CA. At 80 μg/mL CA and 20 μg/mL TCA, the efficacy is 45% which is lower than the efficacy of 80 μg/mL CA, which indicates antagonistic effect of TCA on COM crystallization when combined with CA.

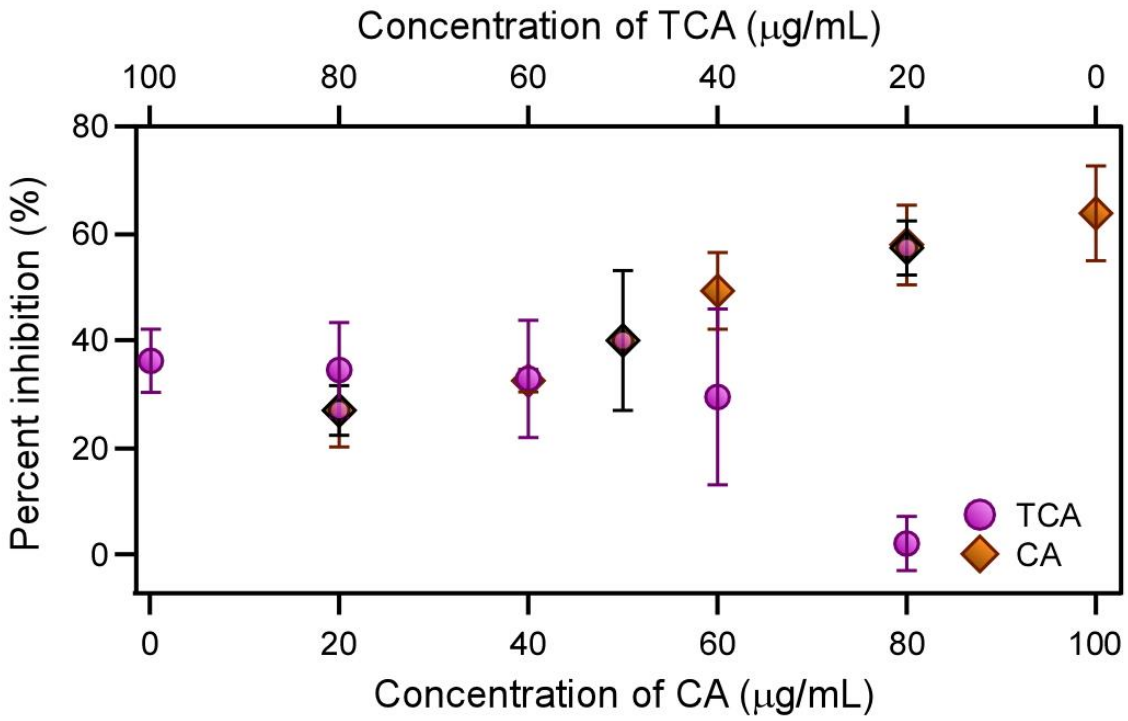

Figure C5 Kinetic studies COM crystallization in the presence of TCA (top x-axis) and CA (bottom x-axis), respectively, and in combination. Error bars equal two standard deviations.

Combination study of TCA and HCA was conducted as shown in Figure C6 where the top x-axis represents the concentration of HCA in μg/mL and the bottom x-axis shows the concentration of TCA in μg/mL. Again, TCA seemed to have either little impact or antagonistic effect as a binary mixture with HCA. The combined OGMs of 20 μg/mL HCA and 80 μg/mL TCA exhibited 27% inhibition which is lower than that of the effect of individual HCA (38%) and TCA (38%) concentrations, respectively.

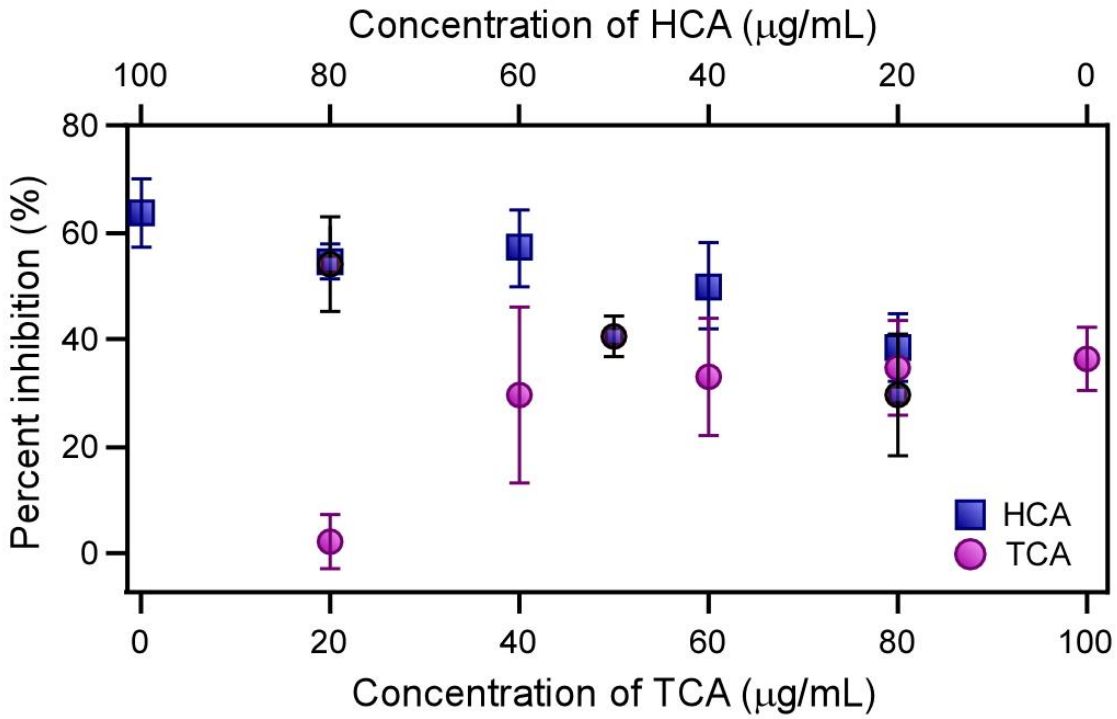

Figure C6 Kinetic studies COM crystallization in the presence of HCA (top x-axis) and TCA (bottom x-axis), respectively, and in combination. Error bars equal two standard deviations.

Combination study of HCA and CA revealed that the efficacy of the binary mixture was comparable regardless of the ratio of CA to HCA, which may be due to the comparable effectiveness of CA and HCA at high concentration (> 60 μg/mL). Also, as previously shown in Chapter 3, CA and HCA distinctively possess different binding affinity to COM crystal surface which eliminates competition for the OGMs to interact with COM surfaces.

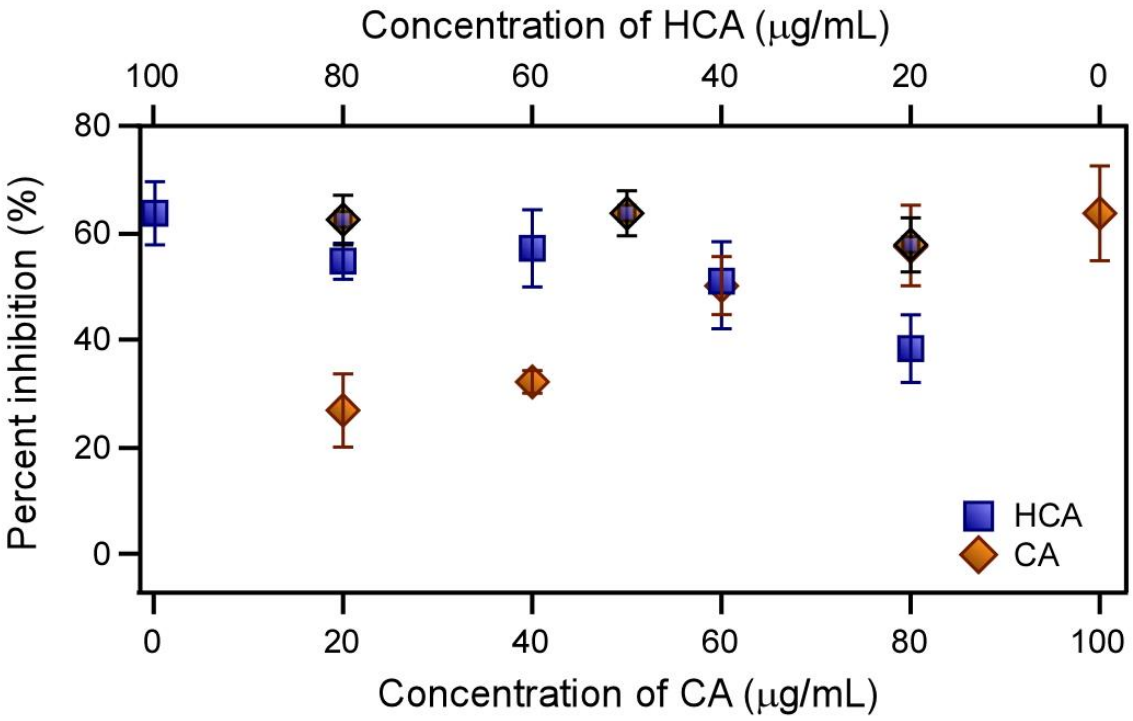

Figure C7 Kinetic studies COM crystallization in the presence of HCA (top x-axis) and CA (bottom x-axis), respectively, and in combination. Error bars equal two standard deviations.

However, to fully determine whether the OGMs inhibit crystallization synergistically or antagonistically, we should construct an isobologram plot and also compare the combination index (Equation 1.1).

C9. Change in supersaturation in the presence of OGMs

Both citrate and hydroxycitrate are capable of forming soluble complex with free calcium ion in the solution which may affect the supersaturation of COM growth solution when these OGMs are present. To this end, we analyzed the supernatant of COM growth solution after seven-day synthesis performed in the presence of varying concentration of CA and HCA, respectively. Normal crystallization protocol was carried out at solution

composition of 0.7 mM $CaCl_2$: 0.7 mM $Na_2C_2O_4$ with 150 mM of NaCl as background electrolyte to keep the supersaturation constant during crystallization process. The solution was kept at stagnant condition in a 60°C oven for three days and subsequently placed at room temperature for additional four days to sufficiently allow the solution to reach equilibrium. Supernatant of the solution was filtered with 0.45 μm filter paper to ensure no crystals would be analyzed. Concentration of calcium ion in each solution was measured using atomic adsorption spectroscopy (AAS) and supersaturation ratio of the supernatant was calculated as shown in Figure C8.

In the presence of HCA at the concentration greater than 0.06 mM, the supersaturation ratio of the supernatant was higher than that in the absence of modifier, which agrees well with HCA's ability to effectively inhibit COM crystallization leaving higher concentration of free calcium ions in the solution. However, the supersaturation ratio of the supernatant is decreased in the presence of CA at the concentration greater than 0.02 mM even though CA shows moderate inhibitory activity for COM crystallization.

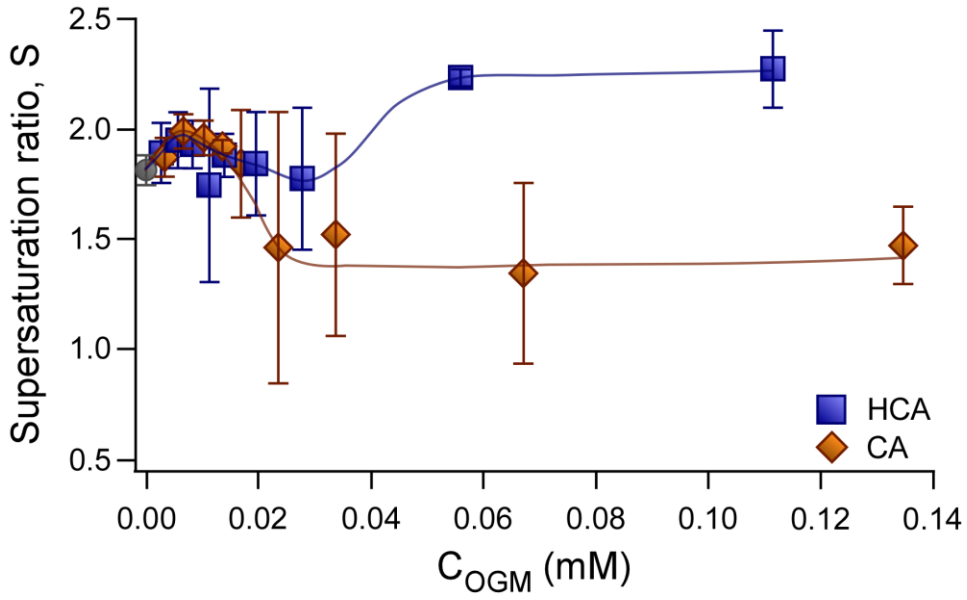

Figure C8 Supersaturation of the supernatant after seven-day synthesis in the presence of HCA and CA at varying concentrations. Three separate samples were prepared and error bars equal two standard deviations.

Appendix D

Chapter 5 Supplementary Information

D1. Speciation model calculation of citrate

Species fraction of oxalate, citrate, and hydroxycitrate presented in Figure 5.2 was calculated using the speciation reaction equations in Table 5.1. Citrate is a triacid with three dissociation constants:

$$K_{a1} = \frac{[H_2C_6H_5O_7^-][H^+]}{[H_3C_6H_5O_7]}, \quad \text{(D1)}$$

$$K_{a2} = \frac{[HC_6H_5O_7^{2-}][H^+]}{[H_2C_6H_5O_7^-]}, \text{ and} \quad \text{(D2)}$$

$$K_{a3} = \frac{[C_6H_5O_7^{3-}][H^+]}{[HC_6H_5O_7^{2-}]}. \quad \text{(D3)}$$

All experiments are based on aqueous solution so we account for water dissociation,

$$K_w = [H^+][OH^-]. \quad \text{(D4)}$$

The net charge of electrolytes in solution is neutral,

$$0 = [H^+] - [OH^-] - [H_2C_6H_5O_7^-] - 2[HC_6H_5O_7^{2-}] - 3[C_6H_5O_7^{3-}] + [Na^+] - [Cl^-], \quad \text{(D5)}$$

or if we simplify the equation by substituting the citrate and water dissociation constant,

$$0 = [H^+] - \frac{K_w}{[H^+]} - K_{a1}\frac{[H_3C_6H_5O_7]}{[H^+]} - 2K_{a1}K_{a2}\frac{[H_3C_6H_5O_7]}{[H^+]^2} - 3K_{a1}K_{a2}K_{a3}\frac{[H_3C_6H_5O_7]}{[H^+]^3} + [Na^+] - [Cl^-]. \quad \text{(D6)}$$

Total amount of citrate in solution equals to the sum of all the species in solution,

$$[H_3C_6H_5O_7]_{total} = [H_3C_6H_5O_7] + [H_2C_6H_5O_7^-] + [HC_6H_5O_7^{2-}] + [C_6H_5O_7^{3-}] \quad \text{(D7)}$$

or if we simplify the equation by substituting the citrate dissociation constant,

$$[H_3C_6H_5O_7]_{total} = [H_3C_6H_5O_7] + K_{a1}\frac{[H_3C_6H_5O_7]}{[H^+]} + K_{a1}K_{a2}\frac{[H_3C_6H_5O_7]}{[H^+]^2} + K_{a1}K_{a2}K_{a3}\frac{[H_3C_6H_5O_7]}{[H^+]^3}. \quad \text{(D8)}$$

Activity coefficients can be calculated based on the Davies equation,

$$\log(\gamma) = -0.5\, z^2\left(\frac{\sqrt{I}}{1+\sqrt{I}} - 0.2I\right), \quad \text{(D9)}$$

where z is the charge of ion and I is the ionic strength.

D2. Species fraction of citrate and hydroxycitrate

We also approximated the fraction of neutral and charged OX, CA, and HCA as a function of distance from COM crystal surface using a combination of mass balances, speciation models (Table 5.1), and colloidal relationships for charged interfaces (Equations 5.10 – 5.12 in Chapter 5). Species profiles of CA and HCA are shown in Figure D1 at bulk pH values 4 – 8 (For OX species profile, see Figure 5.4 in Chapter 5). At pH 4 and 5, the percentage of fully dissociated citrate, CA(-3), at COM crystal surface is less than 1 % and becomes the dominant species at pH 7 in which ca. 64% of CA is fully dissociated at surface as opposed to ca. 80% at bulk. The difference between surface and bulk CA concentration narrows at pH 8. In the case of HCA, there are 20% of HCA(-3) at the crystal surface and ca. 40% in bulk at pH 5, and the concentrations of HCA(-3) at the surface and at bulk become similar at pH 6.

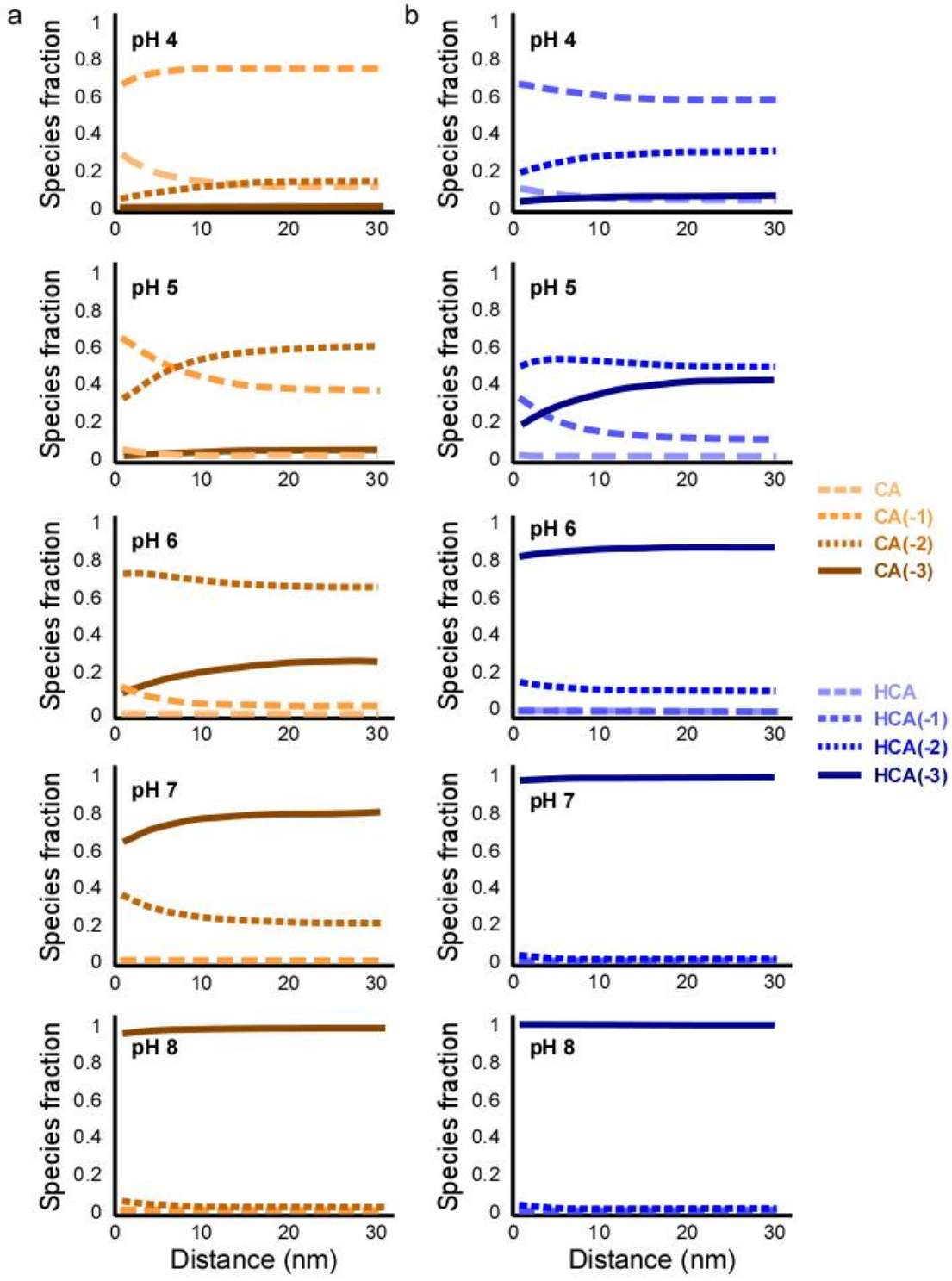

Figure D1 Species fraction of citrate (a) and hydroxycitrate (b) in their neutral, monovalent, divalent, and trivalent states were calculated for pH 4 – 8 as a function of distance from the COM crystal surface, respectively.

D3. Growth kinetics at varying growth solution concentrations

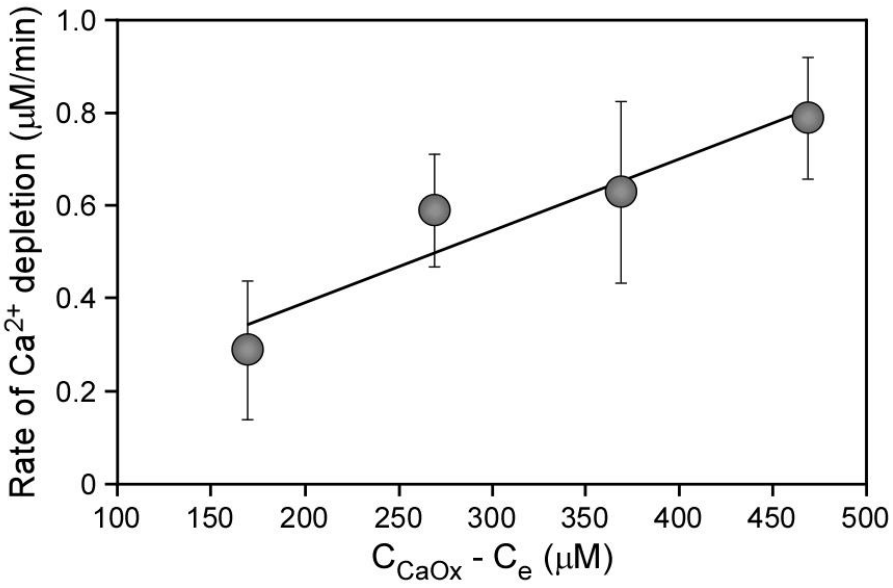

Figure D2 Rate of calcium depletion during COM crystallization in the absence of any modifiers was measured using ISE at varying CaOx concentration. Solid line is linear regression and the error bars equal two standard deviations.

Appendix E

Role of Glutamic Acid Based Peptide

E1. Library of glutamic acid peptide

A library of synthetic 18-mer peptides with glutamic acid (Glu, E) as the binder and alanine as spacer were prepared. We have previously reported the effect of a library of 18-mer peptides with the same sequence but with aspartic acid (Asp, D) as binder. In physiological condition, both aspartic acid and glutamic acid are negatively charged and may interact with COM crystal surfaces.

Table E1 List of E-peptides.

	1	2	3	4	5	6	7	8	9	10	11	12	13	14	15	16	17	18
E1	**E**	**E**	**E**	A	A	A	A	A	**E**	**E**	**E**	A	A	A	A	A	**E**	**E**
E2	A	A	**E**	A	A	A	A	A	**E**	**E**	A	A	A	A	**E**	A	A	A
E3	A	**E**	A	A	A	**E**	A	A	**E**	A	A	**E**	**E**	A	A	**E**	A	A
E4	A	**E**	A	A	**E**	A	A	**E**	A	A	**E**	A	A	**E**	A	A	**E**	A
E5	A	**E**	A	A	**E**	**E**	A	A	**E**	A	A	**E**	**E**	A	A	A	A	A
E6	A	**E**	A	A	A	**E**	**E**	**E**	A	A	A	**E**	A	A	A	**E**	**E**	**E**
E7	A	**E**	A	A	A	**E**	**E**	A	A	A	A	A	A	A	A	**E**	A	A
E8	A	**E**	A	A	A	**E**	**E**	A	A	A	**E**	A	A	A	A	**E**	A	A
E9	A	**E**	A	A	A	**E**	**E**	A	A	A	**E**	A	A	A	**E**	**E**	A	A
E10	A	**E**	A	A	**E**	A	A	A	**E**	A	A	**E**	**E**	A	A	**E**	A	A
E11	A	**E**	A	A	**E**	**E**	A	A	A	A	A	A	**E**	A	A	**E**	A	A
E12	A	**E**	**E**	A	A	**E**	A	A	**E**	A	A	**E**	**E**	A	A	**E**	**E**	A
E13	A	**E**	A	**E**	A	**E**	A	**E**	A	**E**	A	**E**	A	**E**	A	**E**	A	**E**
E14	A	**E**	**E**	A	**E**	**E**	A	A	**E**	**E**	A	A	**E**	**E**	A	A	**E**	**E**

E2. Comparison of the effect of D-peptide and E-peptide

We compared the specificity of selected sequence of D-peptides and E-peptides and their effect on the resulting morphology of COM crystals by comparing the aspect ratio of crystals prepared in the presence of respective peptides at the concentration of 20 μg/mL as shown in Figure E1. Presence of E10 and E12 peptides resulted in increased aspect ratio indicating that these peptides specifically adsorbed on the (010) surface whereas the D-peptides with equivalent sequences had little impact in the overall morphology of COM crystals. This may be attributed to the hindrance of methyl group in alanine for the peptide to effectively interact with crystal surface. Presence of X13 and X14 peptides (X = D or E) resulted in reduced aspect ratio which indicates that the peptides preferentially interacted with {12-1} and/or {021} crystal surfaces. It is worth noting that aspartic acids are reported to have a greater binding affinity to {12-1} and {021} faces than glutamic acids; however, in the case of X14 sequence, E-peptide is slightly more effective in affecting the growth in <12-1> and <021> direction, which supports the importance of spatial arrangement of binding moieties.

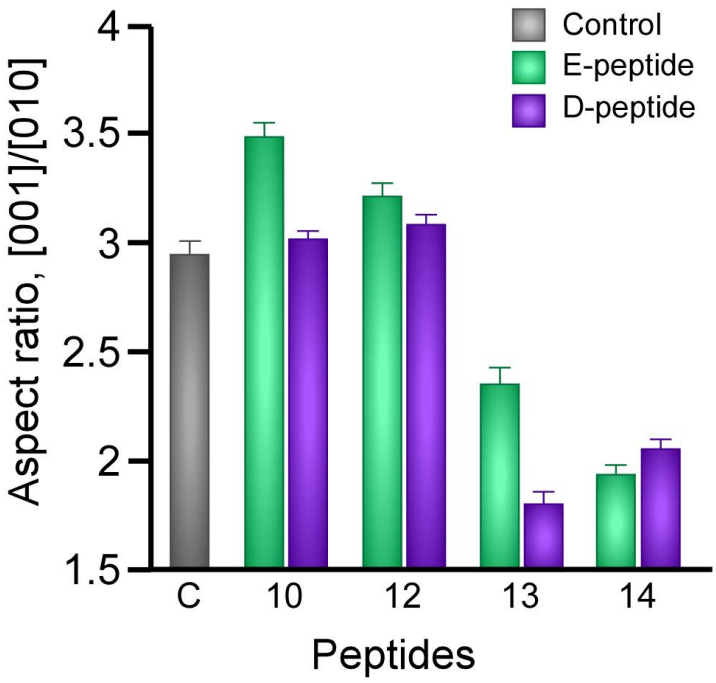

Figure E1 Aspect ratio of COM crystals prepared in the presence of 20 μg/mL peptides with aspartic acid (D) and glutamic acid (E) as their binding moieties, respectively. Error bars equal one standard deviation.

Notable changes in the surface of COM crystals were observed through optical micrographs (Figure E2). In the presence of X13 and X14 sequences for both D- and E-peptides, the COM (100) surfaces became significantly rougher than that of control. Thus, the resulting COM crystals were observed under atomic force microscopy where the topology of crystal surfaces was scanned with a cantilever (Figure E3). In the presence of E-peptides, COM (100) surface developed macro steps with distinct step edges mimicking the hexagonal bulk crystal morphology with straight edges whereas in the presence of D-peptides, COM (100) surface developed macro steps with rounded step edges. It is an intriguing result that two very similar peptides with the same sequence with slight difference in the binding moiety (i.e., glutamic acid possesses one more carbon chain making the carboxylic group more flexible) to reveal pronounced

differences in their binding mode to COM crystal surfaces. A further investigation with *in situ* atomic force microscopy may be employed to decipher the interaction between peptide and COM crystal surface.

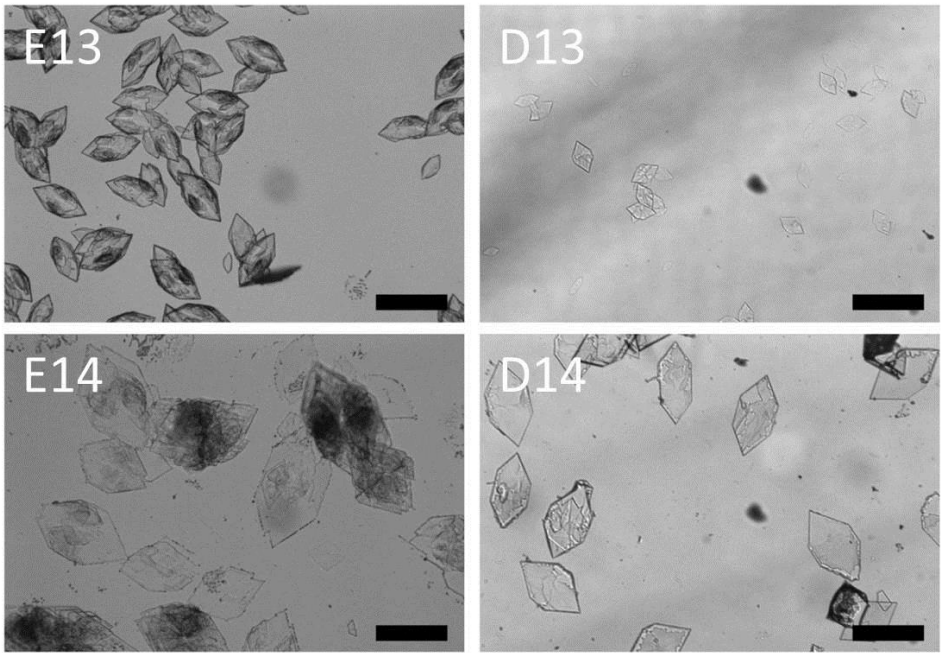

Figure E2 Optical micrographs of COM crystals prepared in the presence of peptides at the concentration of 20 μg/mL. Scale bars equal 100 μm.

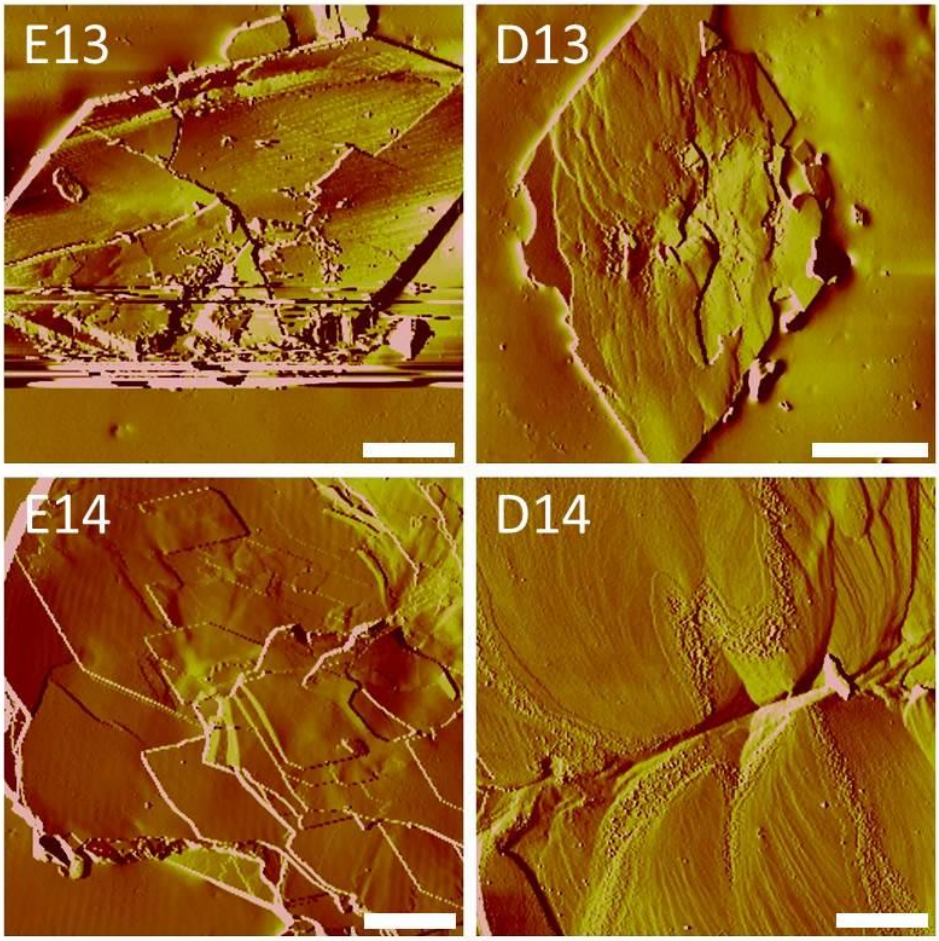

Figure E3 Atomic force microscope deflection mode images of COM (100) crystal surface prepared in the presence of peptides are shown. Scale bars equal 10 μm.

Appendix F

Identifying Hydroxycitrate

F1. Identification of hydroxycitrate stereoisomers

Hydroxycitrate possesses two diastereomers because of the two chiral centers in their molecular structure and exists in four forms of stereoisomers: (2S,3R), (2R,3S), (2S,3S), and (2R,3R) as shown in Figure F1. There have been reports in which researchers synthesized or extracted HCA from natural sources and characterized their molecular structural properties via high performance liquid chromatography, optical rotation, and nuclear magnetic resonance spectroscopy (Qiu and Orme 2008; Olafson, Li et al., 2016). However, the focus of previous studies was for two specific stereoisomers (i.e., (2S,3R) HCA from *hibiscus subdariffa* and (2S,3S) HCA which is found in *garcinia cambogia*). Lewis and Neelakantan successfully identified and isolated (-) hydroxycitrate from the garcinia cambogia fruit and identified it as such stereoisomer by using paper chromatography and comparing the retardation factor which is the ratio of the distance traveled by the substance of interest to the distance traveled by the solvent (i.e., R_f value) (Meldrum and Colfen 2008). Prior to this study, hydroxycitrate was mistaken for tartaric acid or citric acid.

We tested HCA that were purchased from two different manufactures, Sigma Aldrich (i.e., named (+)-HCA) and Chromadex (i.e., named (-)-HCA); however, since Sigma Aldrich does not provide a detailed information on their product we were not able to definitively identify which enantiomers were present; however, we believe it could be a racemic mixture because 1) most laboratory synthesis processes yield racemic mixtures

and not pure forms, and 2) pure forms are very expensive whereas the product purchases was not. HCA purchased from Chromadex is equivalent to the one extracted from *garcinia cambogia* (i.e., (2S,3S)-HCA)) and is in its pure form. We attempted to characterize the two HCAs by analyzing the carbon nuclear magnetic resonance (C-NMR) spectra which is shown in Figure F2 and F3, respectively. Equivalent concentration of both HCA was prepared using deuterated water, respectively. From the two spectra, it is clear that the two samples are not the same enantiomers; however, it still remains elusive which form is present in (+)-HCA.

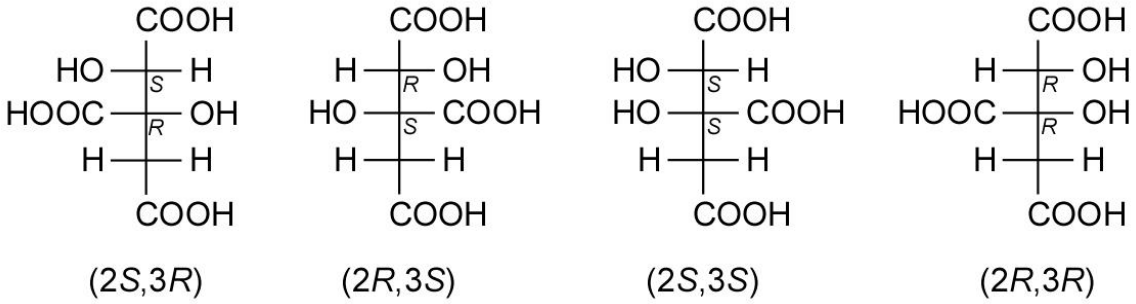

Figure F1 Four stereoisomers of hydroxycitrate: (2S,3R), (2R, 3S), (2S,3S), and (2R,3R).

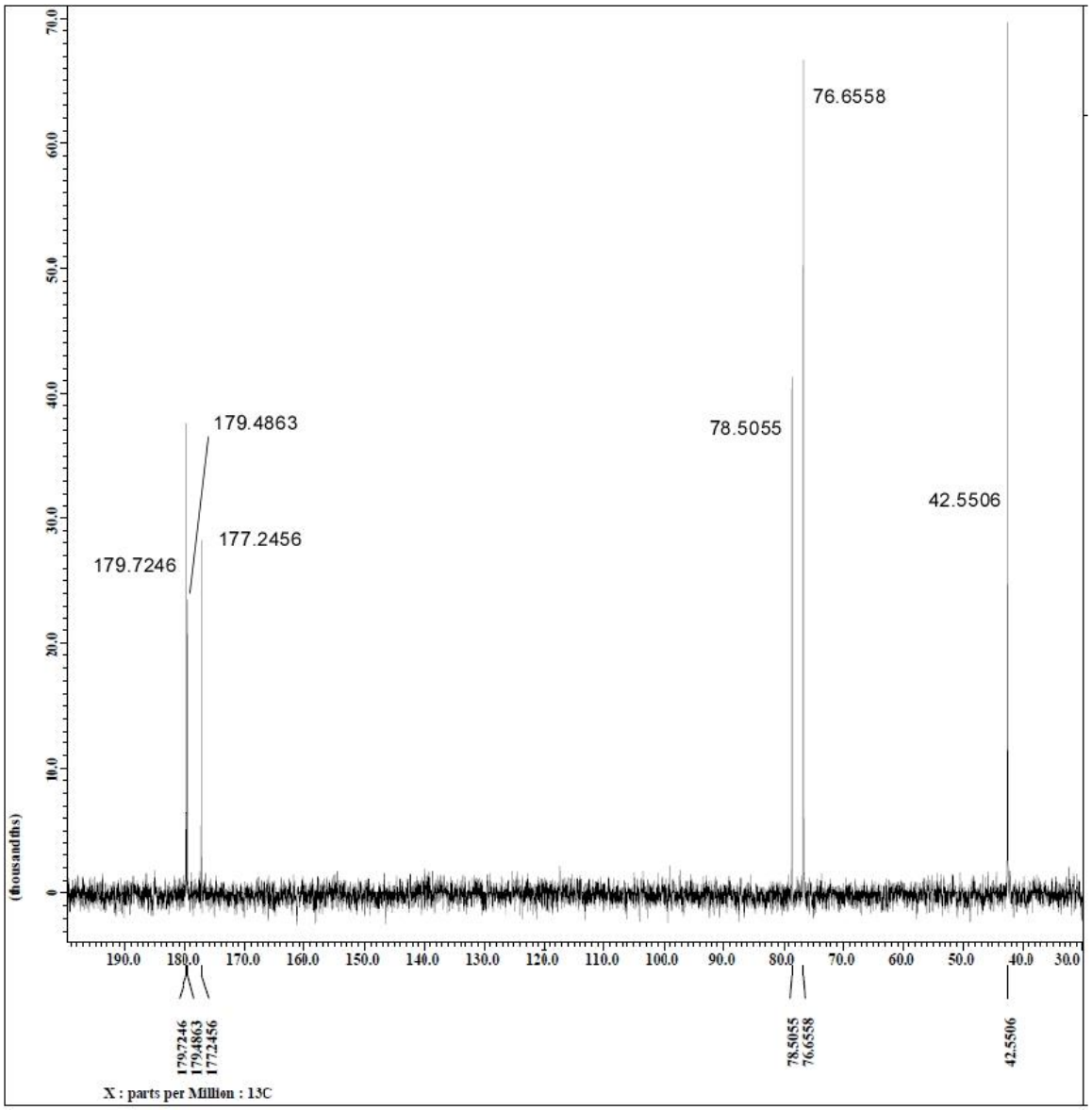

Figure F2 ^{13}C nuclear magnetic resonance spectrum of (+)-hydroxycitrate. Deuterated water was used as the solvent.

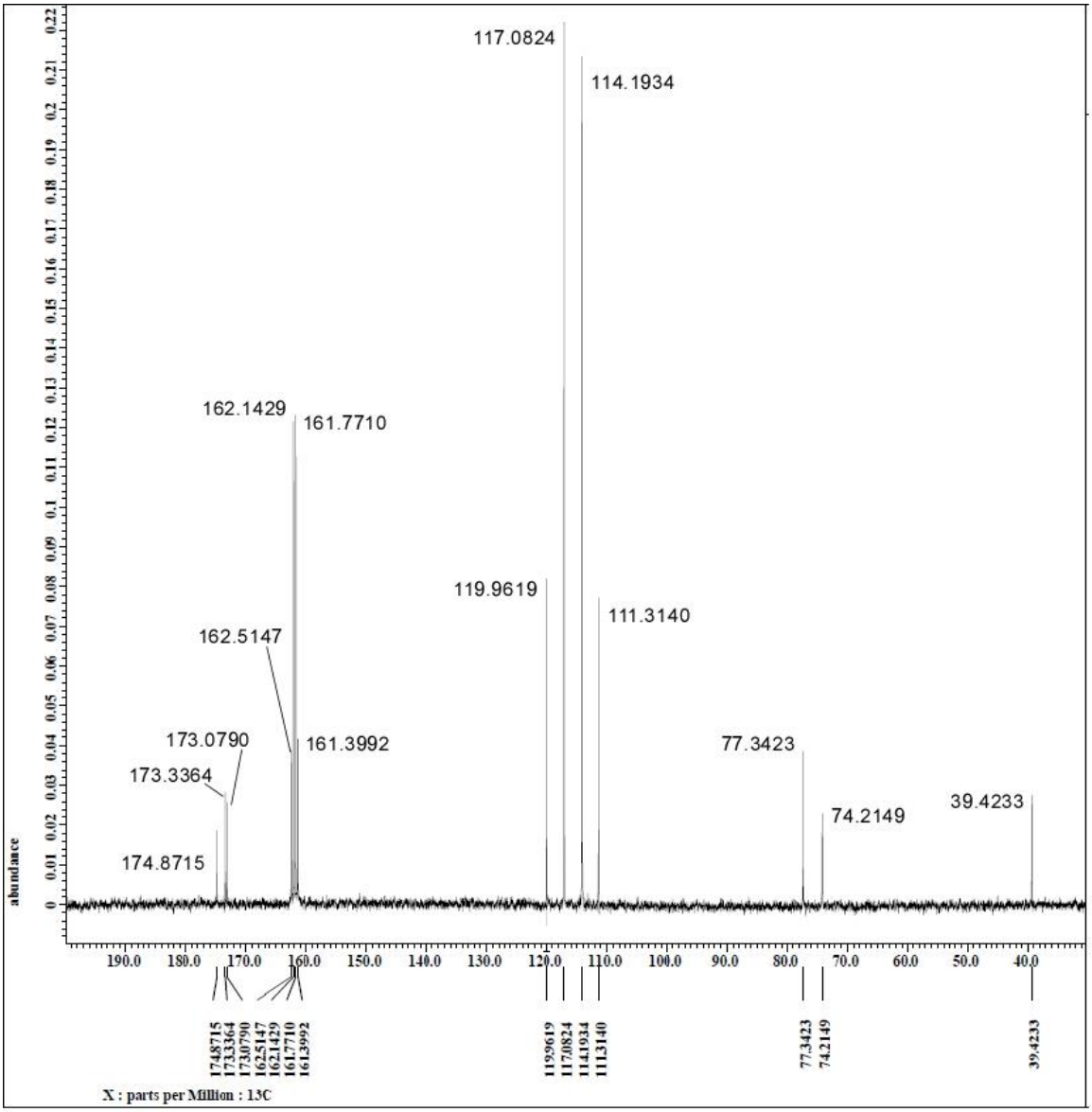

Figure F3 ^{13}C nuclear magnetic resonance spectrum of (-)-hydroxycitrate. Deuterated water was used as the solvent.

Chiral molecules also exhibit optical activities which can be quantified using a polarimeter; however, since rotation is affected by the path length of the light travelled through the sample and the concentration of the sample, specific rotation can be calculated to eliminate those effects using following equation:

$$[\alpha]_{\lambda}^{T} = \frac{\alpha}{l \times c}, \tag{B1}$$

where α is the measured angle in degree, *l* is the path length in decimeter, and *c* is the concentration in g/mL. Hida et al., reported (2S,3R)-HCA obtained in alkaline solution revealed optical rotation of +31º and (2R,3S)-HCA to be -24º (Hida, Yamada et al., 2006). Likewise, Lewis and Neelakantan reported the free acid form of (2S,3R)-HCA (*hibiscus*) to reveal optical rotation of +31º and (2S,3S)-HCA (*garcinia*) to be -20º (Lewis and Neelakantan 1965). Table F1 lists the optical activity of two different HCA samples at the wavelength of 589 nm (Na D-line) and deionized water was used as the solvent. We obtained [α] of -2.6º for (+)-HCA and + 38.3º for (-)-HCA, which could indicate that the (+)-HCA contains a mixture of (2S,3X) and (2R,3X) (X = S or R) which would reveal positive and negative specific rotation values, respectively. Unfortunately, we were not able to determine the enantiomers present in the racemic mixture due to lack of references.

Table F1 Specific rotation of hydroxycitrate

	$[\alpha]_{589}$
(+)-HCA	-2.6
(-)-HCA	+38.3

F2. Effect of (+)- and (-)-hydroxycitrate on COM crystallization

We compared the specificity and efficacy of different stereoisomer. We prepared COM crystals in the presence of (+)-HCA and (-)-HCA, respectively, at the concentration of 20 μg/mL and compared the resulting morphology. As shown in previous chapters, (+)-HCA preferentially interacted with {12-1} and {021} surfaces which resulted in a faceted diamond shaped crystals (Figure F4a); however, (-)-HCA exhibited non-specific

binding on COM crystal surfaces resulting in an oval-shaped COM crystals (Figure F4b). Interestingly, kinetic studies reveal that both forms of HCA exhibit comparable efficacy in inhibiting COM crystallization at the same concentration (Figure F5).

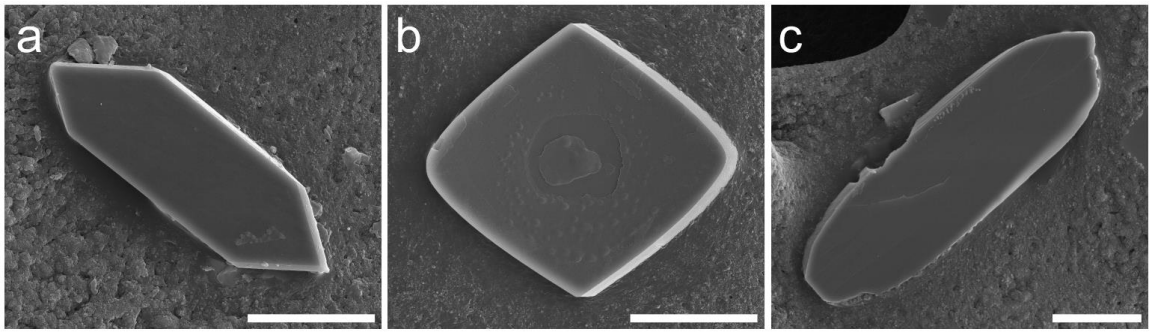

Figure F4 Scanning electron micrographs of COM crystals prepared in the absence (a) and in the presence of C_{HCA} = 20 μg/mL and $C_{(-)\text{-}HCA}$ = 20 μg/mL, respectively.

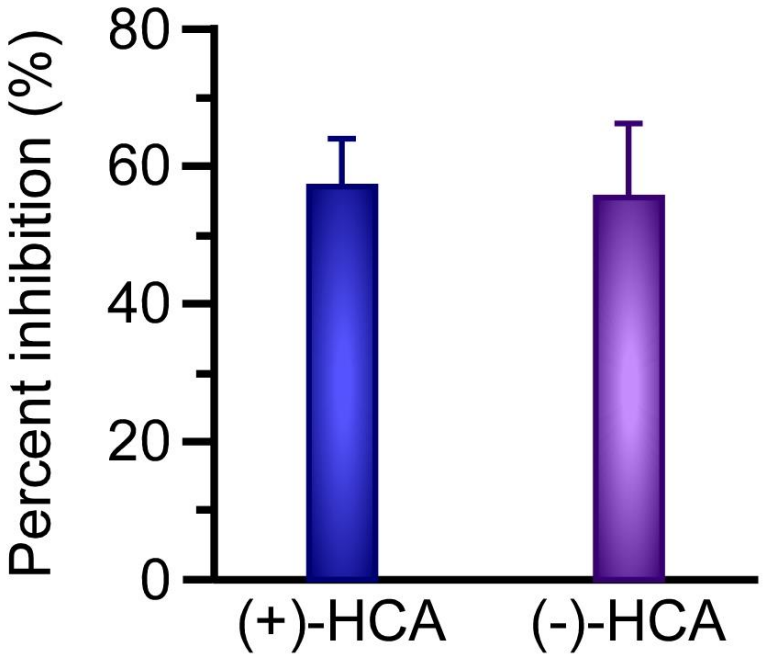

Figure F5 Kinetic studies of COM crystallization in the presence of 60 μg/mL (+)-HCA and (-)-HCA, respectively. Minimum of six separate measurements were averaged and error bars equal one standard deviation.

Interestingly, hydroxycitrate first garnered its popularity due to its alleged beneficial effect in weight loss. There have been several reports of based on laboratory and animal experiments that (-)-HCA inhibits enzyme processes responsible for converting carbohydrates into stored fat and also suppresses appetite (Risthaus, Bosbach et al., 2001; Arias and Fernandez 2008). However, studies showing the effect of (-)-HCA in human are limited and the efficacy in weight loss is based small sample sizes, which was performed without placebo-controlled group. As for the safety of the molecule, it was reported that animal studies indicate (-)-HCA to be no more toxic and citrate. It should also be noted that (-)-HCA has been used in Southeast Asian countries as culinary and medicinal purposes.

Appendix G

Unusual Growth Mode

G1. COM growth in the presence of high concentration of hydroxycitrate

Previously, we discussed the effect of hydroxycitrate on COM crystallization and observed how the surface growth is affected. It should be noted that the concentration range we studies thus far is at least an order of magnitude lower than what researchers have studies with other COM growth modifiers. To this end, we studied the effect of HCA at the concentration that is comparable to previous works of others.

We observed the growth of COM (010) surface in the presence of HCA at 1 μg/mL (Figure G1) and 2 μg/mL (Figure G2), respectively. Figure G1 shows the snapshots from *in situ* AFM studies on the growth of COM (010) surfaces in the presence of 1 μg/mL taken ca. two minutes apart, which revealed interesting movement of steps in both [12-1] and [021] directions. What we observe is in accordance with our previous results in which steps uniformly receded towards screw dislocation center in the presence of 0.1 μg/mL HCA even under supersaturated growth solution resulting in negative velocity. However, as shown in Figure G1, the steps do not move in an orchestrated manner but rather the steps recede back to its screw dislocations and subsequently recovers to move outwards. In Chapter 3, the effects of HCA on (010) surface at low concentrations were extensively investigated using *in situ* AFM studies and a new mode of inhibition mechanism for HCA was proposed; however, it is clear that the effect of modifiers at higher concentration (i.e., concentration ranges that are comparable to the works of other researchers) differ from that at low concentrations.

As previously mentioned, step pinning mode of action is a thermodynamic effect that follows Gibbs-Thomson effect in which the true supersaturation is a function of step curvature. It is reported that when steps are pinned to the point where the radius of step curvature falls below the critical value, the solution at the crystal interface becomes undersaturated and the steps may retreat to increase the radius of curvature (De Yoreo and Vekilov 2003). What we observe in Figure G1 may be an indication that at high concentration, HCA inhibits COM crystallization via step pinning mode of action; however, a more systematic study and a qualitative analysis will be required to determine the mechanism.

Figure G2 represents the snapshots of surface growth of COM (010) face in the presence of HCA at 2 μg/mL during *in situ* AFM study. It appears that multiple source of screw dislocation center is being developed as the modifier is introduced and the steps in growth hillocks propagate in a chaotic manner, which does not follow the rectangular growth hillock shape. As a result, the growth hillocks are not distinguishable from one another making it difficult to perform qualitative analysis of step velocity. It may be due to greater degree of step pinning or lattice strain caused by higher surface coverage by modifier.

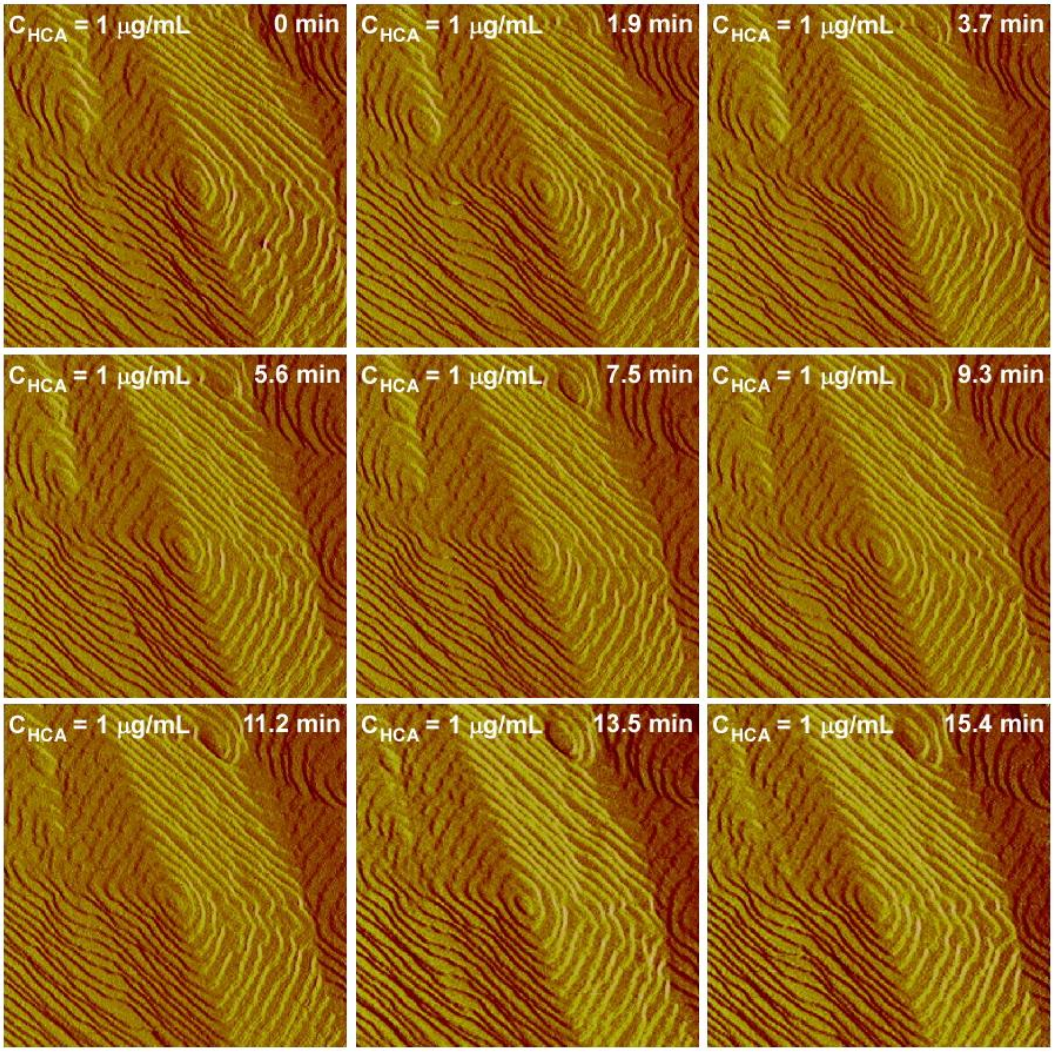

Figure G1 Snapshots from in situ AFM studies of COM (010) surface in the presence of C_{HCA} = 1 μg/mL. All images obtained in deflection modes and the areas are 2.41 μm x 2.41 μm.

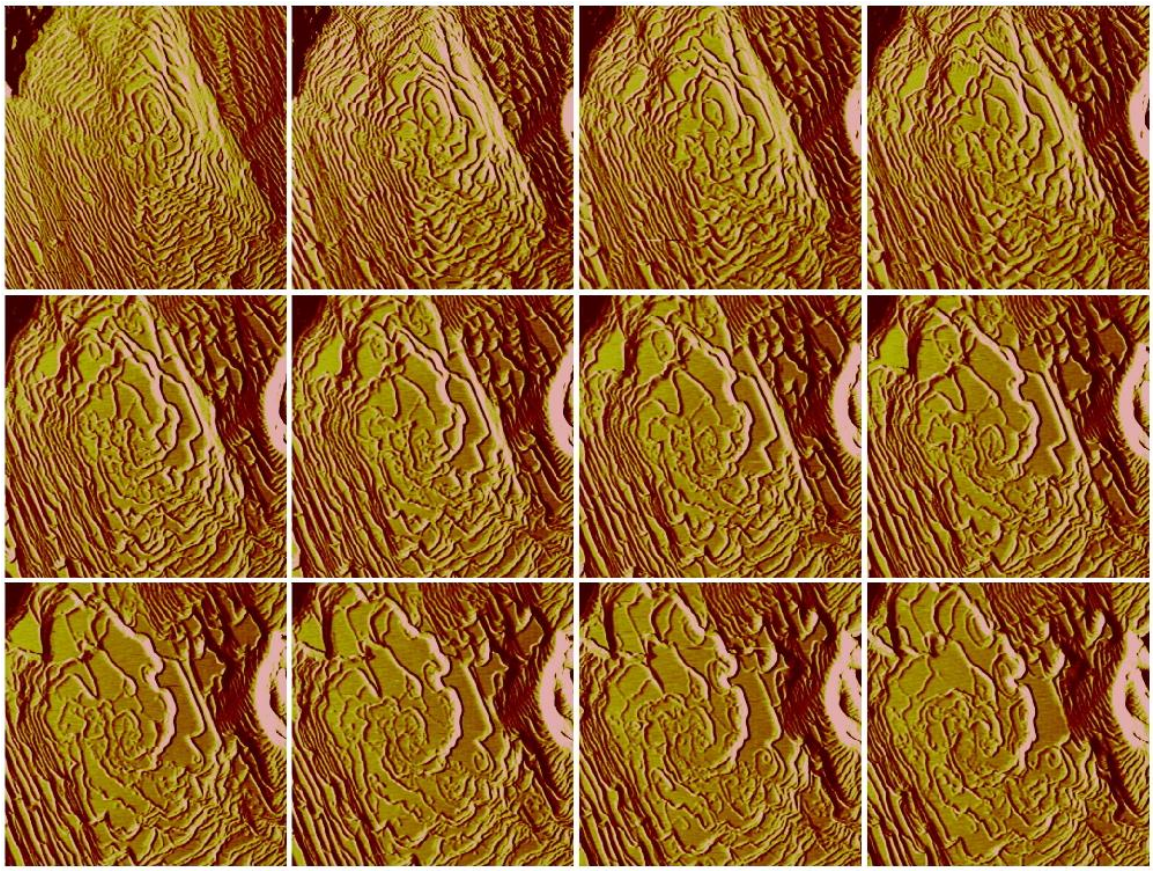

Figure G2 Snapshots from in situ AFM studies of COM (010) surface in the presence of C_{HCA} = 2 μg/mL. All images obtained in deflection modes and ca. two minutes apart. Image area equal to 3.55 μm x 3.55 μm.